HIGH THROUGHPUT FUNCTIONAL MATERIAL DEPOSITION

USING A LASER HOT WIRE PROCESS

By

SUKSANT PANGSRIVINIJ

Submitted in partial fulfillment of the requirements
For the degree of Master of Science

Thesis Advisor: Professor James McGuffin-Cawley

Department of Materials Science and Engineering
CASE WESTERN RESERVE UNIVERSITY

August, 2016

Case Western Reserve University

School of Graduate Studies

We hereby approve the thesis of

Suksant Pangsrivinij

_____

A candidate for the **Master of Science**

Committee chair:

James McGuffin-Cawley

Committee Member:

Badri Narayanan

Committee Member:

John Lewandowski

Date of defense:

February 25, 2016

* We also certify that written approval has been obtained for any proprietary material

contained therein

Table of Contents

List of Tables

List of Figures

15

17

Acknowledgements

I would like to thank my local advisor Prof. James McGuffin-Cawley for his very excellent supervision and guidance during this work. Thank you very much for your calm patience, encouragement, understanding, sense of humor, and both physically and mentally great support. He not only educates me with his knowledge in materials science field, but also teaches me through his real-world experiences outside classes that I can apply to my daily life. I cannot thank you him enough everything he has done for me.

Special thanks to Badri Narayanan for recommending me to enter to the department of materials science, introducing me to Prof. James McGuffin-Cawley and giving me a very big opportunity to participate in this project. I also appreciate the support I always have obtained from Shenjia (Alfred) Zhang including the consumable R&D team at The Lincoln Electric Company for allowing me to use their experiment tools and facilities there and guiding me through everything I should know to complete the project step by step.

Finally, I would like to thank my family and friends in both U.S. and Thailand especially my mother and father for supporting me in this work and degree and being by my side throughout this journey. Without them, I would not even have an opportunity to enter to a great university like Case Western Reserve University (CWRU).

Suksant Pangsrivinij
February, 2016

High Throughput Functional Material Deposition using a Laser Hot Wire Process

Abstract

By

SUKSANT PANGSRIVINIJ

Laser Hot-Wire (LHW) cladding is a wire-based, laser-assisted additive process of fusion joining. As the name suggests the filler wire is resistively heated prior to reaching the weld pool. The LHW process offers great benefits, relative to arc-based processes, in terms of high energy efficiency, excellent metallurgical control and high deposition rate. In work reported on in this thesis, two different material systems, Ti-6Al-4V alloy and the nickel-based superalloy 625, are experimentally evaluated through characterization of specimens created using the LHW process with a range of process parameters. Characterization includes chemistry of deposited metal, microstructure, selected mechanical properties, dimensions, and residual stress. Also, a rigorous analysis of energy efficiency was performed. All results are benchmarked relative to a laser/powder based additive manufacturing process. The result obtained in this work is anticipated to improve the understanding of the LHW process, expand its use to less common alloy systems, and promote its use as an industrially relevant form of additive manufacturing. The project that enabled this work is a collaboration between CWRU, Lincoln Electric, Alcoa Titanium & Engineering Products, and rp+m Incorporated.

1.0 Introduction

1.1 Additive Manufacturing overview

Additive manufacturing (AM) is a name used to describe technologies that are used to fabricate 3D objects by adding cross-sectional layer upon layer of liquid, powder, sheet material or others generated from 3D computer-aided design (CAD) applications whether the material is metal, polymer or others. AM was originally focused on rapid prototyping for preproduction visualization models. Currently, AM is also being used to develop and customize end-use products for several industries. Several benefits of using AM technologies over traditional tooling-based approaches such as casting or machining are its relative low cost for low-volume production of near-net-shape parts, lower net manufacturing costs, faster lead times, and construction of more complex geometries [1, 2].

Additive manufacturing via Laser Hot-Wire (LHW) freeform welding, which is the main focus on this thesis, can be seen as an extension of both robotic welding and cladding processes. The process is a limited arc process of welding and cladding commercially extended and applied by The Lincoln Electric Company. It is a laser-assisted, wire-based robotic process and, as the name "hot wire" suggests, the filler wire is resistively heated prior to reaching the weld pool. This offers advantages in terms of energy efficiency, metallurgical control, and deposition rate.

1.2 Objective

The objective of this research is to focus on the assessment and characterization of a laser-assisted, wire-based additive called "laser hot-wire" (LHW) process capable of high throughput functional material deposition applications into a full 3D freeform additive manufacturing process. Energy efficiency, material characterization, mechanical properties testing analyses are conducted through several shapes and features of specimens fabricated by the LHW process. In addition, these results are benchmarked against specimens created by a laser/powder-based additive manufacturing process with an intention to develop the LHW process to be one of potential alternatives in a future of additive manufacturing industry.

Therefore, with this project, it is expected to address the different needs of current additive manufacturing (AM) specifically in metal materials and deliver, in addition to the assessment of the feasibility of the LHW process for additive manufacturing, a guideline document and test protocols for assessing other new processes. Outcomes to include characteristics of microstructure and measurements of selected properties for two alloy systems.

1.3 Scope and Approach

The scope of this research is to investigate and evaluate two different material systems with the LHW process whether the LHW process can be used in service with desired properties to real-world industry adoption of additive manufacturing or not. Specimens of Ti-6Al-4V and nickel-based superalloy 625 were generated, validated, and assessed as a part of this project using standardized test protocols. The reliability of the technology and the process was assessed by observing the material behavior in terms of property, chemistry and structure heterogeneity. In addition to the reliability analysis, the efficiency of the process in terms of material, energy and time will be determined using the information generated on the structure and property heterogeneity characterization.

1.4 Thesis outline

The above introduction to additive manufacturing and the LHW process is followed by Section 2 which provides a literature review of several welding, cladding, and freeform welding types related to AM using both powder-based and wired-based feedstocks. Section 3 provides details on the experimental methods used in the experiments conducted in this thesis work. Section 4 presents results from all experiments conducted. In section 5, results based on topic in section 4 are extensively discussed followed by conclusions, suggestions for future work and references.

2.0 Literature review

2.1 Relationship between welding and additive manufacturing of metals

Currently, several welding processes, such as arc, laser or e-beam welding, have been applied in additive manufacturing. In this section, a systematic overview of welding processes is provided and comments are offered with respect to their relative relevance to AM. In addition, the technology of cladding is described and related to AM as well.

2.1.1 Fusion welding, cladding, and build-ups

In the following sections, a brief review is provided on methods of local melting and resolidification, which is the basis of all fusion welding techniques. Following this, the specific literature that pertains to how each has been explored as the basis for additive manufacturing is provided.

The process of fusion welding starts by bringing two conformal surfaces into close proximity (conventionally termed "faying" surfaces). A highly localized source of heat is brought to bear which causes melting at a spot along the joint. When the surfaces are sufficiently closely spaced, the liquid bridges the gap and is held in place by capillary forces. By causing relative motion between the heat source and the workpiece (depending on the approach to fixturing one is typically stationary and the other moves), the entirety of the faying surfaces is sequentially raised above its melting point and then resolidified through cooling (usually through a combination natural convection and radiation) [3]. The geometrical arrangement for fusion welding is shown in Figure 1a.

The surfaces to be locally melted are generally perpendicular to the free surface.
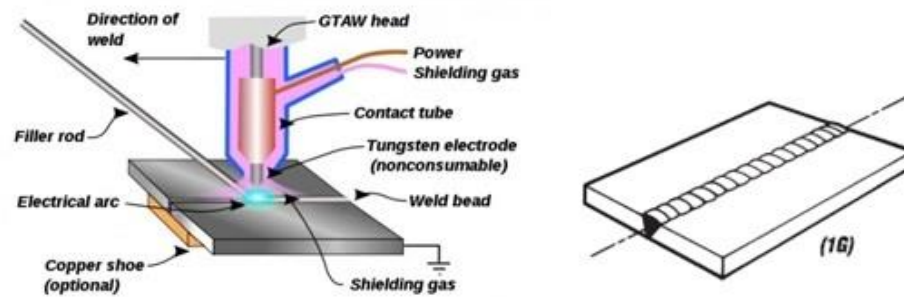
Figure 2.1.1.1: Illustrations of geometrical arrangement for fusion welding (a) during the process (b) weld bead created after process [2, 3]

Cladding (including overlays, hardfacing, etc.) is geometrically distinct [4, 5]. Unlike in welding, this family of processes does not lead to joining of two solid parts. Rather, matter is added across an entire free surface by sequential deposition of molten metal. The geometrical arrangement for cladding is illustrated in Figure 1b. Characteristics include using a raster pattern to cover an area [6], or a helical pattern when covering a cylinder (e.g., pipe), the thickness of the cladding is typically a small fraction of the original substrate, and only a thin layer of the substrate is subjected to transient melting.

Figure 2.1.1.2: Illustrations of geometrical arrangement for cladding (a) on straight-plane substrate (b) on tube-shaped pipe [7, 8].

A welding build-up is the equivalent of multiple layer cladding. That is, sequential addition of successive cladding layers allows the creation of a part that has definite shape and which is often a substantial three dimensional form [9, 10]. The original substrate may, or may not, be incorporated into the final part. An illustration of build-ups is given in Figure 2.1.1.3. Welding build-ups that generate near-net shaped parts are increasingly referred to as freeform welding, a form of additive manufacturing.
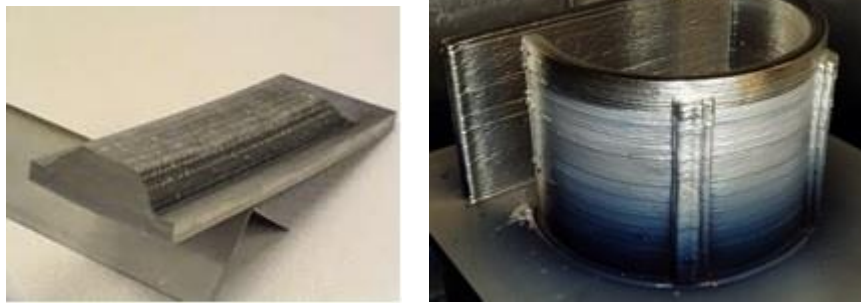
Figure 2.1.1.3: Illustrations of geometrical arrangement for welding build-up (a) on substrate with basic shape (b) with more complicated shape [11]

2.1.2 Energy sources

What distinguishes the basic classes of welding is the nature of the localized heat source. This also is the case with cladding, freeform welding, and additive manufacturing processes for metals. As welding has the longest history and greatest breadth of application, it is most studied. Therefore the significance of using a particular energy source is first comprehensively reviewed in its context. As a basis for comparison, the

range of energy sources is first reviewed in the context of welding. Two broadly applicable welding types are oxy-fuel and arc welding. Both have long histories and both continue to find wide application.

Oxy-fuel welding (usually oxy-acetylene Welding, OAW) employs combustion of a gaseous mixture to generate localized heat. Typically, two compressed cylinders are used with internal pressures ranging from 2,000-2,640 psi (pounds per square inch) for oxygen cylinder and not above 15 psi for acetylene cylinder [12]. Flame temperatures can be in the range of 3,200–3,500 C (5,792-6,332 F). Amongst its advantages is the ability to alter the flame chemistry by controlling the oxygen to fuel flow rates in order to achieve reducing (carburizing), neutral, or oxidizing conditions over the molten metal. Also, by inducing a high flow rate of gases it is possible to switch to "cutting" in which the molten metal is literally blown from the workpiece. Oxy-fuel is therefore most often used when flexibility is a premium, and is less favored in industrial applications which are automated and in which the nominal conditions do not vary greatly. Though, in principle, one can use OAW to do additive manufacturing process, a review of the literature confirms that localized heating by arc, e-beam, and laser offer more desirable characteristics.

2.1.3 Arc welding

The term fusion welding can be used to describe a number of welding procedures. One of the prime power sources remains an electric arc to locally heat to the melting

point in order to irreversibly join metals. Historically, it was after the discovery of the short-pulsed electric arc in 1800 by Humphry Davy [13] and the continuous electric arc in 1802 by Vasily Petrov [14] that fusion welding started to develop. In operation, the arc is struck between an electrode and a workpiece, and one is translated relative to the other to create the joint. The job of the electrode is to conduct the electric current and, through standoff distance and tip geometry amongst other parameters, control the electric arc between a tip of welding gun and the workpiece. Commonly, the electrode is consumable. That is, the heat from the arc melts the tip of the electrode, this molten metal is transferred to the workpiece, and it is incorporated as a "filler" in the joint. It is furthermore typical to distinguish between rod and wire when referring to consumables. Rod is, as the name suggests, relatively short in length (nominally 14" or 35 cm) and large in diameter (1/16 to 3/16" or 1.6 to 4.8 mm), and is also often referred to colloquially as "stick welding." It is essentially always a manual process carried out by skilled welders. Wire, on the other hand, is thinner (ranging from 0.024 to 0.045" or 0.6 to 1.1 mm) and is supplied in long lengths on spools (100s to 1000s of feet in length or, roughly, 30 to 300 m). Both manual and robotic systems routinely use weld wire.

However, it is also possible for the electrode to be fabricated from a non-consumable, most predominantly tungsten or its alloy, and, if required, the consumable (or filler metal) is independently fed into the joint region. Arc welds may be obtained in the absence of a filler metal (i.e., locally melting and resolidifying). These are termed autogenous and have specific advantages and disadvantages. For example, autogenous offers highly accurate and consistent application of heat and may be more economical

[15]. However, this process is not of concern here because attention is to be focused on builds-ups in the context of additive manufacturing, and this necessarily requires consumables.

In terms of motion during welding, "drag" (pull) or "push" are two terms being used to tell two different motions in welding. On one hand, to drag means the electrode is pointed back towards the weld pool. This kind of motion provides maximum penetration. On the other hand, to push means to point the electrode forward. This kind of motion is helpful when welding vertical-up because it leads the heat away from the puddle and permits the weld to solidify quicker [16].

Contamination of the weld area is an important concern in all fusion processes due to the fact that the molten metal occurs in a high specific surface area form in contact with both an atmosphere and a free surface (that may or may not have been recently cleaned).   Reactions can lead to porosity, inclusions, and/or alloy chemistry shifts. To mitigate this problem, inert shielding gases and/or fluxes have been developed (and continue to be improved).   These are used to protect the weld area from air and surroundings.

2.1.3.1 GTAW (Gas Tungsten Arc Welding) or TIG (Tungsten Inert Gas) welding

GTAW generates a joint of weld by using a non-consumable tungsten electrode. In most cases, a filler metal is used in GTAW. Especially in welding dissimilar metals, a mutually compatible filler metal can help form a stronger bond by grading the

composition across joint. For example, it is common to use a nickel filler metal to join steel and cast iron [30]. Although the electrode used in GTAW does not melt due to the high melting temperature (3,422 °C or 6,192 °F), some erosion which often is called burn-off, generally occurs and resultant debris may fall into the joint.

To protect the welded area from such debris and also reaction with atmospheric gases such as nitrogen and oxygen, a shielding gas is commonly used. This helps limit porosity and weld metal embrittlement during welding. The gas also helps transfer heat from the electrode to metal and maintain the arc while welding. Shielding gases must be nonoxidizing and a small family of compositions dominate the industry [17]. Generally, lower cost formulations are used whenever possible. Typical systems include noble gases, primarily argon (and in some cases helium) and mixes that include up to 25% CO_2. For special situations, argon/helium gas mixtures can also be used to permit high penetration depth as is needed such as welding on a thick aluminum. The benefit of using argon as a shielding gas is that it helps remove contaminants at the surface and reduce weld porosity - called an arc cleaning action by forming a plasma to etch weld surface. Thus, mixture of both gases can give the benefits of depth penetration and surface cleaning.

In terms of power supply, GTAW commonly uses a constant current power source, i.e., the electronics of the power supply fix the current to a user specified value regardless of changing the arc distance and voltage. The constant current source can help maintain a steady arc and generally yields a smoother finish to the joined materials

when compared to a constant voltage source. In addition, polarity can be varied with current either alternating current (AC) or direct current (DC) in power supply. This also affects the quality of weld and it strongly depends on the type of metal being welded.

For DC power supplies, there are two types that are two important subclasses; direct current with a negatively charged electrode (DCEN) and direct current with a positively charged electrode (DCEP). In simplest terms, with a negatively charged electrode electrons flow to the base material which at steady state is hotter than that the electrode tip. The ionized shielding gas will flow along the electrode due to electrostatic forces and this eventually allows oxides to form on the surface of the weld. On the other hand, in DCEP, electrons are emitted to the other direction leading the positively charged electrode to reach an extremely high temperatures and which drives the ionized shielding gas to the base material. As a result, the weld surface is cleaned by the ionized shielding gas. Although the surface of using DCEP is cleaner than using DCEN, DCEP is still suitable only for shallow welds due to less heat generated on the workpiece. For deep welds that require DCEN, external parameters are adjusted to create the most favorable conditions and, ultimately, the absence of cleaning may have to be accepted.

With AC power supply, the polarity of the electrode and base material reverses at a fixed specified frequency, with the electrode alternately being positive and negative. This helps to get both benefits of surface cleaning from DCEP and of heating base material from DCEN. However, one disadvantage of AC is the fact that the arc must be

re-ignited after every zero crossing. If a conventional sine wave is used arc loss and reformation becomes impractical. Typically, for GTAW a high frequency oscillator is used which generates a square wave to reignite the arc at every each half cycle during welding. In practical terms, TIG welding can be set up to produce clean welds under conditions of well controlled heat input, and a filler metal may or may not be used.

2.1.3.2 Gas Metal Arc welding (GMAW) or MIG (Metal Inert Gas)

GMAW also produces a weld by heating via an electric arc causing local melting. However, in this case the arc is formed between the filler wire and the workpiece. That is, the filler wire acts as consumable electrode, and it melts into the weld pool. The consumable electrode may simply be a solid wire, but often is "cored" meaning it is a small diameter metal tube which contains granular materials (i.e., powders). Both alloying elements and/or flux formers may be included in the granular materials. Electrode selection depends on the composition of welded metal and the electrode has a great impact on weld quality and mechanical properties of the metal being welded. Generally, the complete weld metal should have the same mechanical properties as the base material. While joining metals, some erosion or burn-off can occur from heating consumable wire electrode and/or filler metal if used which can cause fusion defects to the weld metal. Thus, to protect the welding area, shielding gas is blown along the welding gun.

There are 4 sub-processes of GMAW that can be described by mode of metal

transfer; GMAW-S (Short Circulating Arc), GMAW-P (Pulsed Arc), GMAW-B (Buried Arc or Globular), and GMAW-ST (Spray transfer). Detail of each process is provided as follows.

- Spray Transfer - It is an axial transfer of small discrete drops of metal (as small as or smaller than the diameter of the wire) at rates of hundreds per second without spattering. DCEP is commonly used with spray transfer mode. Although, argon is preferably used as a shielding gas in this process, helium is commonly added to gas mixture to increase ability for penetration when joining reactive materials such as aluminum, titanium or magnesium. Since this process requires higher voltage and current, the drawback of this process is the high arc energy and large weld pool area created because it makes the process harder to join thin sections, as well as limiting vertical and overhead welds. It is generally suitable to join workpieces of thicknesses above about 0.25 in or 6.4 mm. It is a high heat input process that can melt an appreciable amount of base metal, and stay hot enough to react with the atmosphere for a relatively long time.

- Pulsed Arc (Pulsed-spray) -The pulsed-spray creates a small molten droplet in each pulse with low input of pulsing current to melt the filler wire which helps decrease the size of the weld pool and heat-affected zone. That is why it can be used to weld thin sections as well as thick sections. Also, pulsed-spray is better suited to do so-called out of position welds (vertical and overhead). It provides a stable arc and no spatter since short-circuiting does not occur. For shielding gas,

35

the process primarily uses argon with a low carbon dioxide concentration. However, it needs sophisticated power source to supply current pulses with a frequency between 30 and 400 pulses per second. This increases capital cost, but from an engineering point of view it provides several advantages. These include wider processing windows, lower net heat input (which has several advantages such as reduced distortion and a reduced tendency to boil volatile elements to create weld "fume," and, obviously, a smaller heat-effected-zone, HAZ), and higher throughput.

- Short Circuiting Arc – At low voltages relative to that used for spray or pulsed-arc, a mode of transfer that relies on intermittent contact between the workpiece and electrode is obtained. Polarity is chosen so that a droplet forms at the tip of the electrode. With a low voltage and high enough wire feed rate the droplet comes into contact with the workpiece before separating from the electrode creating a short circuit condition. The momentary high current flow causes magnetic forces that, in combination with surface tension, cause the droplet to flow to the workpiece recreating the gap and the arc is re-ignited. This cycle is repeated about 100 times per second. Generally, this process creates low heat input and is suitable to join thinner material with low distortion and residual stress. However, it is dynamic process in which molten metal experiences high forces leading to spatter as a result of ejection of droplets from the pool.

- Buried Arc and/or Globular – With this metal transfer mode a drop is formed on the electrode (as in short circuiting arc), but it differs in that the conditions permit the droplet to grow in size prior to transfer. It was originally developed as a cost efficient way to weld steel by using carbon dioxide as a shielding gas which is lower cost than argon. It can be considered the least desirable of GMAW because it provides an uneven and poor weld surface and larger electrode is also required from using high current. Furthermore, substantial spatter occurs due to uncontrolled short circuits.

2.1.3.3 Arc power and polarity of GMAW

Although a wide variety of conditions are possible, most of welding applications employing GMAW use direct current reverse polarity (electrode positive or DCEP) since this type of polarity provide a stable arc and smooth metal transfer, fast melting of the feed wire, and fast travel speed during welding. On the other hand, a negatively charged electrode is hardly used since special emissive-coated electrode wires are needed and it usually provides an unstable arc.

The electric arc is a low cost powerful energy source that can be localized. For this reason it remains the basis of many welding processes. However, there are other sources of concentrated energy that can be used for welding (and additive manufacturing). The two most widely used are the electron beam (e-beam) and lasers.

2.1.4 Laser beam welding

Laser first became practical for welding in the 1960s. Similar to electron beam, laser welding relies on the creation of a well-collimated "power beam," but in this case it is photons rather than electrons. The first of the two fundamental differences between the two is that electron beam requires a vacuum whereas the laser does not (although it does often require shielding gases to be used). Secondly, the generation of the laser is a much more energy intensive process than the electron beam. System efficiencies for electron beam can be greater than 80% whereas for the laser it is less than 10% [18].

The laser beam welding (LBW) is used to join materials with high welding speed and automatic operation to accurately control the quality of welds. Some of advantages using laser beam welding are high and focus heat source, good depth of penetration, and small heat-affected zones. Besides, the laser beam can be emitted through air without dissipation like electron beam. So, it can be an economical choice for manufacturers who have a limitation of tooling and production pricing.

In welding with laser beam, the pulse of laser energy is transmitted, contacted, and focused into a specific point of the workpiece. It enables power densities in the range $10^3 - 10^7$ W/mm^2 to be applied to the weld. After the workpiece absorbs the focused laser beam, the beam drills into the workpiece, creates a keyhole, and vaporizes the workpiece's surface. The molten metal begins to solidify around the keyhole and eventually form a fusion weld. As a result of the process, high productivity can be

achieved from high travel welding speeds in thinner materials, or in thicker materials, a single pass of the laser beam can also create a deep penetration weld with low thermal distortion. Thus, high melting points and high heat conductivity materials can be welded with this process. However, keyhole characteristics are not really used in AM since each layer is used to build up a part not to create a hole. So, in a regard of AM discussion, laser has been used to melt and re-solidify filler metal to create a build-up.
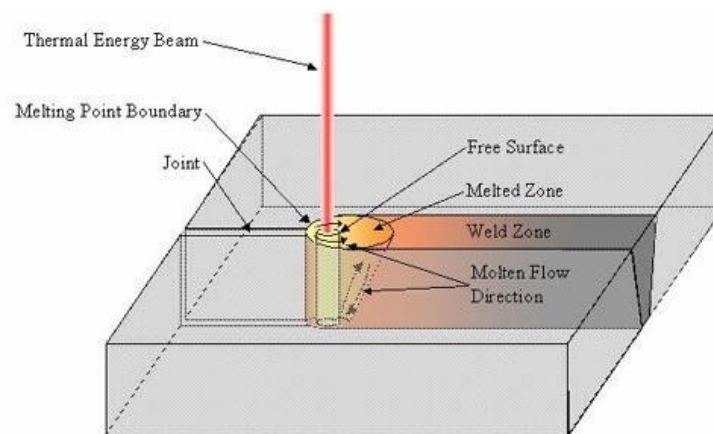
Figure 2.1.4.1 Schematic of laser welding process [21]

For laser sources, there are four types of lasers that are generally applied in laser welding as solid-state lasers (most commonly used are Nd: YAG lasers and ruby lasers), gas lasers, fiber lasers, and high power diode lasers. Firstly, in solid state lasers, Nd:YAG (neodymium-doped yttrium aluminium garnet; $Nd:Y_3Al_5O_{12}$) and ruby lasers are crystals that are applied as a lasing medium for this process. The shape can be rod, disk or flashlamp depending on applications. In comparison of output, Nd:YAG lasers provide much more power than ruby lasers at 0.04-6000 W while ruby lasers gives between 10-20 W [19]. Secondly gas lasers used gas mixture (Commonly used argon, helium, and

nitrogen) as a lasing medium. Power outputs of gas lasers are able to reach 25 kW which

is higher than those of solid-state lasers [20]. Thirdly, a fiber laser, which uses an optical

fiber as a lasing medium, is couple into a flexible fiber. For the power output, ytterbium-

doped (yb) fiber lasers can provide power up to 50 kW [21]. Finally, for the diode lasers,

it can provide power up to 10 kW [21].

Moreover, two operating modes (continuous wave and pulsed) are applied in laser

welding. Continuous wave delivers essentially constant power, whereas a pulsed laser is

often described as a set of periodic square waves. Specifically, in the pulsed laser, there

are three modes of laser welding to consider; conduction, penetration, and keyhole

mode. Power density and pulse duration are factors that differentiate each mode.
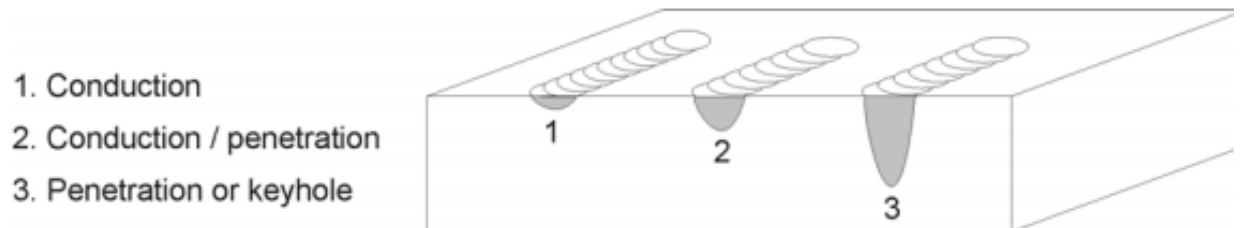
Figure 2.1.4.2 three modes used in laser welding [21]

2.1.5 Electron beam welding

Historically, electron beam welding (EBW) was originally pursued to solve arc

welding problems such as atmospheric gas contamination by operating under vacuum

condition. By necessity, EBW generally takes place in a vacuum to eliminate electron

beam scattering and dissipation problems associated with electron gas atoms/molecules [22], thus gas-solid reaction are not an issue.   For example, materials such as titanium can be welded by a variety of techniques, but EBW under vacuum is the preferred technique to avoid gas contamination of the reactive metal. EBW is also preferred for metals such as niobium, nickel-based superalloys and other refractory metals [23].

In addition, EBW is able to produce a full thickness weld with a high depth-to-width ratio by interchangeably increasing in a wide range of beam current as well as power density. This is a particular advantage in reducing the amount of time spent in welding thick materials (more than 1/2 inch or 12.7 mm) and creates welds of favorable final geometry.
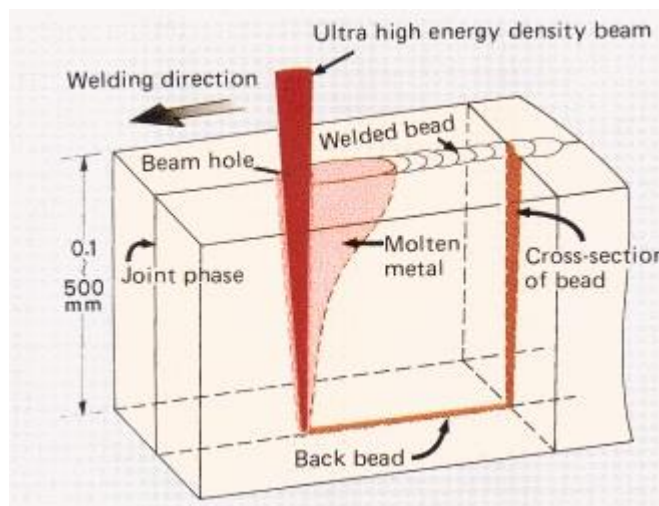
Figure 2.1.5.1: Schematic of e-beam welding process [24]

The EBW process is qualitatively similar to the GTAW in that heat energy is supplied externally to the filler wire. Instead of using an electric arc, an electron beam is (typically at a voltage of 10-150 kV and very low beam currents measured in milliamps [23])

generated by a filament and directed to the joint of weld. When electrons interact with a surface of workpiece, the kinetic energy of electrons is transformed into thermal energy. Very high thermal energy densities are possible due to the ease of focusing the beam. Furthermore, the efficiency of heating is high. Regardless of the angle of incidence, more than 90% of the electrons are absorbed [24].

Furthermore, the EBW process is able to provide two welding modes. These are conductance and keyhole modes. With conductance, the weld is rapidly created at, or just below, the surface with temperature just above the melting point. The thermal conductance generated from heat then penetrates to the workpiece's surface below the joint. A focused electron beam spot and high energy density supported by this mode result in a narrow weld on the workpiece. As a result, the conductance mode is suitable to weld thin materials because, in utilizing high energy density, rapid travel speeds can be achieved which reduce damage of heat affected zone (HAZ) and also absorption of excessive heat on the workpiece's surface.

The other mode of the EBW process is the keyhole mode. This mode is often preferred when deep penetration is required. Even though it is not used in AM, a brief explanation is provided to differentiate with other modes. To be able to get a full penetration, more focused energy and higher accelerating voltage of the electron beam are needed. The electrons from the focused beam melts and vaporizes the subsurface of the workpiece generating a through-hole cavity. A pressure caused from vaporization and sputtering is exerted on the liquid distributing it on the cavity walls of the workpiece.

As the beam is moved along the weld direction, the trailing molten layer begins to fill the hole, solidify and create a fusion weld. The resultant weld from this mode, like the conductance mode, still gives narrow welds with minimal heat affected zone.

In terms of the degree of vacuum, the EBW process can be classified into three main processes as hard vacuum EBW (0.013 Pa or lower), commercial or soft vacuum EBW (13.0 Pa), and non-vacuum EBW (100 kPa or 1 atm). With the highest penetration rate and depth to width ratio, the hard vacuum EBW is the most frequently used in manufacturing industry. [25] The hard vacuum type also provides the highest purity of fusion zone, the best properties of joining sensitive brittle materials, the best ability of welding thick metals and the longest working distance (up to 30 in. or 750 mm). However, soft vacuum process is easier than the hard vacuum to operate because it requires just a simple mechanical pumping as an operational pressure source, whereas the hard vacuum mode requires both mechanical and diffusion pumping.

Given a particular atmosphere, the four parameters that have a great impact on weld shape and dimensions, and resultant mechanical properties, in EBW process are beam current, accelerating voltage, beam focus, and welding travel speed. In practice, these parameters are straightforward to control over relatively wide ranges. In fact, by using the different extreme values, quite different welds can be obtained. For instance, a very high beam focus (yielding high power density) with low speed creates a conical melted zone and a deep penetration while a hemispherical melted zone and shallow weld is a result of lower beam focus with a very fast travel speed.

2.1.6 Hybrid laser arc welding

The process is a combination of laser welding and one other welding process, normally GMAW or GTAW is applied, to achieve advantages of both techniques. The weld beads resulting from hybrid laser arc welding usually have a narrower than arc welding alone, while at the same conditions, it provides deeper penetration than stand-alone arc welding or laser beam welding [26]. Additionally, grain size of the hybrid process is observed to be smaller than that of GTAW process but bigger than that of laser beam process [26]. Therefore, benefits of using the hybrid laser arc welding over the stand-alone process of arc or laser welding are: higher welding speed, deeper penetration, lower weld shrinkage and distortion, lower pores and cracks, good gap bridging ability [27, 28, and 29].

Laser hybrid welding has many benefits over stand-alone arc welding and laser welding. However, since the focus of this is on additive manufacturing, keyholes that penetrate the workpiece are not our objective. In the next section, feedstocks and cladding processes which do not use the keyhole mode will be discussed.

2.1.7. Feedstock

In welding process, wire-based feedstocks are mainly used and their characteristics, differences, advantages and disadvantages are discussed in the next section. Powder-based feedstocks for cladding and AM processes are deferred until in

cladding section.

2.1.7.1 Wires: solid and flux-cored

There are three main types of wire feedstock. Firstly, solid wire-based welding is the most common usage in several industry. It has been widely used in simple arc welding such as GMAW (Gas Metal Arc Welding) power sources. Solid wire is used as a filler metal with an externally supplied shielding gas during the welding process. The wire is usually mild steel and coated to protect it from rusting and also improve arc performance and electrical conductivity [30].

The second most commonly used wire is flux-cored. Flux-cored arc welding (FCAW) is different from solid wire because the process utilizes a hollow wire which contains oxides and/or reactive species that form a flux to isolate the molten metal from the environment.

In the context of welding, the primary role of a flux is to prevent oxidation. The chief advantage of flux-core is that the slag that formed during the process is a sufficient barrier in many circumstances to eliminate the need for shielding gas while still creating a smooth and sound weld. This is termed self-shielding. Gas shielding is sometime, however, used in combination with a flux.

For gas shielded flux cored wires (FCAW-G), the process uses both a slag system and external shielding gas to protect a weld from external atmosphere. The core ingredients of these wires create a slag and can be added additional alloying elements to obtain desired properties of final welds. It helps improve usability of these wires by

using shielding gas. On the other hand, self-shielding flux cored wire (FCAW-S) does not

need external shielding gas. In this case, flux from the wire when burnt generates

shielding gas to protect molten weld pool. This self-shielding flux cored wire is very

portable and more suitable for welding outdoors when external shielding gas is no

needed [30]. However, typically the slag must be physically removed prior to putting

the parts into service. Removal of the slag is necessary if a second layer or pass is

required in order to minimize the likelihood of inclusions. In addition, it may be

required to allow inspection, or to prepare the surface for painting or lubrication.
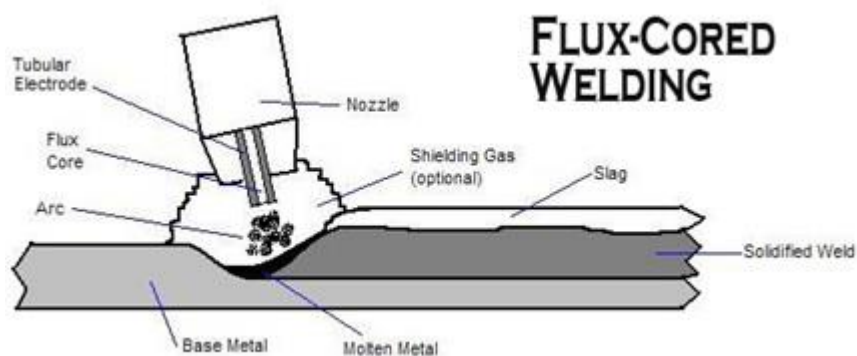
Figure 2.1.7.1.1: Schematic of flux-cored arc welding process [31]

Thirdly, for metal-cored (MC) wire, it has a very similar construction to flux-

cored wire but the performance and functionality parallel to solid GMAW wire. It is

typically a composite tubular wire of an outer metal sheath with a core of powdered

metals and alloys. With the metal-cored wire, it provides versatility to welders in terms

of metal composition and properties because several alloy compositions can be

formulated in the tubular wire to meet specific requirements [32]. It is also more

economical compared to solid wire since small quantities of metal powders are easier

to manufacture than a special melt of steel [33].

Furthermore, MC wire offers higher deposition rate (lbs/hr) since the sheath conducts the electrical current and the current carrying density is greater in metal cored wires. With higher deposition rates, it leads to more efficient productivity and low cost production. This is because the metal powder core of MC wire is less-conductive and requires less current to melt it than metal inert gas (MIG) wire which the entire cross-section of the MIG wire is conductive. Low spattering and low slag volume are benefits of utilizing MC wires as well [34, 35]. Although, MC wire contains both sheath wire and powder, it is introduced in wire feedstock section since it is still be used in wire manner. Powder feedstock will be introduced in cladding section.
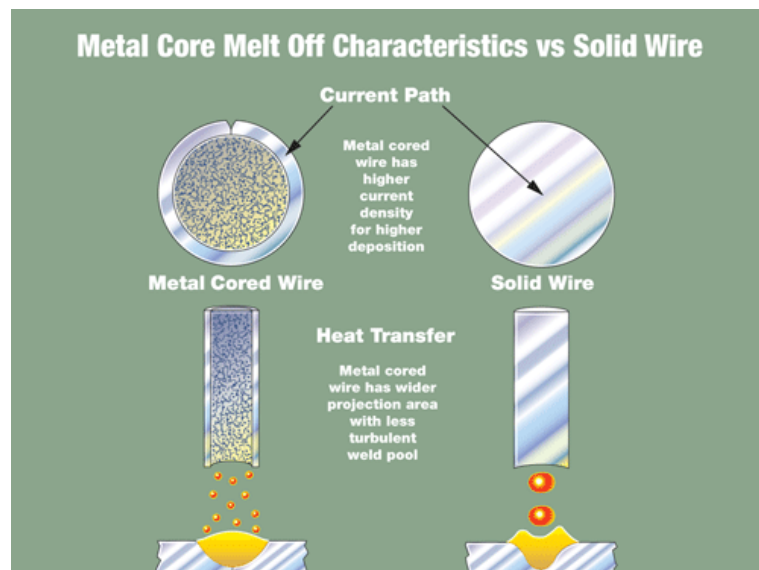
Figure 2.1.7.1.2: A figure comparison between metal-cored (MC) wire and Solid wire characteristics

2.1.8 Cladding

The aim of the cladding process is to add new material (generally with different properties) onto the surface of the substrate (original material). In the case of repair, the clad may be the same as the base material, but when cladding is part of fabrication the clad is generally of different composition. Examples include hardfacing (cladding with a wear resistant alloy [36]) or for enhanced corrosion resistance [37]. A fundamental premise of cladding is the creation of a strong metallurgical bond between overlayer and substrate. Therefore some melting of the substrate must occur. Mixing of this melted substrate with the cladding alloy is termed "dilution." In this usage higher dilution means more dissolved substrate which may compromise the properties of the overlayer. Ideally, the lowest dilution that reliably produces a strong bond is used.

In terms of feedstock, other than wire-based options, powder feedstocks are also utilized in cladding and AM. There are many additive processes such as Selective Laser Sintering (SLS), and Electron Beam Melting (EBM) that use powder feedstocks which will be explained in the section 2.3 named "powder additive processes for metals". Generally, for cladding and additive manufacturing processes that work with powdered materials, laser or e-beam energy sources is traced along an X and Y plane across a powder bed of spread material laid down by a roller inside the machine. As the power sources interact with the powdered surface, it fuses and re-solidifies to form a layer of solid. Once one layer is completed, the powder bed drops at a certain size incrementally and the roller rolls the powdered material over the powder bed surface prior to the next pass of power sources. The process continues repetitively until the 3D

48

part is finished. Key advantages of powdered-based additive processes are support structure provided, high geometrical accuracy (+/- 0.05 mm) , better temperature and shielding gas control from using sealed build chamber, etc.

Nevertheless, on the downside, powder feedstock is more expensive than wire feedstock across the board. For instance, AM-grade Ti-6Al-4V powder is 50% more expensive than the cost of Ti-6Al-4V wire [38]. Moreover, porosity has still been an issue with the processes and some post-heat treatment, such as Hot Isostatic Pressing (HIP), is still necessary. Also, the deposition rate is lower compared to wire feedstock (which can also be seen as a result of energy usage calculation in the discussion part) and the build size is limited to the bed size for all the powder bed processes [39, 40].

On the other hand, there are also advantages for wire feedstock in cladding processes compared to powder feedstock. Apart from lower cost of wire feedstock, it also supports higher deposition rates as compared with powder bed. Additionally, it provides a wider selection of wire products versus powder feedstock [40]. Especially in LHW process, by using both laser and resistance heating of the wire, the same amount of material can be melted faster. This consistent result means higher deposition rate can be gained from using wire feedstock [Lincoln Electric, 2013] [41, 42]. Moreover, wire feedstock are better in usage efficiency and environmental friendly as almost 100% of the wirefeed is fed to melt pool during the process. No feedstock reclamation is needed [42, 43, and 44].

Material Feedstock	Titanium 6Al-4V	Tantalum	Inconel 625	Stainless Steel 316
Wire—0.035" Diameter (0.9 mm)	$58/lb.	$545.30/lb.	$26.73/lb.	$5.19/lb.
Wire—0.045" Diameter (1.1 mm)	$54/lb.	$545.30/lb.	$23.30/lb.	$4.63/lb.
Wire—0.062" Diameter (1.6 mm)	$50/lb.	$524.88/lb.	$22.17/lb.	$4.57/lb.
Wire—0.093" Diameter (2.4 mm)	$48/lb.	$502.30/lb.	$21.43/lb.	$4.81/lb.
Wire—0.0125" Diameter (3.2 mm)	$45/lb.	$438.96/lb.	$21.02/lb.	$4.75/lb.
Wire—0.0156" Diameter (4.0 mm)	$44/lb.	$438.96/lb.	N/A	$4.69/lb.
Powder—AM Grade	$77/lb.	$522/lb.	$48/lb.	$10/lb.

Table 2.1.8.1 approximate costs of a variety of wire in size VS powder as material feedstock according to a survey of the U.S. commercial market in June 2015
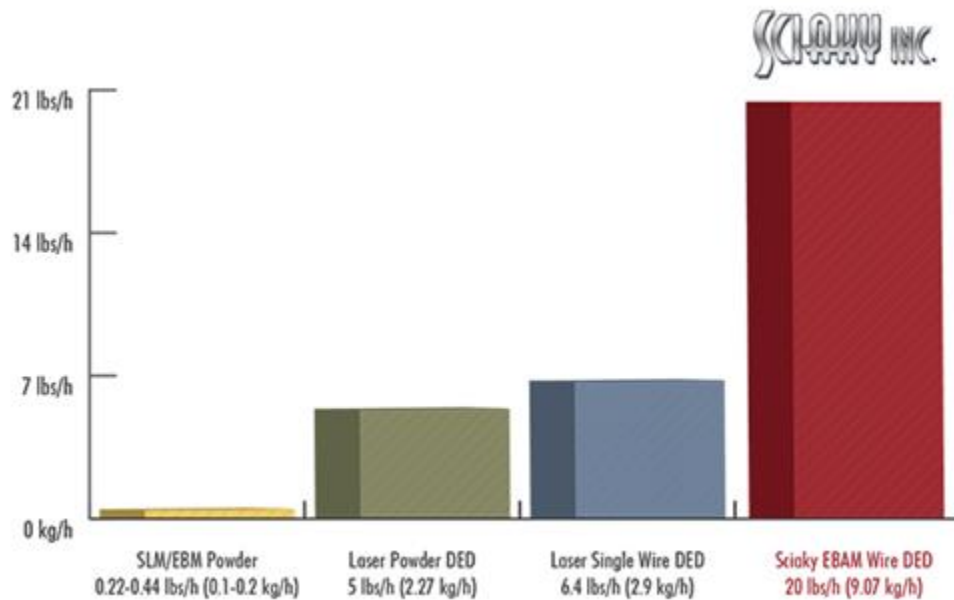
Figure 2.1.8.1 graphical representation of metal additive manufacturing deposition rate of powder feedstock VS wire feedstock

In this section, metal cladding processes using a variety of energy sources will be reviewed.

2.1.8.1 GMAW and GTAW Cladding

Arc welding technology, such as GMAW or GTAW, is also widely used for metal cladding. The geometry of cladding conditions is shown below.
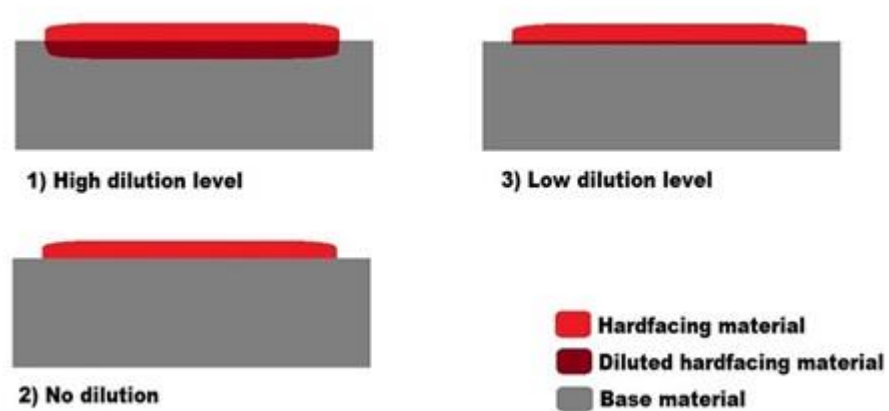
Figure 2.1.8.1.1 Different dilutions level in arc cladding [45]

The first two cases in this figure are both undesired. Case 1 represents a high dilution level due to the high heat input. This result is typical of cladding using conventional arc welding processes. Although a strong metallurgical bond has been created, the composition might not be desirable since the coating becomes an alloy of the substrate and new added material. In practice, multiple layers are usually required to solve the issue and get the desired properties in the working face. Case 2 might be thought of as an ideal in that the clad alloy is undiluted; however, there is often modest,

or intermittent, metallurgical bond between the added material and the substrate. This condition is frequently obtained when thermal spray coating is used [46]. Quoted values for the interfacial bond strength may be less than one quarter of the alloy yield strength. While there are applications appropriate for thermal spray, it is not generally suitable to applications with impact loads or deformations. Case 3 (low, but finite, dilution level) accomplishes both strong metallurgical bond to the substrate without markedly changed the clad alloy composition. With optimized process, the dilution is less than 5% and this is accomplished through accurate control of heat [47].

Thermal management, in particular the control of spatial and temporal thermal gradients, is as important in cladding as it is in welding. Although the geometry differs, both effectively impose heat sinks. The goal in both is to be able to exert engineering control over residual stress and avoid defects such as cracking. In addition to controlling defects, it was found that external preheating of the filler wire in GMAW resulted in lower dilution levels and improved use of arc energy (i.e., greater thermal efficiency) compared to conventional GMAW claddings [70]. Also, dilution of the added material is found to be dependent with wire feed rate, welding travel speed, voltage, and current used. Moreover, in a comparison of the pulsed and continuous current used of GMAW, the right selection of pulse parameters were able to produce comparatively finer microstructure and lower dilution which could be beneficial to the corrosion properties of repaired parts [48].

2.1.8.2 Laser Cladding

Laser cladding [49] also offers control of spot size and energy intensity. In the laser cladding, there are several advantages relative to welds quality and manufacturer compared to e-beam energy sources such as simpler tooling requirements, no need of a vacuum chamber, and shorter cycle times which bring to cost advantages [49, 50]. In order to get high quality of clad layer, correct parameters are required while performing laser cladding process to obtain low dilution and great metallurgical bond between layers. Moreover, compared to arc welding, the laser clad samples show narrower dilution zone, less porosity, and better fusion bonding [51].

2.1.8.3 E-beam Cladding

Electron beam has also been used to improve performance of metals by means of surface treatments or cladding processes. To succeed in e-beam cladding, beam power density and duration, alloy composition, and alloy properties are all factors that needs to be considered and controlled. Due to its ability to achieve higher energy densities and smaller spot size than are associated with arcs, e-beam cladding offers more control over residual stress and lower dilution levels. Besides, in a recent investigation, it was shown that porosity and crack rate were reduced or there was no crack at all in some cases [52]. The same study also demonstrated that, by appropriate selection of the e-beam parameters, the chemical composition of cladded material was a homogenous throughout the melted zone (identical with that of the parent material). It also provides

53

superior properties, including low dilution, high wear and corrosion resistance and high hardness in high stainless steel and mild steel [53, 54].

2.1.8.4 Laser hot-wire cladding (LHWC)

Conventionally, in welding and cladding, the filler metal is at room temperature and it is termed "cold wire." One of the disadvantages of using cold wire is that the temperature difference between the filler metal and melt pool is large. When this occurs, it creates surface tension, buoyancy and electrostatic driven instabilities in the melt pool, which results in welding bead irregularities and less than optimum mechanical properties [55, 56]. Furthermore, the maximum deposition rate achievable with a cold wire is ultimately limited by thermal conduction from the melt pool through the radius of the wire. A pre-heated wire allows complete melting in a markedly shorter time.

A technical approach that minimizes these effects is the use of a "hot-wire." This technique is to use of AC or DC current flow to resistively pre-heat filler wire to very near to the melting temperature of the wire as it is fed into the melt pool. The chief advantage is that achievable deposition rates can be much higher with a hot wire. In addition, this can be used to reduce the peak temperature of the melt pool temperature at the same feed rate. In this case, the hot-wire offers additional degrees of freedom in metallurgical control relative to the cold-wire technique [57]. Notable is the reduced likelihood of gas porosity since pre-heating the wire drives off moisture and other absorbed species from the wire surface [58, 59].
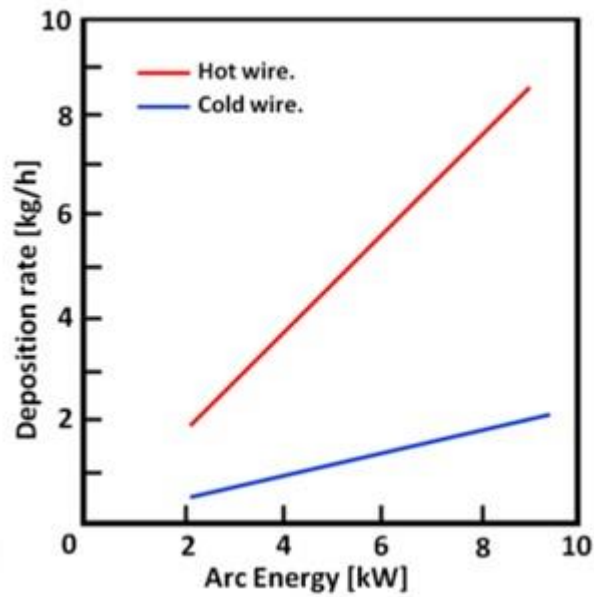
Figure 2.1.8.4.1: Deposition rates in hot wire and cold wire TIG [60]

In principle, a hot-wire can be used with GTAW, laser, or e-beam (GMAW is also used in a lab scale process at the present time). In practice, hot-wire appears to be restricted to GTAW and laser because of electromagnetic interference in others. The geometry is illustrated in Fig. 2.1.8.4.2. The resistive circuit is the same regardless of whether a laser or GTAW torch is used to create the melt pool.
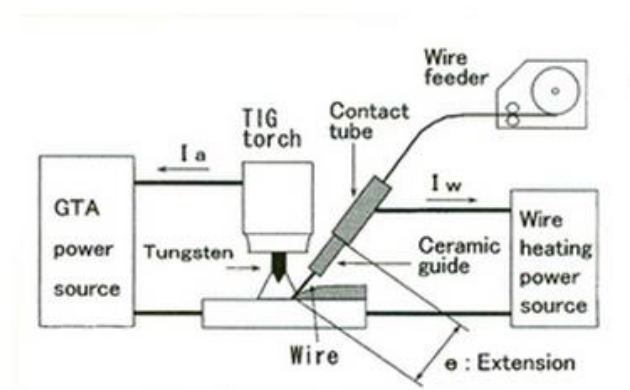
Figure 2.1.8.4.2: Graphical illustration of hot wire welding (GTAW is used in this illustration)

The hot wire gas tungsten arc welding process has been used in a wide range of welding, cladding, and also build-up methods. For instance, GMAW usually has a higher deposition rate than GTAW. However, with hot wire support, GTAW is able to provide a comparable deposition rate, which also remains superior quality than GMAW [61]. One of major problems using hot wire GTAW is the presence of an electric current in the feed wire and its associated magnetic field distorts the arc path (this is termed "magnetic arc blow" in the welding). It often moves against the welder, which makes it more difficult to control. To solve this problem, instead of using continuous heating and conventional arc, pulsed wire current (pulsed heating) and pulsed arc current have been applied and the wire current flows during the arc base period only with sufficient low arc current, the magnetic arc blow problem is reduced or eliminated. The current waveform of pulsed heating and pulsed arc is demonstrated below. The price for this is increased complexity and a restriction of the processing window.
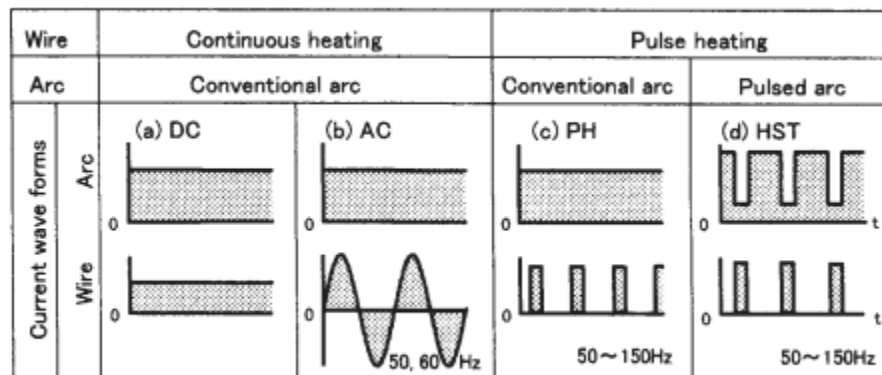
2 Current waveforms of hot wire TIG welding methods.

Figure 2.1.8.4.3 Current waveforms of hot wire TIG welding methods [62]

For laser hot-wire cladding (LHWC) process, this process uses two energy sources

which are laser and electric power source to resistively pre-heat filler wire during welding. These have the advantage of not interfering with each other as this arc-free process reduces distortions and increases the stability of weld beads [63]. For LHWC, with high deposition rate, a weld can achieve higher travel speeds and thinner clad layers, resulting in a higher productivity and efficiency. The LHWC process also provides low dilution from using low heat input of laser which helps reduce damage around the area being welded (HAZ) with low distortion [64] and support general metallurgical control such as the ability to obtain desired meta-stable phase [65]. In practice, the widest application of LHW process is cladding to protect surface of the workpiece rather than joining.

In terms of microstructure, wire feed rate and compositional chemistry of added alloy influence a variety of microstructures. The LHWC process offers a high degree of control over this. For instance, with hot wire filler metal, a fast wire feed rate provided acicular ferrite while a low wire feed rate resulted in a combination of bainite-martensite microstructure [65]. This characteristic of LHWC makes it well-suited to a work in which an intention is to repair worn or damaged parts. And, it is suggestive of a process that lends itself to metallurgical engineering.
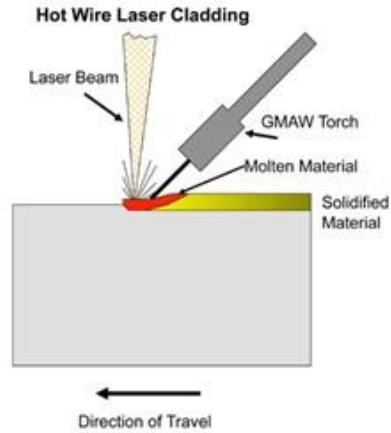
Figure 2.1.8.4.4: Position of weld equipment in Hot Wire Laser Cladding [63]

2.1.9 Build-up welding

Welding build-up can be seen as a multiple layer cladding. One thing that differentiates build-up welding and cladding is the relative roles of the substrate and added material. In cladding, the substrate and layer of added material generally differ in chemistry. The geometry and mechanical integrity are determined by the substrate. The role of the clad is the change only the surface of the part, for example to improve corrosion or wear behavior. In the case of build-up welding, the deposited materials is generally the same or similar to the substrate. A larger volume may be deposited relative to cladding.

The entire range of welding/cladding technologies can be applied to producing build-ups depending on typical engineering concerns of cost, equipment availability, property requirements, etc.

2.2 Freeform Welding

Freeform welding can be seen as a further generalization of build-ups. In this case the build-up process is controlled so that an arbitrary geometry is formed and when it is complete the build-up is separated from the original substrate (which is available for reuse or is discarded). Since it is not included in the final object, the material used for the substrate is therefore chosen for stability, availability, and low cost. (In some instances the part design is such that the substrate can be incorporated into the final object.) Some advantages of freeform welding are cost and time saving and ability to join a variety of materials with different compositions [66, 67].

Freeform welding has received a lot of attention in recent years, but in fact it can be documented that it is essentially as old as arc welding itself [68-70]. Initially, welding was used to join parts, Baker [69] realized that welding is not limited to the use of joining but also to create freeform shapes to use in daily life, such as receptacles, containers, or any other useful shapes [71]. Evidently, after the arc welding was discovered around 1900, it has been used to create freeform shapes since approximately 1920 by depositing fused metal into a metal base plate to form contiguous layer, superpose with new layers until the desired shape is complete [71, 72]. A timeline of welding history is provided below.

In the present, near-net-shape parts manufactured by freeform welding are being broadly investigated and are increasingly used in several industries. Many of the basic welding processes are exploited in freeform including: arc welding, electron beam

welding, laser welding, etc. Advantages relative to other additive manufacturing methods for metals are that freeform welding is not limited by part size (parts up to 19' x 4' x 4', or cylinders 8' dia. are made) [73], build rates are quicker, a broader array of materials, and lower cost feedstock. On the other hand, there are some of disadvantages for freeform welding as well. Support structure might be needed if the built part requires to be built in vertical or other abnormal positions [74-76]. In addition, there are existing technical problems relative to converting CAD file to be in a readily built format. Sometimes, the converted file is reduced in quality and details which cause incompleteness to the built part. One of these problems can be seen from the LHW case where manual programming for each layer is still needed to be created by welding operators and converting CAD file into program or coding for welding robot to understand still needs more future research and information. Moreover, a recurring theme in freeform welding experiments [77-79 and 80-83] demonstrates that the shape and dimensions of the weld bead are a main focus of freeform welding because they determine quality and desired properties of finished parts.

2.2.1 Timeline of welding history [68-70]

B.C. - Copper is thought to be the first metal to be welded followed by bronze, silver, gold, and iron in Egypt

- Small gold circular boxes were created pressure welding lap joints together

- The Egyptians and the eastern Mediterranean people started welding pieces of iron together

A.D. - Gold brazing was created and recorded for first time in welding history by Pliny

- The manuscript described mixing flux for silver brazing was written by monk Theophilus

1375 - Black smiths of the middle ages welded various types of iron tools by pounding hot metal until it bonded

- Zinc was discovered and forge welding was introduced by blacksmiths

14th - 17th

Centuries - Brazing a silver/copper alloy using a soldering process was introduced by Benventuto Cellini

- The word weld (originally well) has been started to use widely

18th Century - Blast furnaces were used a lot during this time in welding history

- Oxygen cutting process has been established by Lavoisier

19th Century

1800 - The electric arc is invented by Sir Humphrey Davy. The arc was created using 2 carbon electrodes   powered by a battery

1836 - The use of open flames (acetylene) was used to create more complicated tools and products by Edmund Davy

1850S - The electrical generating devices and arc lighting was used and become popular

1881 - Fusion welding was established by Auguste de Meritens where lead battery plates were welded with a carbon electrode

1890   - Carbon arc welding, metal electrode arc welding, and casting metal in molds were used and patented

20th Century

1900   - Several welding process have been developed during this period such as seam welding, spot welding, flash butt welding, and projection welding. Coated metal electrode was first discovered by Strohmenger that helps to obtain more arc stability by using a coating of lime

1919   - American welding society was conducted by Comfort Avery Adams tne a.ternating current was invented by CJ Holstag even though it became popular later in 1930 with the heavy-coated electrode

1920   - Automatic welding with the use of arc voltage and bare electrode wires was found by P.O. Nobel and used widely. It was often used for repairing motor shafts and crane wheels.

- Gas shielding techniques were introduced since several researches demonstrated that the atmosphere of oxygen and nitrogen caused brittle and porous to molten weld metal.

1929   - Lincoln Electric Company produced covered electrode rods and sold to the public

1930   - At the New York Navy Yard, Stud welding was developed and became popular in the construction and   shipbuilding industries

- Submerged arc welding process was used to build longitudinal seams in pipes, shipyards, and in ordnance factories

1940   - Gas tungsten arc welding (GTAW) was developed by C.L. Coffin to weld with non-oxidizing gas atmosphere (helium and argon gases). It was an ideal to weld aluminum, magnesium, and stainless

1948 - Gas shielded metal arc welding (GMAW) was created at Battelle Memorial Institute. It is similar to GTAW, however, replaced the tungsten electrode with a continuously fed electrode wire. It was for welding non-ferrous metals

1950 - CO_2 welding process was used because of economical reason and electrode wires of small diameter and refined power supplies were introduced to increase convenience to welders.

1960 -There were advancement of welding techniques being developed such as dual-shield (inside-outside electrode) welding, innershield, electroslag welding, plasma arc welding, and also electron beam welding which utilizes a focused beam of electrons as a heat source in a vacuum chamber.

1991 - Friction Stir welding introduced by TWI

1999 - 300 percent increase in flu penetration into a weld was developed by the Edison Institute

2000 - Magnetic pulse welding and diode laser welding were developed and improved

2008 - Development of laser-arc hybrid welding has been established

2013 - low-carbon steel and aluminum welding utilizing a lap joint and laser technology and gas metal arc welding-brazing have been established

This timeline of welding history was created by these generous references as follows:

1) Howard B. Cary. "Welding History". Modern Welding Technology. 4th edition (1998)
2) Hobart Institute of Welding Technology
3) Jeff Grill. The Harnessing of Heat: A Welding History. www.weldguru.com. (2002)

2.2.2 Freeform arc welding

Arc welding is one of the most common welding processes that have been applied to create parts from freeform welding. It provides ease of access, material availability, and reasonable operational and machine costs since it does not require complicated system compared to laser or e-beam welding [84]. It is therefore not surprising that it has been adapted to freeform as a low-cost method of producing near-net shape freeform fabrication. For instance, a method called "3D micro welding method" or "3DMW" which consists of GTAW, rapid prototyping, and self-propagating high temperature synthesis (SHS) [85-89] has been used with a variety of materials including refractory nickel alloys, stainless steel, Ti-Al alloys, Ti-Ni and Ti-Fe intermetallic alloys. The objective of these studies was to explore and optimize of welding parameters and also compare mechanical properties yielded between welded bead joint and the base substrate. The authors investigated that effect of arc current, bead height, bead width, and contact angle and demonstrated that they are important parameters which also affect mechanical properties of the welds.

From their experimental results, it was found that increasing arc current expands bead width but also decreases bead height and contact angle. This is because higher energy input and heat were used to create a weld. As far as several shapes, such as ring, arch, Arabic numeral, pyramidal, and helix shapes were created, the interface between adjacent beads were completely welded and no cracks were found [89].

In terms of the microstructure of titanium-based build-ups [86], needle-like dendritic microstructure of alpha phase titanium was found to develop during bead formation, as expected, due to the rapid cooling of the melt. Specifically in nickel alloy experiments, the authors found that the tensile strength, elongation, density and Vickers hardness are comparable to those of the commercial superalloy [90, 91].

Furthermore, in 2015, arc welding has been officially applied to use in 3D metal printer named the "Value Arc MA5000-S1 3D printer" [92]. This create a more affordable opportunity for more people because several current 3D metal printers that uses selective laser sintering (SLS), direct metal laser sintering (DMLS), or electron beam melting (EBM) technologies are comparatively more expensive. Even though, post-machining might be required for very detailed objects, material costs can be decreased by a factor of 10 and material availability is largely increased. Additionally, the arc welding printer also provides benefit of faster printing (up to 500 cubic centimeters per hour) compared to conventional machines (100-200 cubic centimeters per hour). This can be considered as a new and big step of arc welding in applying to fabricate potentially and commercially freeform objects.

Moreover, sometimes problem of freeform welding with substrate on base is parts are not easily removable and damage could occur during removing process. In the same year of 2015, since freeform arc welding still use a service of substrate, low-cost and no-cost substrate release mechanisms that is used to remove built parts from substrate with minimal energy were investigated and published according to (Haselhuhn et. al, 2015). From the same paper, it was reported that aluminum oxide, boron nitride, and titanium nitride coatings were discovered to be substrate release agents for removing aluminum parts from iron substrate [93]. The researcher claimed that this solution helps reduce overall costs of freeform 3D metal parts production and also minimize waste and concomitant environmental impacts because of reusable substrates [94]. This result certainly provides a method to remove freeform welding part without needs of specialized tooling [93].

2.2.3 Freeform e-beam welding

Electron beam freeform fabrication (EBF) has been used as a rapid metal deposition process to design, create, repair build-up parts using a layer-additive approach from a number of weldable alloys such as aluminum alloys, titanium alloys, nickel and ferrous based alloys [95]. The EBF process also employs a vacuum environment and wire feedstock as an additive filler metals. With e-beam process, the wire feedstock efficiency is close to 100 percent [96]. Additionally, it is found that grain morphologies are related to deposition rate. In other words, lowering deposition rate

from its maximum rate provides a finer detail of microstructure.

Interestingly, to investigate quality of weld, a technique of Near Infrared (NIR) Camera system is used in e-beam freeform process to record images of melt pool and solidification areas and also measure temperature of melt pool while producing a build-up [97]. This system supports an automated closed loop control (CLC) system that can provide feedback to welders and help adjust welding parameters such as beam power, wire feed rate, or wire feed height to optimize desired properties. As a result, cross section of parts created by CLC system yield a better result compared to manual control of welding parameters [100]. Thus, the NIR system certainly improves the quality of weld through investigation during the welding procedure.

However, there are some disadvantages of using e-beam as well such as, limitation of work chamber size, time delay with vacuum environment, high equipment cost and evaporation and spattering effect [101, 102]. To overcome some of these, laser beam welding, laser hot wire welding or other additive manufacturing processes are being developed. The literature of laser beam welding that uses to work on freeform welding will be discussed on the next session.

2.2.4 Freeform laser beam welding

Using laser in freeform welding can provide high deposition rate and precise focus spot as similar as using e-beam. The advantages of laser over e-beam are simpler tooling and lower capital equipment cost since no vacuum chamber is applied [100, 101]. For

laser additive technique, both powder-based and wire-based processes have been used. However, wire-based system is proved to provide better material quality, greater surface finish, higher deposition rate and also cleaner work environment [103, 104].

Sometimes, the problem of not getting the desired quality and accuracy of finished parts can occur. To improve the quality, a combination of additive and subtractive manufacturing techniques has been developed. This means each layer is deposited as a near net shape using laser and then finish machined in a CNC milling operation before depositing next layer [105]. This helps to develop parts that need complex shape and high accuracy. It also offers an economic way and high efficiency to save waste materials compared to conventional machining. A reliable mechanical connection between layers and desired mechanical properties are also found [106].

Moreover, to get more efficiency, a 3D scanning system along with iterative learning control system has been developed and applied to control consistency of deposition rate when surrounding disturbances occur. It allows capability of offsetting the wire feed rate on next deposition layer when the deviation of layer heights appeared. This creates a well balance of overall part instead of concaved surface. The results of using a combination of the iterative learning control and 3D scanning for automatic deposition are satisfactory and applicable to use in industry level [102].

2.2.5 Freeform metal-cored wire welding

Interestingly, in freeform welding application, there are some reports showing

that metal-cored wire has been used to produce parts also. In case of freeform

fabrication using e-beam, metal and also ceramic powders were incorporated via cored

wire sealed by sheath metal. Using metal-cored wire in the experiment as a feedstock,

the author found that it appears to be the most adapted solution since they can add

specific desired composition and place inside a rolled strip. However, there is also some

disadvantages in using metal cored wire. For example, during the process, when the

wire is heated and melted, the temperatures of the powder and the air trapped in the

wire get increased and eventually lead to porosity issue. Thus, after discovering this

problem, the researcher permitted longer time to heat filler metal resulting the trapped

air to evacuate [107, 108]. Additionally, they were able to achieve desired and

continuous composition variation which eventually brought them to desired mechanical

properties of the fabricated part [107, 108]. The illustration of trapped air during the

experiment is shown below.
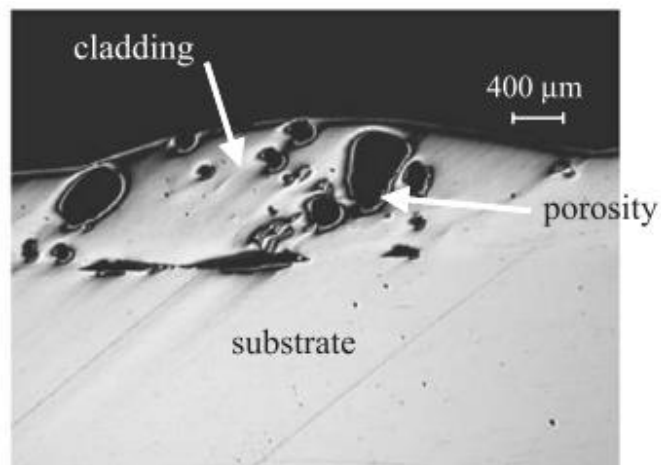
Figure 2.2.4.1 Air trapped inside the cladding layer at wire feed speed 19 inch/min and travel speed at 11 inch per min

Certainly, metal-cored wire also is one of the options for potential feedstock in freeform application using laser beam. Therefore, with metal-cored in freeform fabrication, desired composition variation in wire feedstock and good mechanical properties from those compositions are achievable. Nevertheless, porosity issues and higher consumables cost of metal-cored wire compared to solid wires are still need to be considered when choosing AM procedures.

2.3 Powder additive processes for metals

2.3.1 Powder: Laser beam

For powder-based feedstock, laser beam is widely applied to use in additive manufacturing world also. Main advantages of using laser beam as a heat source and powder feedstock over e-beam are simpler tooling (no need of vacuum chamber), shorter cycle times which lead to lower cost, and also lower training costs [108]. However, one issue that is usually found with powder-based technology is efficiency of powder absorptance during the process. A few research papers have demonstrated that powder absorptance is highly dependent on the type of wavelength of laser sources which are Nd-YAG and CO_2 utilized during irradiation in this case. Specifically, for metal powders (Ni-alloy), the absorptance reduces with increasing wavelength whereas the opposite behavior is gained from polymer materials (Epoxypolyether-based) [107-109]. Powder absorptance also affects to laser power used to sinter each layer of the powder

particles. Thus, with appropriate choice of laser wavelength and materials, one can save

energy used and operating costs from the powder-based laser beam process because

the greater the absorptance of a powder, the less the laser energy needed during the

process. The illustration below shows relationship between optical absorption and

wavelength.
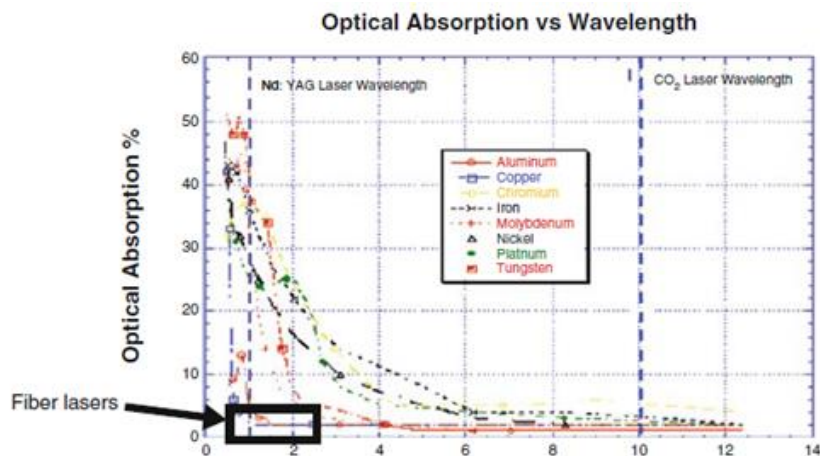
Figure 2.3.1.1 Optical Absorption % (absorptivity) of selected metals VS wavelength [110]

In terms of laser absorptance, it was reported that the absorptance of powders is

multiple times higher than that of dense metals since there are multiple reflection of the

guided wave propagation during the process [111]. Because of its characteristic that has

rough surface and voids between particles, a layer of powder now acts as a gray body to

emit radiation constantly at some wavelength. This circumstance brings to multiple

reflections which also influence to increase optical penetration depths to be larger than

in bulks or dense surfaces [112, 113]. As a result, absorptance in powder-based is higher

than that of dense metals. The figure below illustrates the multiple reflection effects.
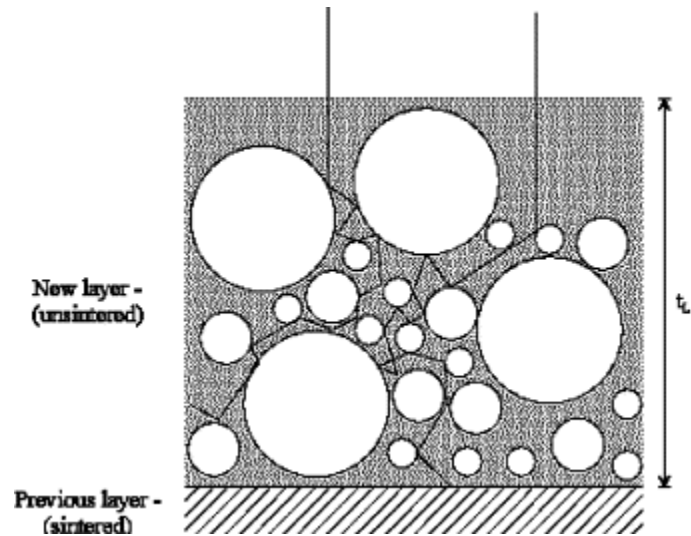
Figure 2.3.1.2 Optical penetration of a laser beam in a powder with the wave-guidance and multiple reflection effects [111]

Although, to use powder-based laser beam processes, such as selective laser sintering (SLS) or direct metal laser sintering (DMLS), finer details can be obtained compared to LHW process. However, some of disadvantages that is related to the built parts are soft, rough, and porous. Humidity control and well powder handling can improve the quality of process and the parts [126, 127]. Another interesting disadvantage is lower deposition rate is gained compared to LHW process although the parts can be more accurate in dimension and size [126, 127]. Furthermore, mechanical properties, such as hardness and tensile strength of built parts can be improve by post-processing. With SLS or DMLS system, it is difficult to accomplish the desired quality in appearance with the best mechanical properties. It generally requires post-processing which can influence a better mechanical properties like the part built from LHW process. From this report of Gibson, Ian and Dongping (1997), they found that coating is able to increase tensile strength and hardness of the test part surface. Also, higher dimensional

and surface accuracy can be gotten from performing surface finishing after the process [128, 129].

2.3.2 Powder: E-beam

Metal powders can also be sintered and used in AM to form a solid part or structure using an e-beam as the heat source. One of the processes that used e-beam source is "Electron Beam Melting" or EBM which is similar to Selective Laser Sintering (SLS) that uses laser as a heat source. With the EBM and pre-alloyed metal powders, a fully dense metal parts are successfully practical. With fully dense properties, this definitely help increase mechanical properties of the test part such as strength [130]. Compared to conventional processing techniques, e-beam with powders has shown capability to reduce lead time, be able to achieve in creating complicated geometries and also produce a high purity weld zone since all works are done inside a vacuum chamber. However, part quality is still an issue to be solved since it is quite challenging to examine each layer deposited without destructively testing the test parts [131]. For powder-based AM, after processing requirements are needed, such as removing excess powder, cleaning the built parts and hot isostatic pressing (HIP) to reduce porosity. Also, another trade-off is a longer and more expensive build time since the electron beam must be scanned across patterned areas pixel by pixel [132, 133].

2.3.3 Blown powder (directed energy deposition)

The process is developed for creating complex prototypes, tooling, and production parts directly from CAD solid models. Laser Engineered Net Shaping (LENS) or Laser Powder Forming can be seen as similar as laser hot wire process in terms of they both are used to repair or modify existing hardware/components. This technology works by using a metal powder injected into a molten pool created by a focused and high powered laser beam. The laser beam is then scanned on the substrate and the metal powder is deposited under the beam interaction zone to produce the desired cross-sectional geometry. The desired part is then deposited layer by layer sequentially until a three-dimensional desired component is complete.

Due to high travel speed, very fine grain structures can be gained from high cooling rate (up to 10,000 C/s). This leads mechanical properties of parts manufactured by LENS to be metallurgically equivalent to properties of wrought products [134]. Additionally, to prevent atmospheric contamination and obtain better control of properties, inert gas is also used to shield the melt pool and support adhesion between layers. Moreover, other benefits of using the LENS technology to create parts are large and fully dense metal parts, excellent metallurgical properties, three and four axis systems for complex part fabrication, ability to tailor deposition parameters such as speed and accuracy, and also wide variety of materials [135, 136, and 137].
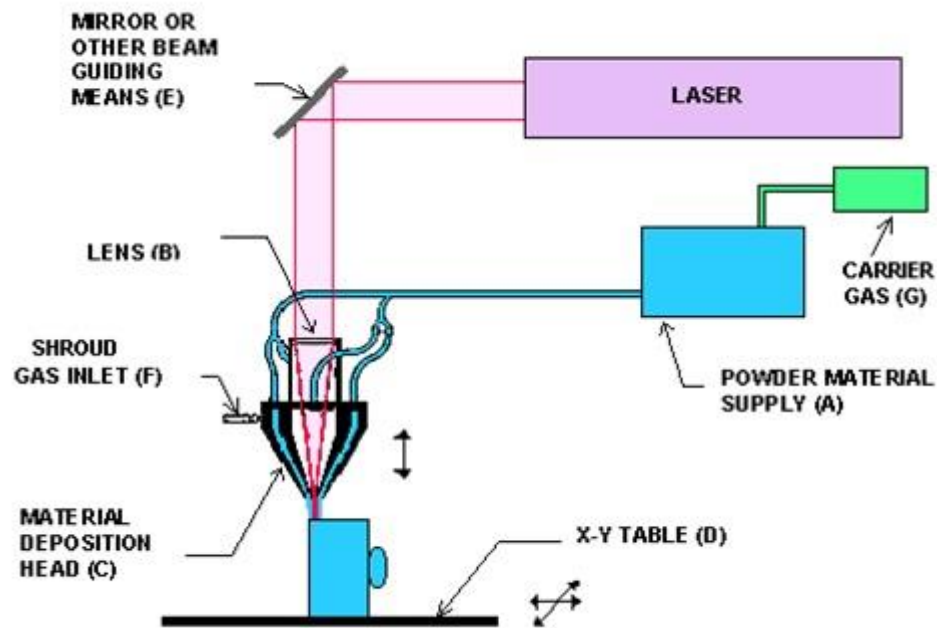
Figure 2.3.3.1: Schematic of LENS process [136]

3 Experimental Methodology

3.1 Experimental method

3.1.1 Material used in LHW process

In this project, there are two different metal materials systems used to conduct experiments with LHW process which are nickel-based superalloy 625 and Ti-6Al-4V. For nickel alloy 625, it is targeted at corrosion resistant properties for extension of life cycles of surfaces. For Ti-6Al-4V, its properties are high strength-to-weight ratio compared to iron-based alloys, high melting point (roughly at 1670 C or 3035 F), high corrosion resistance particularly oxidizing and chloride-containing process streams [138,

139] which are currently in use in several industries, such as oil and gas, automotive, and

aerospace industries. These two alloys systems were selected with an intention to assist

the extension of additive manufacturing (AM) to corrosion sensitive application areas

and demonstrate AM as an alternative to forgings of important lightweight structural

alloys. Since the LHW process has been investigated, improved, and commercially

applied by an Ohio-based manufacturing company (The Lincoln Electric Company). Thus,

feedstock of filler metal wire that is used in the LHW experiments is solid and tubular

wire of nickel alloy 625 and Ti-6Al-4V which are already available as a product of the

company. The usual wire size used in all experiments is 0.045 inch or 1.14 mm in

diameter.

Figure 3.1.1.1: welding wire in spools used in the experiment

Besides, in the LHW experiments, pre-existing substrate (base metal) with the

composition similar to the welding wire are always used during the process in case of Ti-

6Al-4V in order to ensure consistency in terms of mechanical properties of any

single/multiple layers or build-up created. All the substrates used are all provided by The

Lincoln Electric Company.

3.1.2 Experimental process

3.1.2.1 Procedure during the experiment

6-axis
welding
robot

Argon box

Figure 3.1.2.1.1 : FANUC welding robot that is used in creating test parts by LHW process

The development of the LHW process includes three aspects: chemistry control
(oxygen, nitrogen, alloying), metallurgical control (grain size/morphology), and shape
build-up. The laser system used in this research is YLS-15000 IPG Photonics Fiber Laser
and Fanuc welding robot is applied to the whole experiments. Particularly to laser
system, a Yb-fiber laser which contains wavelength at 1,070 nm is utilized. For the
welding supply machine, Power wave S500 model is utilized along with 0.045 inch (1.2
mm) Ti-6Al-4V and nickel alloy 625 wire-based feedstock. Every specimen was built on
the fixed table system and laid down to pre-existing substrate (base metal) which is the
same material as the wire to maintain consistency of desired properties. In this case,
robot is the one who moves to create parts.

Figure 3.1.2.1.2: (a) Ytterbium fiber laser system and (b) FANUC robot welding with the argon box and part built inside the box

[1]Initially, before starting welding, code programming was built to determine direction, position, size and character of specimen (single pass, multi-pass, or weave) by using an index program where the welder[1] always runs preliminary tests first. This procedure is to check completeness of what welder intended the robot to do. So, robot

---

[1] Max Radke and Michael Latessa are welding engineer at Lincoln Electric Automation and were creating all test parts using welding robot and equipment at Lincoln facilities.

arm is order to move only without feeding wire or generating a real weld. After the

preliminary tests, the welder then uses the robotic controller to turn power on to be

ready to weld. All specimens created in this research created by LHW process were

made by the Lincoln Electric Automation Division which are a part of this project[1].

During the process, wire which is resistively pre-heated by welding power

supply as a source (about 1 kW) is fed to targeted position of melt pool on the substrate

and radiated laser (about 6-8 kW) then heats and melts the fed wire. The melted wire

re-solidifies and cools down accordingly along the welding direction. To protect the melt

pool during the process, argon gas is used to cover melt pool in each pass. The

illustration of the LHW welding process is demonstrated below.
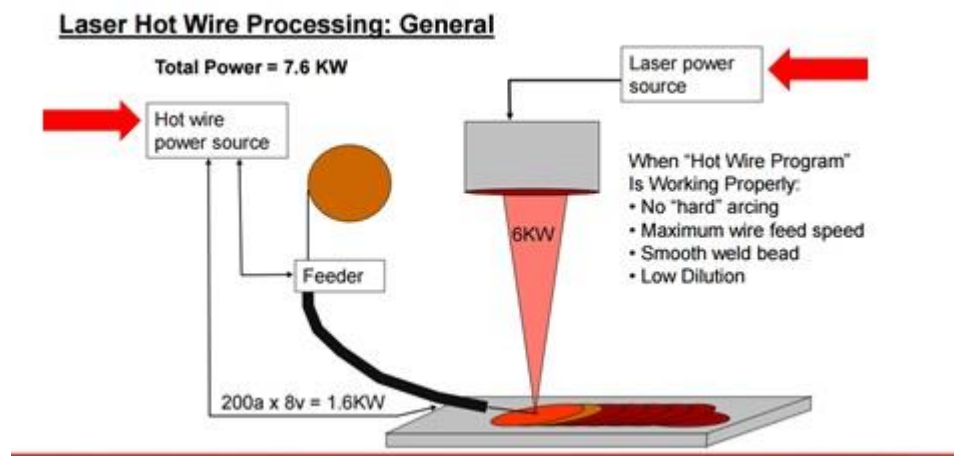
Figure 3.1.2.1.3: Schematic of the LHW welding process

The process described above is for a single pass. If multiple layers needed,

once each single layer is completed, next layer is programmed on top to get the vertical

build up for. However, with multiple beads laid down in a single plane, a specimen can

be created to get a bigger width and length. The illustration below demonstrates

multilayer build-up of Ti-6Al-4V.
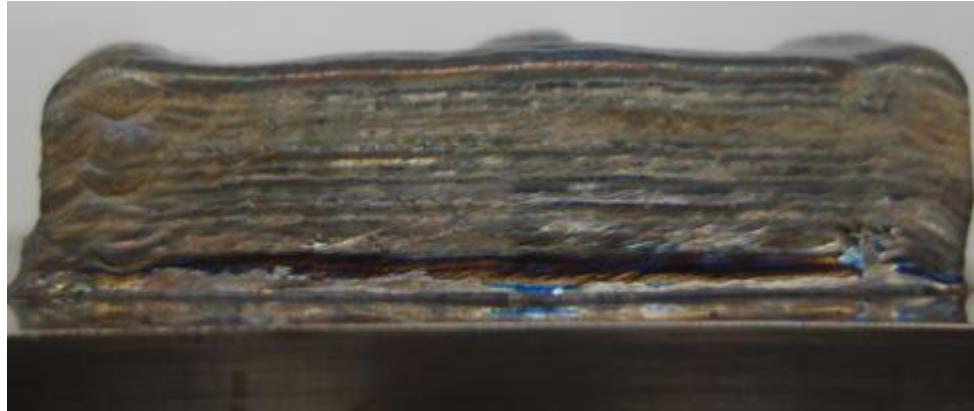
Figure 3.1.2.1.4: Multilayer build-up of TI-6Al-4V at height of approximate 1 inch showing each step of each layer

With two different material systems, different welding techniques and

parameters were used. Details will be discussed in section 3.1.3.

3.1.2.2 Procedure after the experiment

After creating specimens by using the LHW process, the specimens were then

prepared to investigate in terms of mechanical properties, chemistry analysis, and

microstructural inspection. Initially, the specimens were cross-sectional cut in both

perpendicular and parallel to the welding direction with an intention to perform

microstructural inspection as shown below.
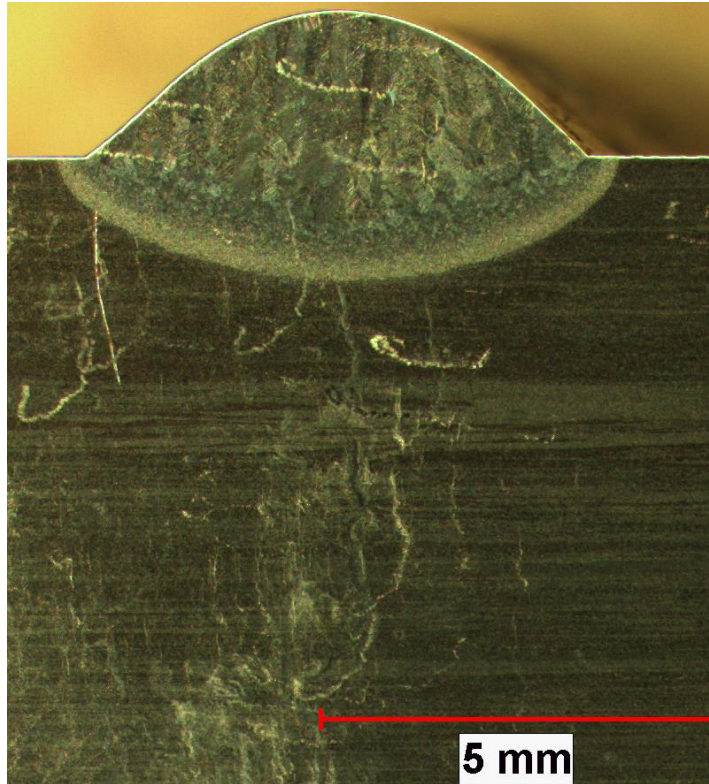
Figure 3.1.2.2.1: a cross-sectional cut of a Ti-6Al-4V single stringer bead created in shielding gas and argon box condition at travel speed = 10 inch/min, wire feed speed = 325 inch/min and laser power 5,500 kW

Before performing microstructural analysis, mounting of specimens were essential to permit those specimens to be handled conveniently and reduce possible damage after getting cut. Mounted specimens were then attached to specimen holder and were grounded with rotating discs of abrasive paper flushed with a coolant solution to decrease heat and debris on the specimens. This grinding process have many stages since the specimens usually need a number of different coarseness of the abrasive paper to grind and clean up. The coarseness of the paper can be determined by a number. This number means grains of silicon carbide per square inch. The higher the number is

shown, the finer of abrasive paper is.

Figure 3.1.2.2.2: A mounted specimen of the Ti-6Al-4V test part

So, the grinding process started from using a coarser paper (low number) and then move up to finer paper for next stage. Each stage helped clean up scratches from the previous stage [140]. After finishing the grinding process, the specimens were washed with soapy water followed by water and let to dry. This step prevented possible contamination occurred during the grinding process on the specimens' surface.

After the grinding process, to remove damage from the fine grinding and gain a highly reflective surface, the specimens required polishing process. In this polishing process, Ti-6Al-4V and nickel alloy 625 specimens need different methodology to accomplish. For Ti-Al-4V specimens, a 30% hydrogen peroxide in 0.05 micron colloid silica disc was utilized to polish. On the other hand, diamond suspension of 6, 3, and 1 micron polishing discs and oily lubricant were used to polish nickel alloy 625 specimens. While 6 micron polishing disc was used to remove the scratches from the finest grinding stage, 1 micron disc was used to create a smooth surface for the specimens.

Certainly, etching process was applied to both kind of specimens to reveal the microstructure through selective chemical attack. This process helped clean specimens'

82

surface also by removing thin deformed layer that might be occurred during the grinding and polishing processes. One thing in etching process that needs to be carefully taken care of is over-etching (too long etching). If a specimen was over-etched, small pits would be possible to present of the surface of specimen and prevent the main features to be seen. Re-grinding and re-polishing processes might be needed to solve over-etching.

After the etching process, the specimens were ready to be microstructurally investigated. Optical microscopy at The Lincoln Electric Company was used to document and evaluate the prepared specimens. Microstructure evaluation in details will be discussed in section 4 (Result) and section 5 (discussion).

3.1.3 LHW Welding procedure data, parameters, and characteristics

3.1.3.1 Ti-6Al-4V by LHW process

3.1.3.1.1 Variations in shielding

Particularly for experiments with Ti-6Al-4V material, oxidation during or immediately after deposition was a particular concern. The presence of air in contact with Ti-6Al-4V is know to produce a high enough concentration of interstitials or both oxygen and nitrogen to modify (and compromise) mechanical properties. Since oxidation negatively affects the final mechanical properties of the test part, a systematic series of protection schemes were designed, developed, and evaluated to ensure that oxygen and nitrogen level are limited to acceptable levels.

Firstly, trailing gas shielding is mounted at the head of welding gun. The

objective is to extend the time that the shielding gas, which is argon in this case, covers

the hot metal. That is, to allow the Ti-6Al-4V to cool to a low enough temperature to

suppress kinetics of oxidation before exposure to air.
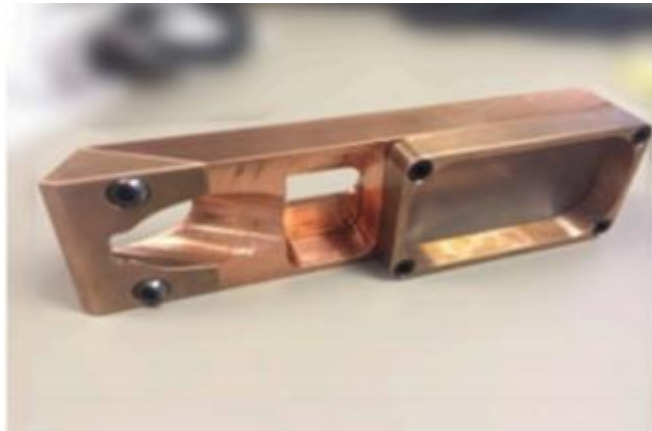
Figure 3.1.3.1.1.1: Trailing gas shielding used to protect contamination of Ti-6Al-4V during LHW process

However, chemistry results showed that the nitrogen and oxygen levels of first

few experiments exceeded the maximum levels allowed by the ASTM F136 standard for

Ti-6Al-4V (which correspond to oxygen and nitrogen contents <0.2% and <0.05%,

respectively). Thus, in order to reach the standard and cover argon gas atmosphere

around the area, argon chamber or argon box is created and used in latter experiments.

The size of the box is about 1.13 meter length x 0.60 meter width x 0.60 meter height

(44.5" length x 24" width x 24" height). The purpose is to fill up argon gas via argon

diffuser as shown below to protect molten weld pool from being contaminated from too

much oxygen and nitrogen contents. Generally, in the experiments, argon gas is filled at

60 cubic foot per hour (CFH) or 1.7 m^3/h for five minutes. With this argon box, since

argon is heavier than oxygen, it sinks in the bottom of the box surrounds near the part

and pushes oxygen up to the top during the process. This prevents the Ti-6Al-4V part to

pick up more oxygen content than not using argon box.

Figure 3.1.3.1.1.2 Argon chamber used to protect contamination for Ti-6Al-4V during the LHW process

In brief, trailing gas shielding and argon box are helpful in keeping oxygen and

nitrogen in the expected level and provide better mechanical properties compared to

normal condition (without both). Results in details will be elaborated in results section

(section 4).
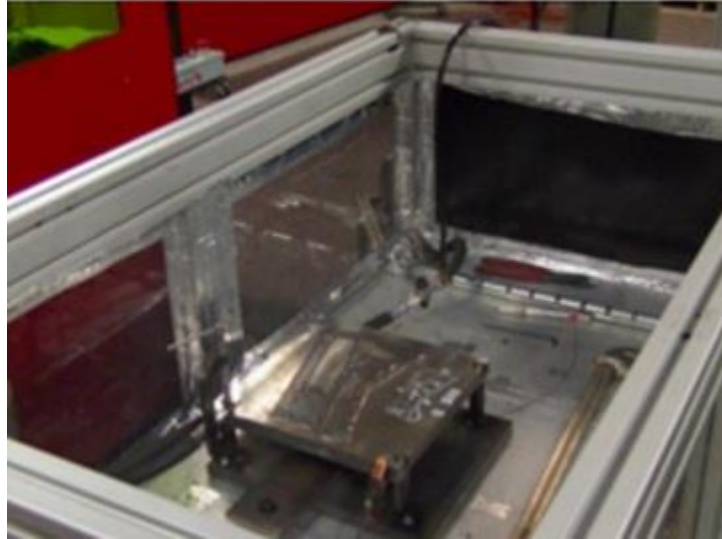
Figure 3.1.3.1.1.3: Sample in position in the argon box

3.1.3.1.2 Welding procedure data and parameters used

Initially, for Ti-6Al-4V material, single-layer of overlapping bead and weave

samples were produced with and without trailing gas shield.

Figure 3.1.3.1.2.1: Single-layer overlapping beads of Ti-6Al-4V with (right) and without (left) trailing gas

shield

While there are many weave patterns exist in real-world industry, the weave

pattern that was used in this entire research is the one being illustrated in the table

below. There was no argon chamber developed at the time of this experiment. For

metallurgical control, different power levels and travel speed were produced. The effect

of power-velocity (p-v) on grain size and morphology and chemistry analysis will be

discussed on section 4. Welding parameters used for stringer and weave beads of Ti-6Al-

4V material are tabulated as shown below.

Weld type	Parameter	Range
Stringer Weave	Hot wire power	0.75 – 1 kW
	Laser power	5-8 kW
	Travel speed	40 – 60 inch per minute
	Wire feed speed	300 -370 inch per minute

Table 3.1.3.1.2.1: A table showing welding parameters and ranges used for stringer and weave beads

Secondly, six-layer pillar or build-up were constructed which was intended to

perform initial assessment of grain size in multi-layer build-ups. Results will be explained

on section 4 as well.
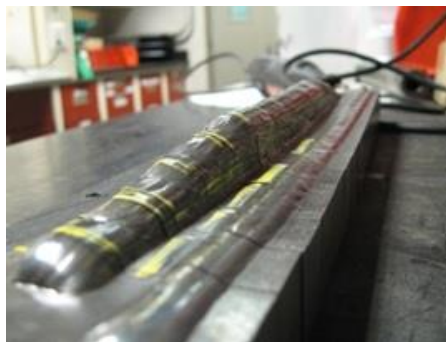
Fig 3.1.3.1.2.2: Six-layer pillar (build-up) constructed by using the LHW process

Other several shapes were also fabricated as can be seen below with different objectives. While a Ti-6Al-4V massive part was constructed to perform non-destructive evaluation (NDE), "E" and "Pi" shapes and three-layer titanium pads were built to investigate N_2 and O_2 measurements, grain structure analysis and parameter optimization. Welding parameters used were similar to those of stringer and weave beads.
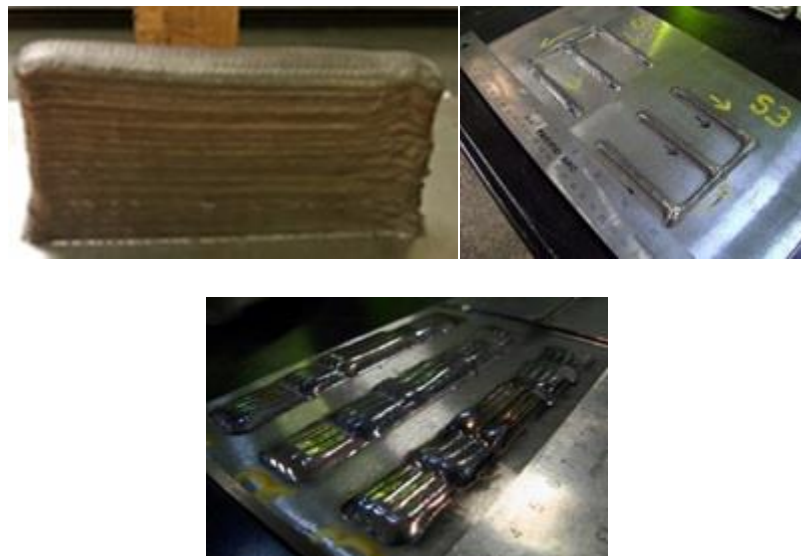
Figure 3.1.3.1.2.3: Specimens of LHW welding specimens: Left: Ti-6Al-4V massive part (nominally 50mm x 150mm x 25 mm from which NDE and mechanical property specimens were taken; Center: Demonstration of intersecting features using "E" and "pi" figures; Right: Three-layer titanium pads used for N_2 and O_2 measurements and parameter optimization

Particularly to "E" and "Pi" shapes, the build sequence is schematically illustrated in figure below. This shape includes a start at the base of a pre-existing bead and an end at the base of another. The block Pi in figure below requires a start and a separate end against a pre-existing bead. Completion of this shape requires both drag and push

motion.
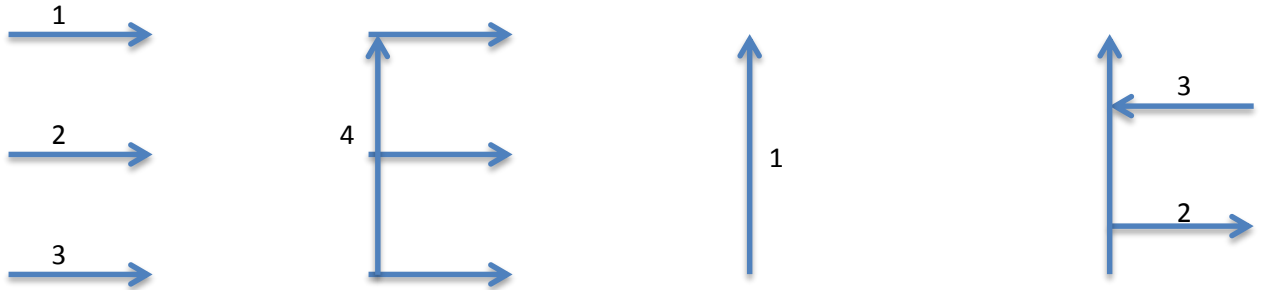
Figure 3.1.3.1.2.4 (Left) Paths executed in a drag mode (number: 1, 2, 3, and 4) by the robot to create the block E in four passes and (Right) Paths executed in a drag mode (number: 1 & 2) followed by a single push mode (number: 3) pass to create the block pi

Apart from stringer beads, weave beads, multi-layers build-up, the LHW process was also used to experiment in building a test part equipped with several shapes and features (such as Pi and E shape) to preliminarily investigate how complicated the LHW process can be utilized. A CAD file screenshot of the test part is illustrated below. With this CAD file, two test parts were created using the LHW and direct metal laser sintering (DMLS) methodology which is a laser/powder based additive manufacturing process. Thus, these two similar CAD file parts were benchmarked and compared in terms of energy usage, possible defects, microstructural characterization, and mechanical properties. These results can be found in the Section 4 of the results section.
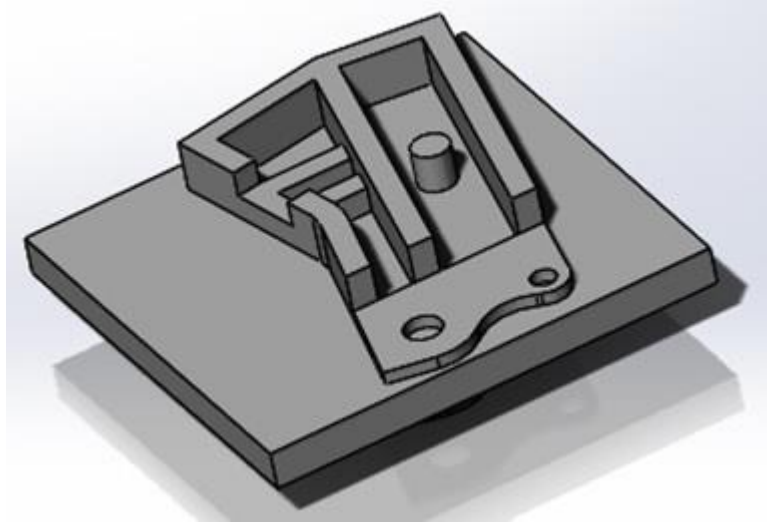
Figure 3.1.3.1.2.5 CAD file screenshot of a test part with shapes and features

For welding parameters used in creating the test part with LHW process, they are tabulated and shown below.

	Imperial Units			
	Laser Power (kW)	Wire Feed Speed (ipm)	Wire Power (kW)	Travel Speed (ipm)
Layer 1	6000	325	0.75	60
Layer 2-17	6000	325	0.83	60

	Metric Units			
	Laser Power (kW)	Wire Feed Speed (m/min)	Wire Power (kW)	Travel Speed (m/min)
Layer 1	6000	8.3	0.75	1.5
Layer 2-17	6000	8.3	0.83	1.5

Table 3.1.3.1.2.2: Welding parameters for the test part with several shapes

Particularly in building this test part, to stacking up multiple layers at the same position, a relative flat layer is needed. Thus, the test part can be a near-net-shape part which requires machining. With that objective, a technique of laser start/end as a function of wire start/end manipulation was used. If the wire and the laser started and ended at the same time, areas of taller deposition would result and make the entire part unbalanced. With multiple layers deposited over time, the part would tend to be a

concave shape instead of single-straight plane for the whole part. This would make it harder to program next layer of weld since the deposited previous multiple layers could cause collisions between the part and the oriented welding torch.

Figure 3.1.3.1.2.6: the test part showing after the first layer of weld pass

So, a solution to tackle with this problem is to start the laser beam first by letting it travel roughly 0.25 inch (6mm) and then start the wire. This reduced the possibility of concave-shaped build-up by permitting the filler wire to flow at the beginning of each pass. A similar procedure was used at the end of each weld where the wire would stop approximately 0.25 in (6 mm) before the end.

Moreover, in order to eliminate the wire sticking in the solidified weld puddle, the robot was programmed to lift slightly as it approached the end point. This is the cause of the wider section at the end of each weld. As the robot reached the end of each pass, the laser beam would be turned off. Also, the test part was created on both sides of the Ti-6Al-4V with 17 layers being deposited on each side which were identified as "A" and "B" sides.

Figure 3.1.3.1.2.7: 17 layers on "A" side were deposited

3.1.3.2 Nickel alloy 625 by LHW process

With nickel alloy 625 material overlay, the objective is to investigate this particular material using LHW process for surface modification and corrosion protection for substrates. In the experiments, both stringer (single direct bead) and weave (wider weld from side to side along the weld joint) beads were created on nickel alloy 625 substrate for characterization in terms of dilution, bead profile, and microstructure. A pillar or a build-up of multiple layers were built to assess heterogeneity

A range of welding parameters used in experimenting nickel alloy 625 by LHW

process are shown below.

Figure 3.1.3.2.2: Welding parameters used with Nickel alloy 625 during the LHW process

Besides, in as-deposited specimens, the dilution or a portion of melt-back filler

metal into substrate plays an important role in determining the mechanical properties of

the weld [141]. To be able to control desired dilution, welding parameters are very

important to be controlled. Definitely, a low dilution is highly desirable in this research

since cladding process needs the final deposit composition to be close to the corrosion

resistant filler metal. One can find dilution of a weld bead by using the formula below

where A_{fm} = area of filler metal deposited and A_m = area of melt-back metal. Results of

dilution in details are discussed in results section (Section 4).

$$\text{Dilution} = A_{fm}/(A_m + A_{fm})$$

Figure 3.1.3.2.3: Graphical representation of dilution calculation in a weld bead

Apart from stringer and weave beads, nickel alloy 625 pillars were deposited for fracture testing under corrosive environment. The notch was orientated along the height direction of the pillar, as through-the-thickness cracking resistance was of interest for nickel alloy overlays as ca be seen below. The specimens was investigated with x-ray before being sent out for machining and testing.
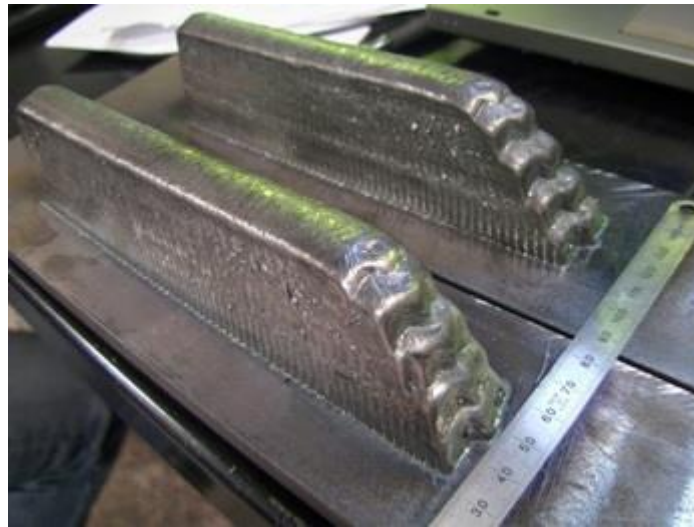
Figure 3.1.3.2.4 Nickel 625 alloy pillars for fracture toughness tests under corrosive environment. This staircased shape make it easier to be analyzed in each layer deposited

3.2 Analytical method

3.2.1 Energy analysis

3.2.1.1 Ti-6Al-4V by LHW process

A definition of energy efficiency is to use less energy to accomplish the same process. For high throughput functional material deposition using a laser hot-wire (LHW) process project, one of important tasks to complete is to calculate energy usage of the process to determine how much of the energy is used to create a part and how much is lost. These values of energy usage then can be used to calculate energy efficiency and also to double check and compare with the absorptivity of titanium being radiated by the laser power sources.

The energy usage was estimated in both materials. The schematic of LHW process is illustrated below identifying energy inputs and energy losses in the LHW system.
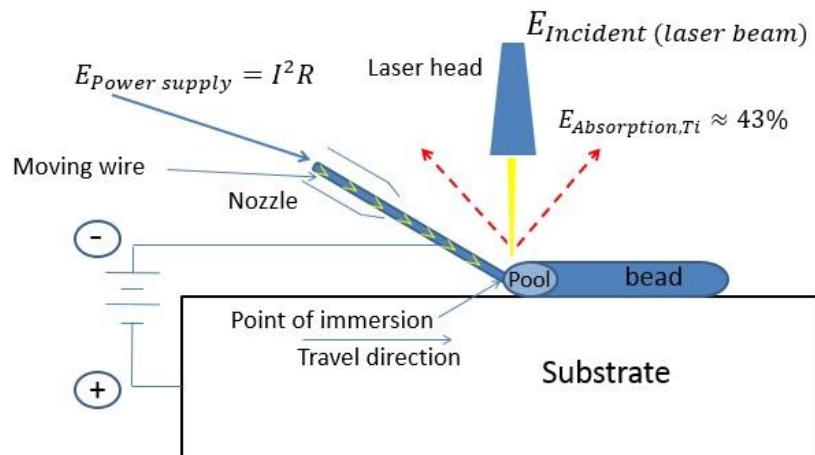
Figure 3.2.1.1.1: Schematic showing energy input and loss in LHW process

Therefore, the first step is to consider how the energy is partitioned in laser hot wire (LHW) process. In LHW processing, the total energy delivered to the workpiece is the sum of

- The resistive heating of the feedwire through the DC circuit ($E_{Power\ supply}$),

- The laser flux ($E_{incident\ of\ laser\ beam}$)

The current flow in the feedwire is assumed to be fully converted to heat, while only a portion of is absorbed, in fact, the majority is reflected. The degree of reflection and absorption depends both on laser wavelength and the emissivity of the metal which is titanium in this case.

For the case of titanium illuminated by an ytterbium (Yb) fiber laser, it is found from literature results that for Nd-YAG laser work as the respective wavelengths are similar (1,070 and 1,064 nm, respectively). Xie & A. Kar (1999) report that the reflectivity of Nd-YAG on solid titanium is 87.0%, but drops to 56.7% for the liquid at the melting point [142]. Therefore, we assume that 43.3% of the laser energy is absorbed by the melt pool in LHW process.

Specifically, this analysis begins looking at the following case (usual welding parameters used in the experiments):

- Titanium bead on titanium plate

- 1 kW in DC circuit

- 8 kW laser power

The energy delivered to the metal in the workpiece is therefore,

$$P_{wp} = 1 + (0.433 \times 8) = 4.46 \ (kW)$$

This fundamentally means, in order to achieve a power of 4.46 kW, a total 9 kW (1 kW in DC circuit and 6 kW laser power) is required in the LHW process.

Now, attention turns to considering how this heat input above is partitioned. Initially, the observable changes in the material are separated into 3 sections: bead, dilution and heat-affected zone (HAZ) as our observable changes in the material.

(1) Bead: There is the added mass of the bead (i.e., the melted and resolidified feedwire).

(2) Dilution: there is the region of the substrate that has been melted and resolidified – for which we adopt the term the dilution region.

(3) HAZ: there is a visibly changed heat-affected zone, or HAZ.
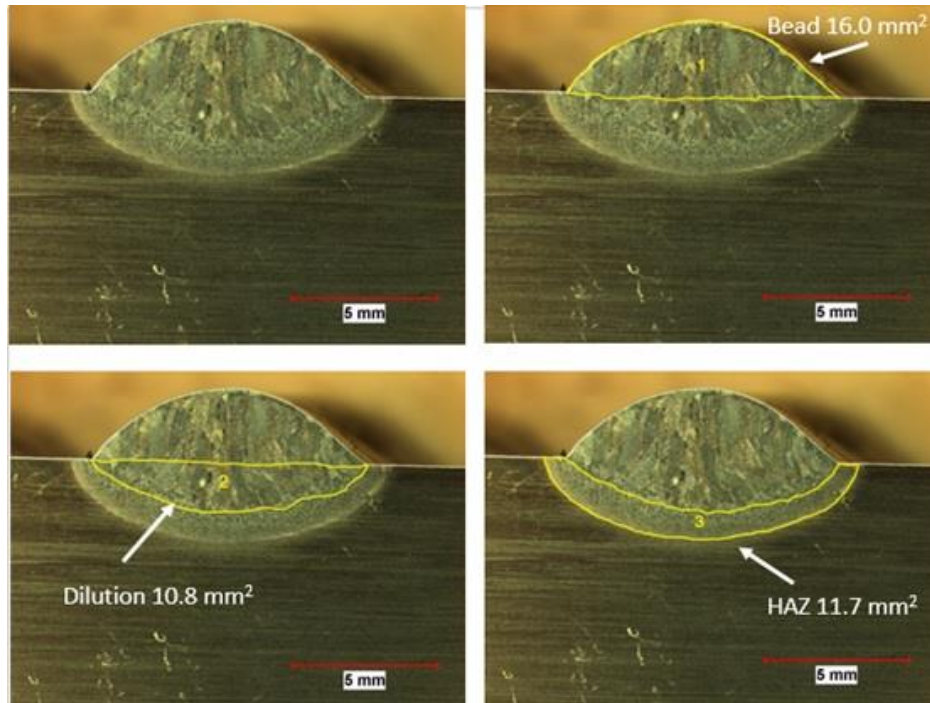
Figure 3.2.1.1.2: Observable changes in our titanium sample: (1) bead, (2) dilution, and (3) Heat-Affected Zone

The total energy used to produce these respective changes in state:

$$\Delta E_{used} = \Delta E_{bead} + \Delta E_{dilution} + \Delta E_{HAZ}$$

With this equation, the respective temperature changes including specific enthalpy changes needs to be calculated and summed to be the total ΔE_{used}. Additionally, in order to get total energy, mass of a substance which passes per unit of time to become bead, dilution, and HAZ needs to be identified first. This mass can be called "mass flow rate" or "mass affected per unit time". Thus, the "mass affected per unit time" for the bead is simply the deposition rate. For the associated dilution, and HAZ, it is the cross sectional area multiplied by the travel speed and density.

Furthermore, after the temperature reaches melting temperature, the assumption is made that the peak temperature of the bead and the dilution region is the same and the 150°C superheat (temperature changes that are above melting temperature) is reasonably assumed to use in the calculation.

Specifically in heat-affected zone (HAZ), referring to Yang et al. (2000), the assumption is made that the low temperature side of the HAZ is 995°C and the top side is, of course, the melting point $1,650^\circ$C. So, the approximation of the average temperature which is $1,320^\circ$C, can be used for the whole HAZ volume.

Moreover, to find ΔH_{SHL} (the energy to create melted and superheated metal), integration the heat capacity, C_p, from room temperature to the onset of melting, addition the effective latent heat of fusion for the alloy over the melting range, and integration of the heat capacity of the liquid for the superheat (Poulsen 2000) are formulated to the equation. Specifically for titanium, the enthalpy for the alpha to beta phase transformation is also included. According to (Mills 2002), beta-transus or temperature that TI-6Al-4V changes from alpha phase to beta phase is approximately 995 +/- 15 C and approximate temperature that Ti-6Al-4V goes over its melting point (T_{liq}) is 1,650 C. Also, Density of Ti-6Al-4V is 4,420 kg/m^3.

Physical Properties	Value	Reference
Liquidus temperature (K)	1923.0	[Mills, 2002]
Solidus temperature (K)	1877.0	[Boyer et al., 1994]
Evaporation temperature (K)	3533.0	[Boyer et al., 1994]
Solid specific heat ($J\,kg^{-1}\,K^{-1}$)	$\begin{cases} 483.04 + 0.215T & T \le 1268K \\ 412.7 + 0.1801T & 1268 < T \le 1923 \end{cases}$	[Mills, 2002]
Liquid specific heat ($J\,kg^{-1}\,K^{-1}$)	831.0	[Mills, 2002]

Table 3.2.1.1.1 Material properties for Ti-6Al-4V [143]
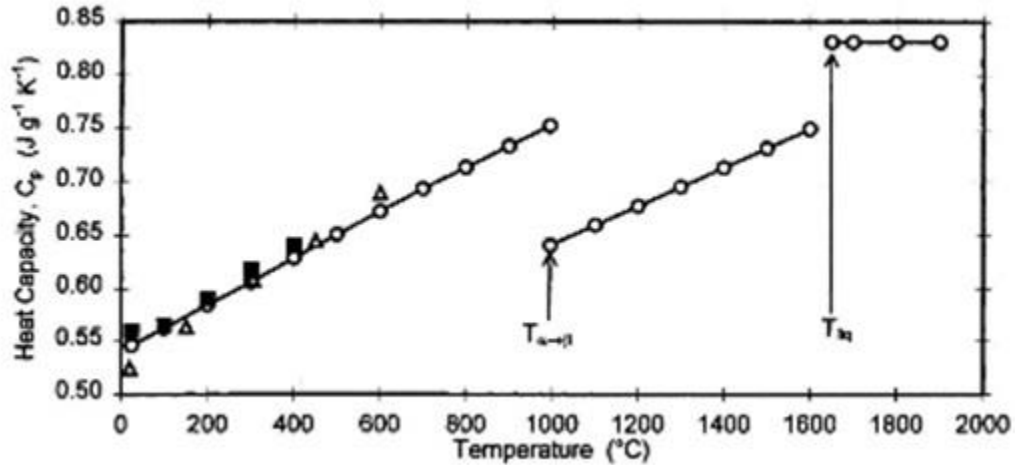
Figure 3.2.1.1.3 Heat capacity of Ti-6Al-4V as a function of temperature [143]

Besides, according to Cezairliyan and McClure (2002), the value of the enthalpy

of fusion or ΔH^{fus} is equivalent to 282 J/g and the enthalpy of transformation from beta

to alpha phase (ΔH_{950}^{tran}) is 48 +/- 10 J/g. Therefore, with all above explanation, the

equation is created as can be seen below.

$$\Delta H = \int_{298}^{1268} C_p^\alpha dT + \Delta H_{1268}^{trans} + \int_{1268}^{1923} C_p^\beta dT + \Delta H_{1923}^\beta + \int_{1923}^{Superheat} C_p^{liq} dT$$

All temperatures in the following having been converted from Celsius (C) degree

to Kelvins (K). To be consistent with the manner in which the effective heat of fusion

was collected by McClure and A. Cezairliyan, an assumption made here is that melting

occurs at a fixed temperature of 1923 K rather than across the observed 40 K interval

between the solidus and the liquidus. Also, the last integration associated with the

liquid requires the superheat to be measured. Substituting in the values from the

tabulated data and integrating gives:

100

$$\Delta H = 632,800 + 48,000 + 458,500 + 286,000 + 166,200$$
$$= 1,591,500 \text{ J/g} \approx 1,600 \text{ kJ/kg}$$

This compares very well with the graphical representation of enthalpy change given Mills (2002) as can be seen below.
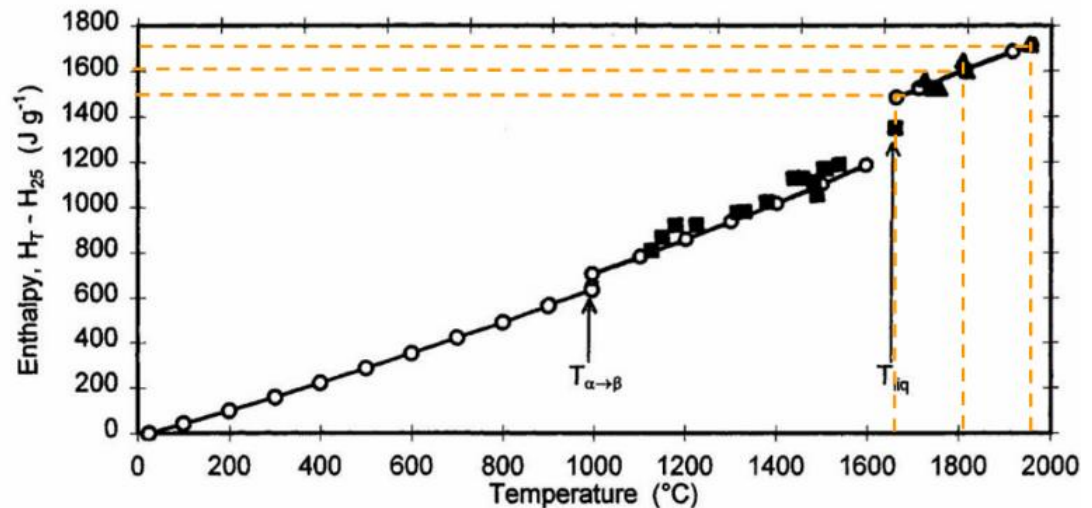
Figure 3.2.1.1.4 Ti-6Al-4V graphical representation of enthalpy change as a function of temperature (Mills 2002)

This graphical representation is particularly useful in assessing the impact of different degrees of superheat on the total energy required. The answer is seen to be only weakly sensitive to superheat. That is, at the melting point the change in enthalpy is roughly 1,400 kJ/kg and with 300 C superheat it is around 1,800 kJ/kg. Approximately 12.5% changes from 1,600 J/g to 1,800 J/g

For HAZ, considering from this graph, ΔH_{HAZ}^{eff} or the average of enthalpy would be assumed from average of temperature between phase transformation change temperature (995 C) and melting temperature (1650 C) which is marked in red.
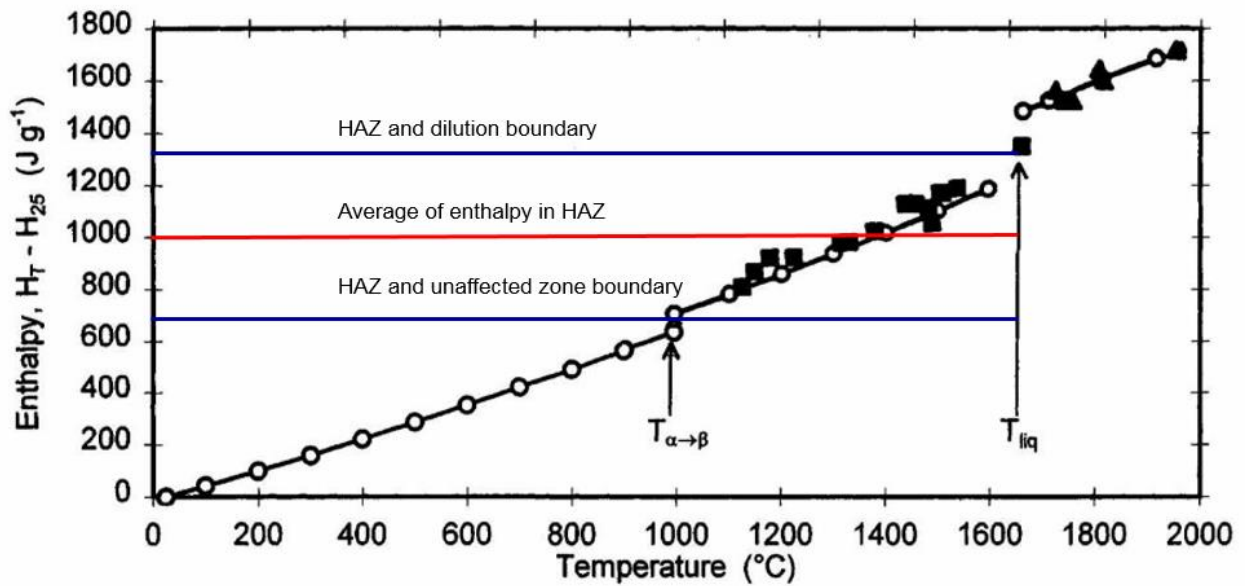
Figure 3.2.1.1.5 Ti-6Al-4V graphical representation of enthalpy change as a function of temperature showing the average of enthalpy at roughly 900 kJ/kg as indicated in red line [177]

So, the average of enthalpy is about = $\Delta H_{HAZ}^{eff} \approx 1,000 \frac{kJ}{kg}$. After obtaining all of these values, one will be able to determine energy efficiency used with LHW process for Ti-6Al-4V. The result of this energy evaluation will be elaborated in section 4 and will be discussed in section 5.

3.2.1.2 Nickel alloy 625 by LHW process

For the case of nickel alloy 625 illuminated by an Yb-fiber laser, A literature results for Nd-YAG laser work as the respective wavelengths are similar (1,070 and 1,064 nm respectively). Xie & A. Kar (1999) report that the reflectivity of Nd-YAG on solid nickel is 77.0%, but drops to 67.4% for the liquid at the melting point [144]. Therefore, we assume that 32.6% of the laser energy is absorbed by the melt pool in LHW.

Specifically, we begin looking at the following case:

- Nickel bead on nickel plate

- 1 kW in DC circuit

- 8 kW laser power

The energy delivered to the metal in the workpiece is therefore,

$$P_{wp} = 1 + (0.326 \times 8) = 3.6 \ (kw)$$

Bead 14.2 mm²

HAZ 5.0 mm²

Dilution 3.0 mm²
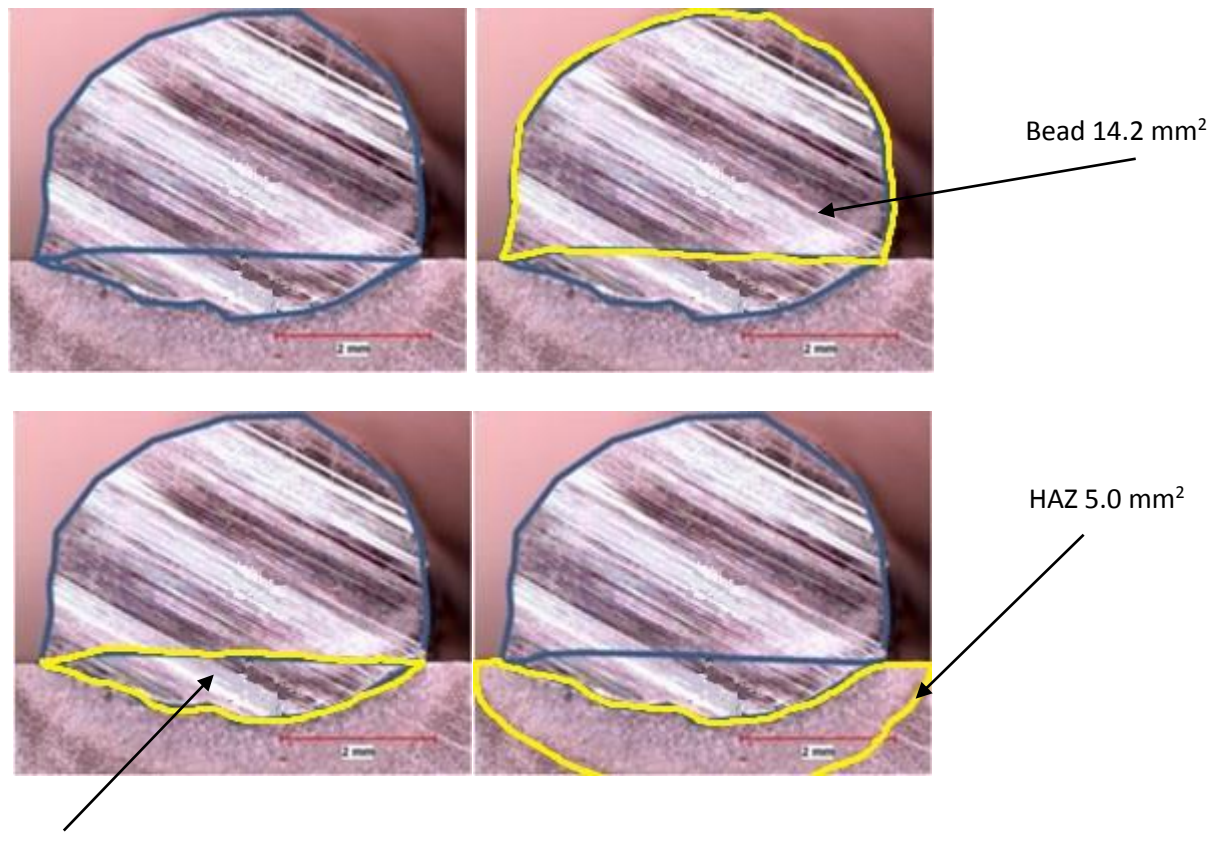
Figure 3.2.1.2.1: Observable changes in our nickel alloy 625 sample

The total energy used to produce these respective changes in state:

$$\Delta E_{used} = \Delta E_{bead} + \Delta E_{dilution} + \Delta E_{HAZ}$$

To find ΔH_{SHL} (the energy to create melted and superheated metal), the equation is similar to the one that is used in Ti-6Al-4V case. However, the nickel case is simpler than the titanium in that the material has no phase transformation change up to the melting point. As is standard practice, tabulated data was fit to get an expression of C_p as a function of temperature for solid 625 alloy as can be seen below.

Chemistry composition of nickel alloy 625

Nickel	58.0 min
Chromium	20.0-23.0
Iron	5.0 max
Molybdenum	8.0-10.0
Niobium	3.15-4.15
Carbon	0.10 max
Manganese	0.50 max
Silicon	0.50 max
Phosphorus	0.015 max
Sulfur	0.015 max
Aluminum	0.4 max
Titanium	0.4 max
Cobalt	1.0 max

Temperature (F)	Temperature (C)	Specific heat (J/kg C)
0	-18	402
70	21	410
200	93	427
400	204	456
600	316	481
800	427	511
1000	538	536
1200	649	565
1400	760	590
1600	871	620
1800	982	645
2000	1093	670

Table 3.2.1.2.1: (Top) Table showing chemistry composition of nickel alloy 625 and (Bottom) Table demonstrating specific heat values at different temperature [122] Melting range for Nickel is 2350-2460 F or 1290-1350 C

$C_p= 0.2437*T(K) + 338.94$
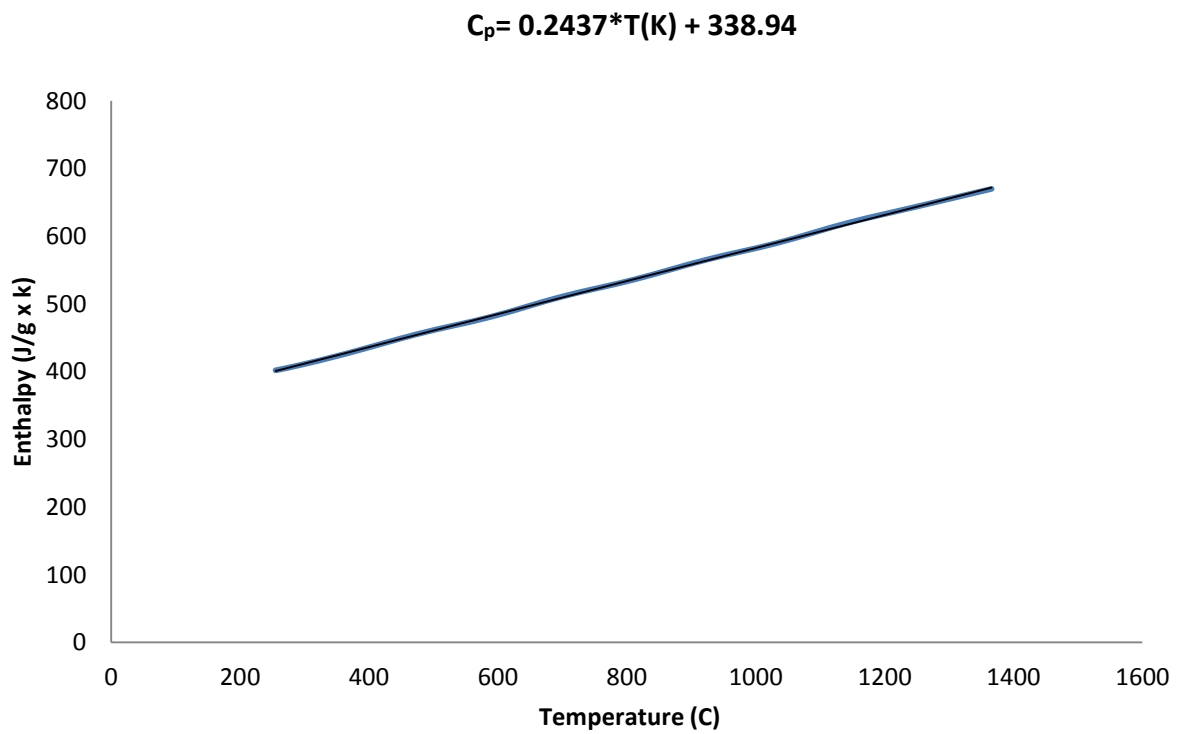
Fig 3.2.1.2.2: Heat capacity at different temperatures for nickel-based super-alloy nickel alloy 625 [122]

Also, an effective latent heat of fusion for the alloy was located as indicated below.

Absorptivity[a]	$A = 0.5$
Specific heat	$C_p = 410 \text{ J kg}^{-1} \text{K}^{-1}$
Thermal conductivity	$k = 9.8 \text{ W m}^{-1} \text{K}^{-1}$
Latent heat of fusion per unit volume[b]	$L = 1.726 \times 10^9 \text{ J m}^{-3}$
Initial temperature	$T_0 = 300 \text{ K}$
Melting temperature	$T_m = 1623 \text{ K}$
Density	$\rho = 8440 \text{ kg m}^{-3}$

Table 3.2.1.2.2: Latent heat of fusion, density, and other properties for nickel alloy 625 [145]

One can calculate the average latent heat of fusion by performing a division of latent heat of fusion per unit volume over the density as follows:

$$\Delta H_f = 1.726 \times 10^9 / 8,440 = 2.045 \times 10^5 \text{ J/kg}$$

However, it proved to be necessary to use a rule of mixtures for the specific heat of the melt. (The calculation shows there property is expected to be reliably estimated.)

Element	C_p (J/mol x K)
Cr	39.33
Fe	41.8
Ni	38.49
Nb	41.8
Mo	34.3

Table 3.2.1.2.3: List values of constant-pressure heat capacity for various liquid elements [146]

According to [146], the authors report that "the values of the heat capacities of liquid alloys have often been estimated by proportional addition of the heat capacities of the constituent elements, ie. The Neumann-Kopp law". Therefore, to apply with this theory, one can approximately estimate C_p as follows:

C$_p$ (625) = 38.33 J/mol-K =   0.643 kJ/kg-K

Then, the average enthalpy for nickel alloy 625 can be calculated by using pre-defined

values as indicated below:

$$\Delta H = \left[\frac{0.2437 \cdot T^2}{2} + \ 338.94 \cdot T\right]_{298}^{1623} + 2.045 \times 10^5 + [643 \cdot T]_{1623}^{1823}$$

ΔH = [871,068 − 111,824] + 204,500 + [1,172,189 − 1,043,589]

ΔH = 759,244 + 204,500 + 128,600 = 1,092,344

ΔH = 1,092,344 J/kg ≈ 1,100 kJ/kg

This means, in order to melt the nickel, it requires approximately 1,100 J/g or

kJ/kg with the assumed superheat of 200 C.
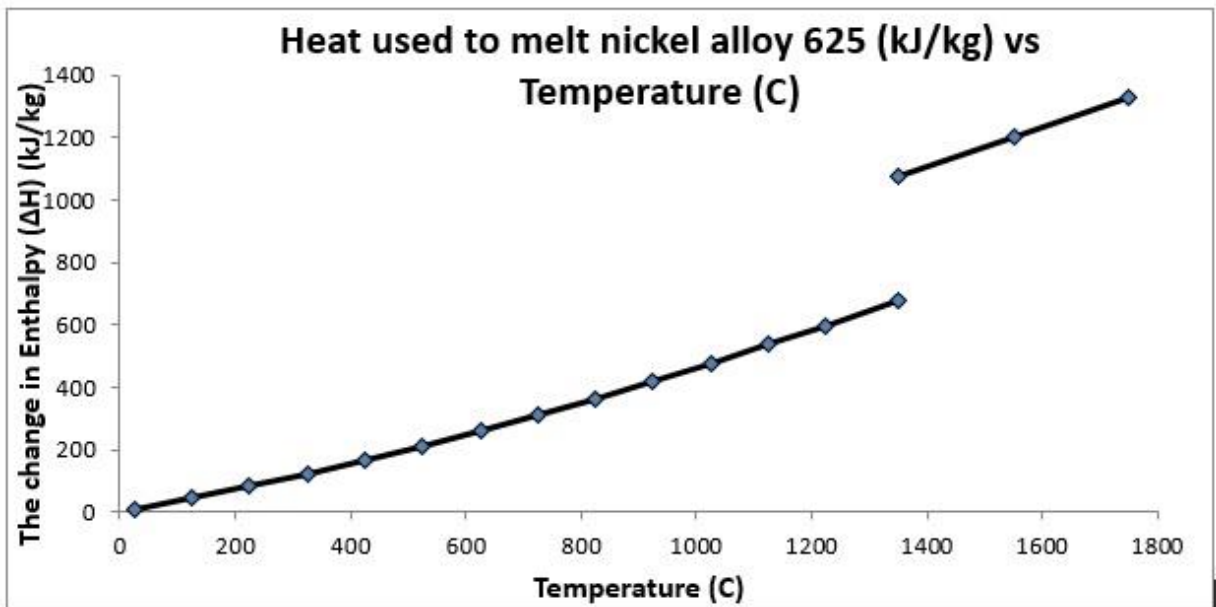
Figure 3.2.1.2.3 Nickel alloy 625 graphical representation of enthalpy change as a function of temperature
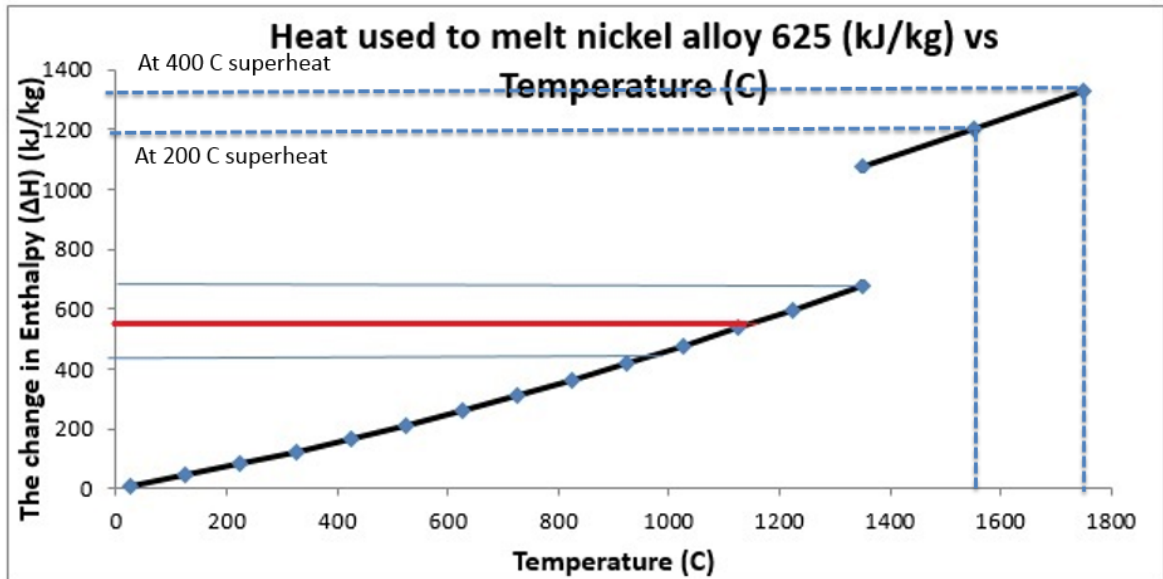
Figure 3.2.1.2.4 Nickel alloy 625 graphical representation of enthalpy change as a function of temperature which indicating red line as the average of enthalpy of HAZ area [147]

Considering from this graph, ΔH_{HAZ}^{eff} or the average of enthalpy would be assumed from average of temperature between lowest approximate temperature of HAZ according to E. F. NIPPES AND J. P. BALAGUER (1986) and [148] at 800 C and melting temperature (1300 C) which is marked in red. So, one can find $\Delta H_{HAZ}^{eff} \approx 550 \frac{kJ}{kg}$

After obtaining all of these values, one will be able to determine energy efficiency used for nickel-based superalloy 625 material case. The result of these both materials will be explained in details in section 4 of results section.

3.2.2 Microstructural investigation

3.2.2.1 Grain size measurement

In microstructural evaluation, grain size measurement has been used to initially

108

identify property of microstructure. The objective of grain size measurement is to determine whether the microstructure varies as a function of position away from the substrate, which is the de facto heat sink. What it termed "grain size" is really the width of columnar grain colonies in a cross-sectional image of the build-up (illustrated in figure 3.2.2.1.1). In some e-beam build-ups, very coarse structures have been observed [149].
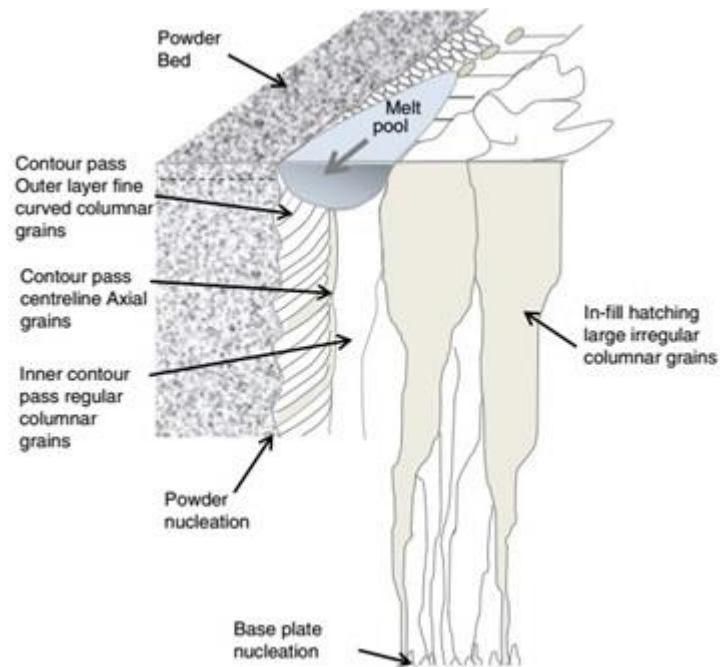
Figure 3.2.2.1.1: Diagram showing large irregular prior beta grain boundaries at the top surface which is bigger than those at the bottom of the part. E-beam process is used in this case. This also illustrates how competitive grain growth leads to larger grain sizes as a function of distance away further from substrate [150].
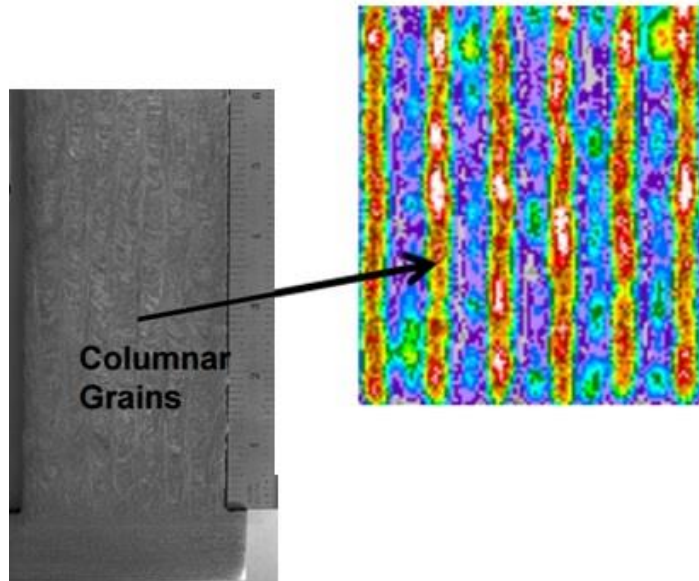
Figure 3.2.2.1.2: A build-up of large scale aerospace components created by e-beam process showing columnar grain structure [151]. The authors state on the difficulties encountered with NDI to inspect parts with such structure due to bigger grain size is able to block scanned signals from NDI (non-destructive inspection)

Turning attention to work carried out in this project, these experiments sought to determine if the same is true for the laser hot-wire. Ideally, the microstructure would be uniform small grains, i.e., very limited coarsening is preferred to allow non-destructive Testing (NDI) and reduce the likelihood of internal strength-limiting structural defects. The image below illustrates a cross-sectioned microstructure of Ti-64 stringer (i.e., single pass bead) and its substrate manufactured at Lincoln Electric using the LHW process.
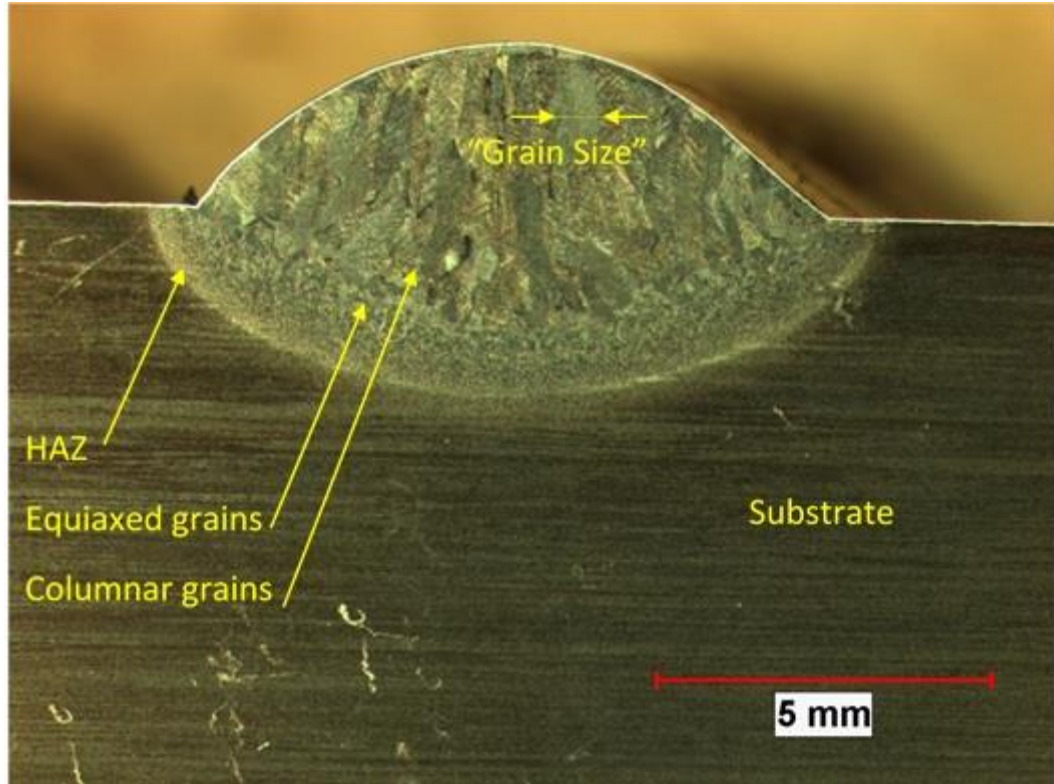
Figure 3.2.2.1.3: Optical micrograph of a transverse section of a single Ti-64 weld bead (i.e., a stringer) on a titanium plate. The heated affected zone within the substrate, a region of equiaxed grains, and extended columnar grains all are visible. The definition of effective grain size is the width of the columnar grains measured parallel to the top of the substrate (illustrated for one grain by the arrows). This quantity varies with distance from the substrate

However, the assessment of coarsening is most relevant to multilayer deposition associated with an arbitrary build up. As a reference specimen, a six-layer build up from Ti-6Al-4V was also studied and reported in result section.

Measurements were also performed on both longitudinal sections (i.e., sectioned along the travel direction – perpendicular to the section) and transverse sections. In this project, the standard "line intercept method" was used in performing grain size measurement. This method can be done by counting number of grain boundaries intercepted by a test line (again, constrained to lie in a plane parallel to the

surface of the substrate) per unit length. A sample calculation, using the image in Fig.

3.2.2.1.3, is as follows:
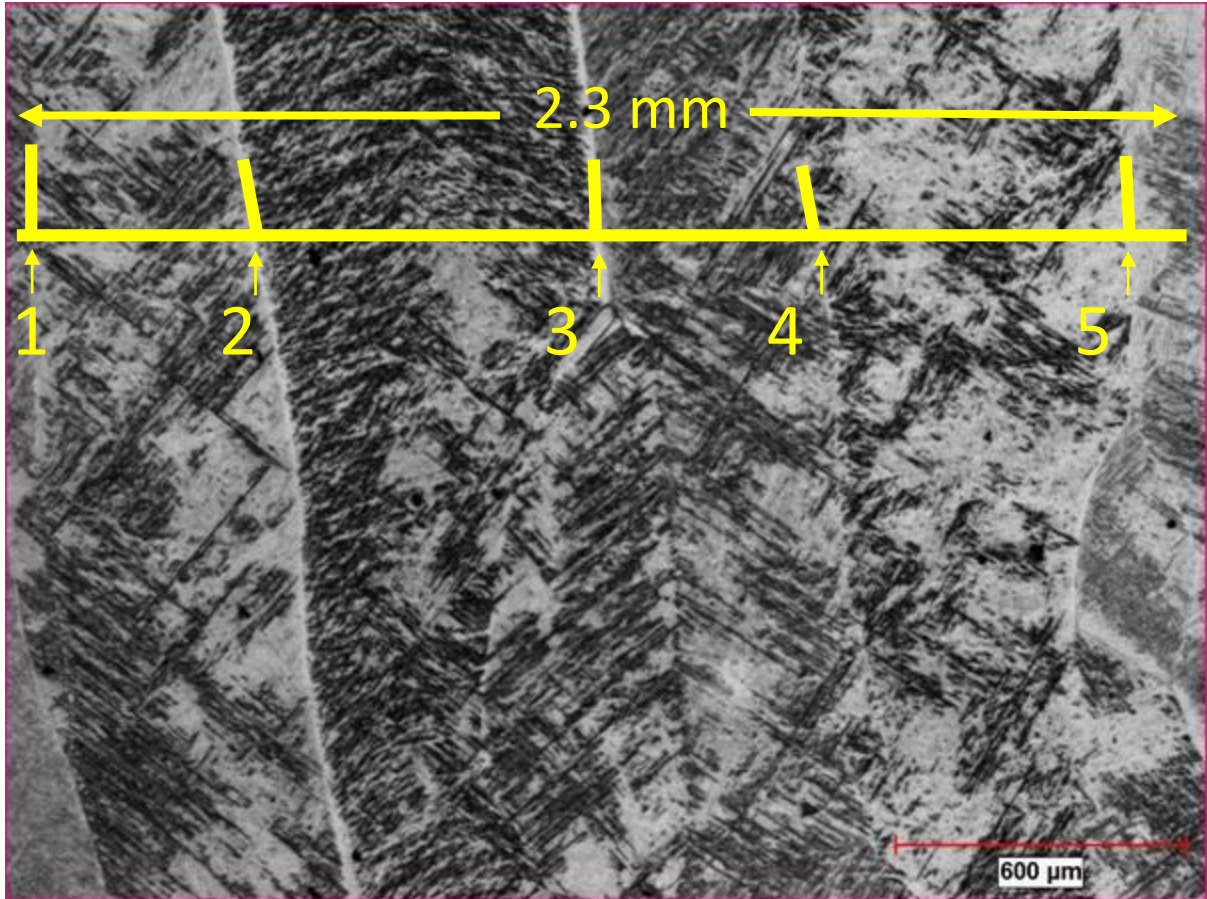
Figure 3.2.2.1.4: A microstructure of titanium build-up showing columnar grain size

Therefore, from the above picture of grain size, one can estimate grain size using

line-intercept method is simply **2.3/5 = 0.46mm or 460 micron**.

Moreover, in order to benchmark against laser powder bed process, another

demonstration test part with several features was created by both the LHW and the

laser powder bed processes which illustrated below.

Fig 3.2.2.1.5 the test part created by LHW process to benchmark against the similar test part created by laser powder bed process

200 µm
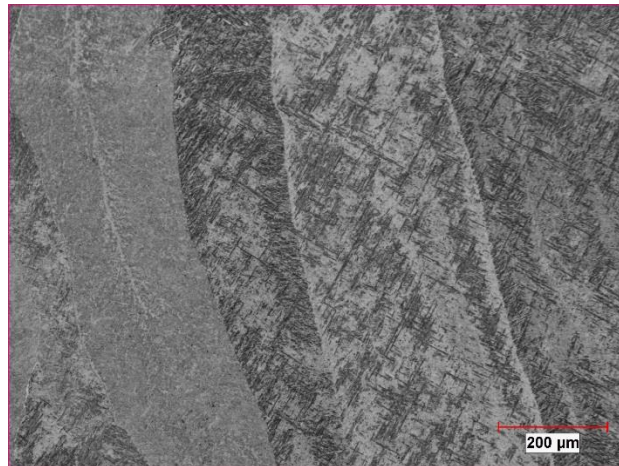
Figure 3.2.2.1.6 100x magnification grain size picture of Ti-6Al-4V created by LHW process

According to figure 3.2.2.1.6 below, with the line intercepted method, it is found that grain size of the sample part created by LHW process is about 240 micron (1200/5). This can be estimated by perform a division of the yellow line which represents a drawn line covering all grains in this picture and number of grain showing in this picture which is separated by red line. The equation for this division will be (1200 / 5) and it is equivalent to 240 micron.

113
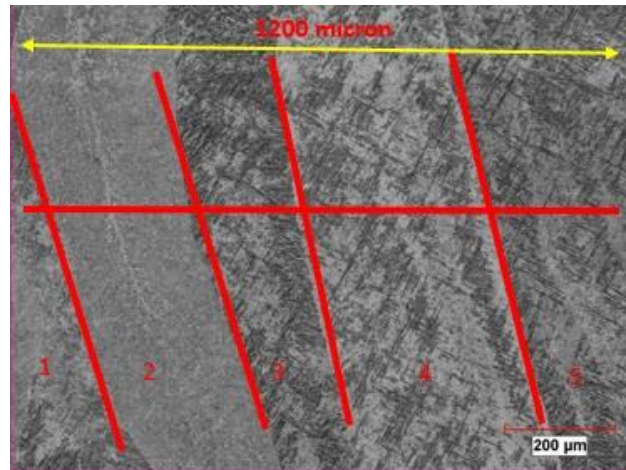
Figure 3.2.2.1.7 similar picture to figure 4.2.1.6 showing how to use line intercept method to measure grain size measurement

The average grain sizes of transverse and longitudinal directions are tabulated and compared in the result section (Section 4). Apart from six layers build up, build-ups of weaves and stringers and demonstration part with features were created, sectioned, measured, tabulated and compared to the six layer build-up. Weave bead is a type of weld bead that uses a technique so called "transverse oscillation" (perpendicular to welding direction) to deposit weld metal. The technique helps to accomplish the width of the deposited weld bead. As all three techniques (weave, stringer, multi-layers) might be used in additive manufacturing, it was desirable to understand the degree of difference in characteristic grain sizes.

3.3 Geometrical evaluation

3.3.1 3D Laser scanning

To document information of specimens built and evaluate those specimens in details, 3D laser scanning method was used in the test part which was explained above and is illustrated below. Both of the test parts that were created using the LHW and laser powder processes were documented photographically and scanned to obtain a 3D CAD file of the parts. CAD file, 3D scanner, and also scanned file of the two additive manufacturing processes are illustrated below respectively.
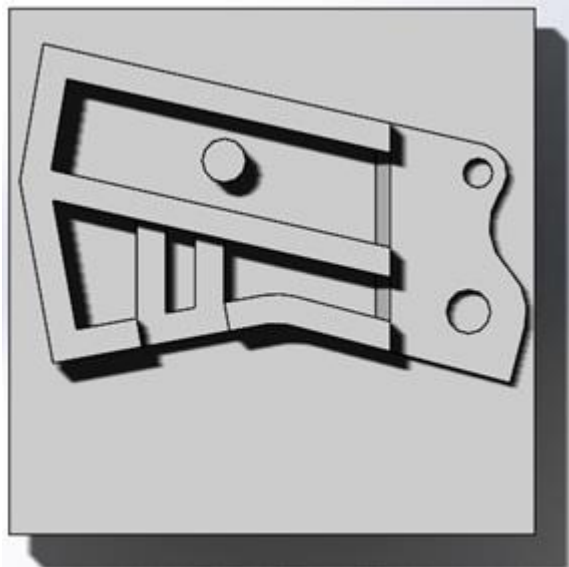
Fig. 3.3.1.1 A CAD file of the test part before getting created by both the LHW and laser powder bed processes

Fig. 3.3.1.2 3D scanner that was used to document the test part
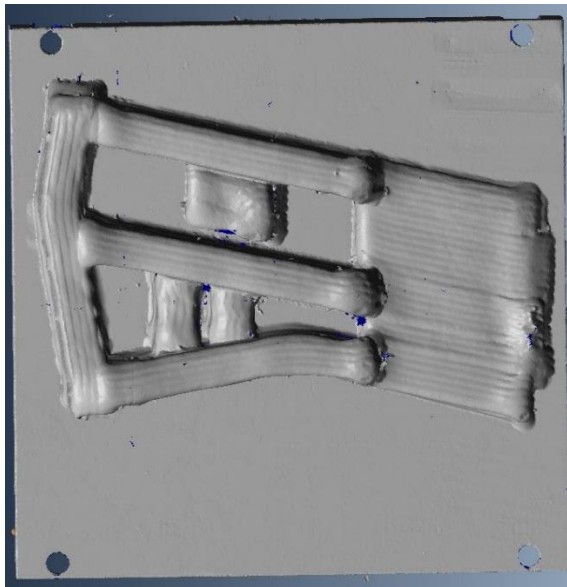
Fig. 3.3.1.3 3D-scanned file of the test part created by the LHW process
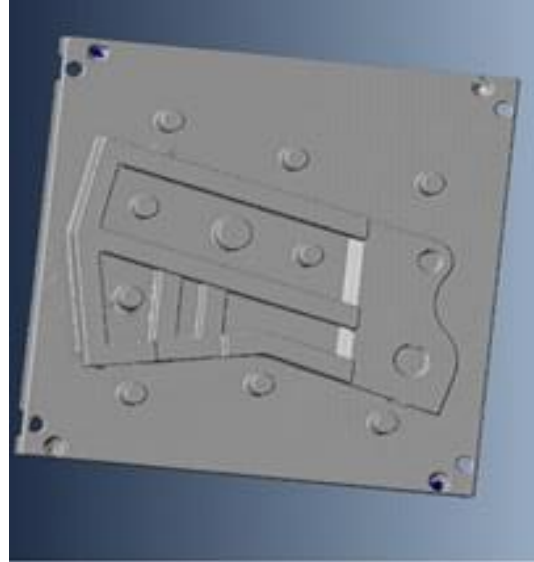
Fig. 3.3.1.4 3D-scanned file of the test part created by the laser powder bed process
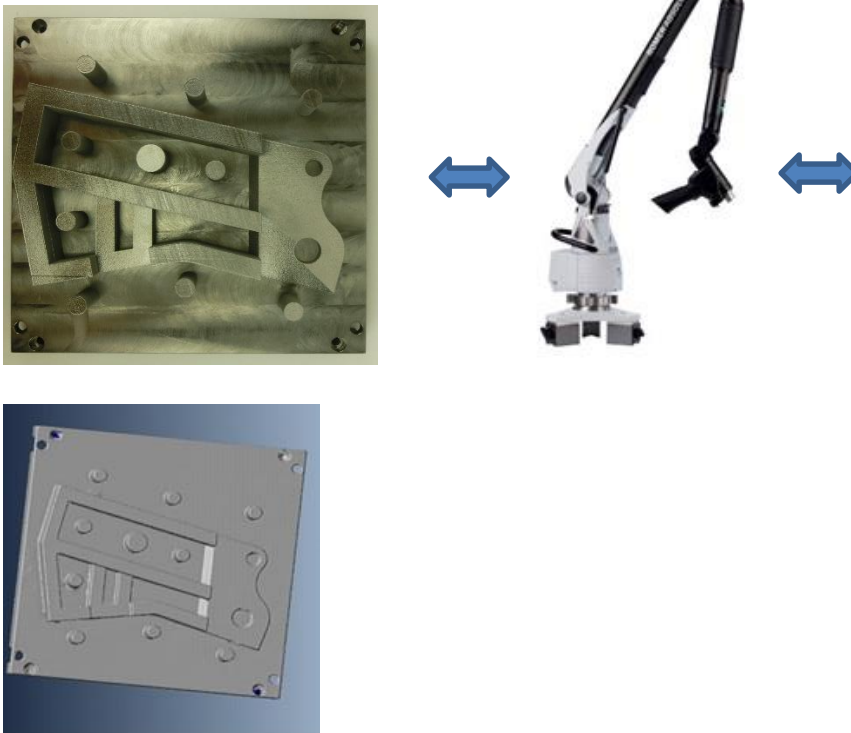
Fig. 3.3.1.5 Schematic illustration explaining how the test part can be transferred to a scanned CAD file

by using 3D scanner

In addition to figure 3.3.1.1, only one big pin in the top middle part is shown and it was designed to be a feature of the whole part. However, for figure 3.3.1.4, with laser powder bed process, extra nine pins were added all around the test part design to create a support structure for the second side of the build. Otherwise, without these supports, the part was expected to not balance and interrupt the build process.

3.3.2 Curve measurement in Ti-6Al-4V material

To perform a residual stress calculation by measuring curve occurred to the test part after finishing the build-up. The two figures below show how curve of the substrate after the process by real photo and scanned file accordingly.

Figure 3.3.2.1. A photo of bent plate of the LHW test part from front side view

Figure 3.3.2.2. 3D scanned file showing bent plate of the LHW test part
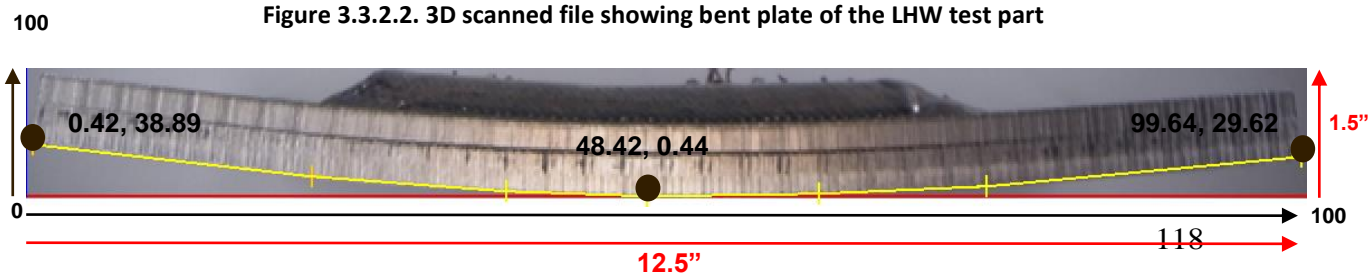
Figure 3.3.2.3. A photo of LHW bent plate identifying x and y coordinates by using digitizer

application

In performing a calculation of curve measurement, a digitizer application has

been used to identify x and y coordinates for 3 pairs on the left, center and right sides as

shown in the figure 3.3.2.3. To make it easier for calculation, once these 3 pair of

coordinates are identified, all of coordinates are converted to inch unit. As can be seen

in the figure 3.3.2.3, in black horizontal and vertical axes, scale is ranged from 1 to 100.

On the other hand, with the same figure, red horizontal and vertical axes are labeled in

12.5 inches and 1.5 inches accordingly referring to measurement of the real sample.

To measure curve of the plate, a radius of curvature of a circle that is relatively

created by these 3 pairs of coordinates has to be calculated. Once the radius of

curvature is known, once can use the information to calculate the amount of stress

causing the plate to be curved.

To find the equation of the circle passing through the 3 points, (x,y) of the center

needs to be identified by:

$$x_c = m_1 m_2 (y_1 - y_3) + m_2 (x_1 + x_2) - m_1 (x_2 + x_3) / 2 (m_2 - m_1)$$

$$y_c = (-1 / m_1) [(x_c - (x_1 + x_2) / 2)] + (y_1 + y_2) / 2$$
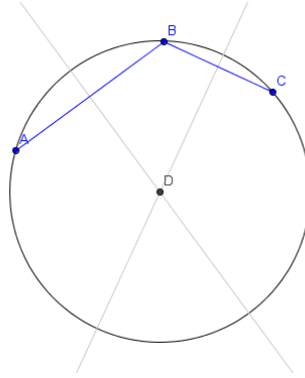
Figure 3.3.2.4. A circle that is created from 3 pairs of coordinates point A, B, and C. With 3 pairs of coordinates, one can find radius of curvature from related circle [184]

The above formulas are based on finding the intersection of the perpendicular bisectors of the 2 lines joining the 3 points, as can be seen in the figure 3.3.2.4.

As stated before, x and y axes must be converted to real world unit and inch is used in this case. As x and y axes have different length scale, each axis has to be converted individually as shown:

For x-axis (horizontal axis):

100 scale = 12.5 inches

1 scale = 12.5 / 100 = 0.125 inch

For y-axis (horizontal axis):

100 scale = 1.5 inch

1 scale = 1.5 / 100 = 0.015 inch

Once the unit is converted, the 3 pairs of coordinates are converted accordingly as

follows:

(x_1, x_2, x_3) = (0.42, 48.42, 99.64) in scale unit $\approx$ (0.05, 6.05, 12.455) in inch unit

(y_1, y_2, y_3) = (38.89, 0.44, 29.62) in scale unit $\approx$ (0.58, 0.006, 0.44) in inch unit

With the formulas, slope m_1 and m_2 can be calculated as follows:

$m_1 = (y_2 - y_1) / (x_2 - x_1)$ = (0.006 - 0.58) / (6.05 - 0.05) = -0.574 / 6 $\approx$ -0.095

$m_2 = (y_3 - y_2) / (x_3 - x_2)$ = (0.44 - 0.006) / (12.455 - 6.05) = 0.434 / 6.405 $\approx$ 0.067

Then one can obtain x_c and y_c by:

$x_c = [m_1 m_2 (y_1 - y_3) + m_2 (x_1 + x_2) - m_1 (x_2 + x_3)] / 2(m_2 - m_1)$

x_c = [(- 0.095) (0.067) (0.58 - 0.44) + (0.067) (0.05 + 6.05) − (- 0.095) (6.05 + 12.455)] / 2 [(0.067) - (-0.095)]

x_c = [-0.0008 + 0.40 + 1.75)] / 0.324 $\approx$ 6.63 inches

And

$y_c = (-1 / m_1) \{x - [(x_1 + x_2) / 2] + (y_1 + y_2) / 2$

y_c = (-1 / -0.095) {6.63 − [(0.05 + 6.05) /2] } + [(0.58 + 0.006) / 2]

y_c = (10.52) (3.58) + 0.293 $\approx$ 37.95 inches

Therefore, radius of curvature from the center of the plate = $\sqrt{(x_2 - x_c)^2 + (y_2 - y_c)^2}$

= $\sqrt{(6.05 - 6.63)^2 + (0.006 - 37.95)^2}$ = $\sqrt{0.34 + 1439.74}$ = $\sqrt{1440.08}$ $\approx$ 37.94 inches

According to figure 3.3.2.3, radius of curvature from center bottom of the plate is about 37.94 inches. With the same methodology, radius of curvature from the center top of the plate is about 37.48 inches. Thus, the middle center point or the average of the center top point and the center bottom point is 37.71 inches. With this information, one can find strain as follows:

Strain = dl / lo = σ / E = $(l_1 - l_o) / l_o$ = (37.94 − 37.71) / 37.94 ≈ 0.006 inch

And, Young's modulus of Ti-6Al-4V is roughly equivalent to 115.8 GPa or 16.8 x 10^6 psi

So, stress of the curve plate = Strain * Young's modulus

= ε * E = 0.006 * 115.8 x 10^9 GPa = 694 MPa

Therefore, approximately 694 MPa caused a curvature in the test substrate. Compared to average yield strength of Ti-6Al-4V, it is about 880 MPa. This is sensible according to figure 3.3.2.1 because if amount of stress was more than ultimate tensile strength or up to level of GPa, the plate would be broken from that amount of stress.

4 Results

4.1 Energy analysis results

4.1.1 Ti-6Al-4V by LHW process

As discussed in section 3.2, one can calculate total energy used to create all

microstructural changes in each zone (bead, dilution, and HAZ) by using the equation below which each variable is clarified and investigated as demonstrated in section 3.2. With values obtained from those variables, the total energy used to created observable microstructural changes (bead, dilution, and HAZ) or ΔE_{used} is equivalent to;

$$\Delta E_{used} = \Delta E_{bead} + \Delta E_{dilution} + \Delta E_{HAZ}$$

$$= [\rho * A_b * v_t * \Delta H_{SHL}] + [\rho * A_d * v_t * \Delta H_{SHL}] + \left[\rho * A_{HAZ} * v_t * \Delta H_{HAZ}^{eff}\right]$$

$$= \left[(A_b + A_d) * \Delta H_{SHL} + A_{HAZ} * \Delta H_{HAZ}^{eff}\right]\rho * v_t$$

$$= \left[(16 + 10.8)(mm^2) \cdot 1,600 \left(\frac{kJ}{kg}\right) + 11.7(mm^2) \cdot 900 \left(\frac{kJ}{kg}\right)\right]$$

$$\cdot \left(4,420 \frac{kg}{m^3}\right) \cdot 11 \left(\frac{mm}{s}\right) \cdot 10^{-9} \left(\frac{m^3}{mm^3}\right)$$

$$= [(42,880 + 10,530)] \cdot (4,420) \cdot (11) \cdot (10^{-9}) = 2.60\ kW$$

In conclusion, the total energy that was used to create an entire microstructural changes are 2.60 kW.

In addition, if each portion is separated, the energy used to generate the bead, dilution and HAZ is 1.24 kW (47%), 0.84 kW (32%), and 0.52 kW (19%) as can be written down below.

$$\Delta E_{used} = \Delta E_{bead} + \Delta E_{dilution} + \Delta E_{HAZ}$$

$$\Delta E_{bead} = 1.24\ kW$$

123

$$\Delta E_{\text{dilution}} = 0.84 \; kW$$

$$\Delta E_{\text{HAZ}} = 0.52 \; kW$$

With the results above, there are couple of different ratios that are informative. The first is the ratio of energy used to produce the bead to the electricity converted from wall plug directed to the workpiece:

$$F1 = \frac{\text{Energy used to produce the bead}}{\text{Electricity converted from wall plug to workpiece}} = \frac{1.24}{28.00} \approx 4.4\%$$

In addition, the ratio of energy used to produce all of the microstructural changes to the electricity of both laser and power supply directed from wall plug to the workpiece is

$$F2 = \frac{\text{Energy used to create all of the microstructural changes}}{\text{Electricity converted from wall plug to the workpiece}} = \frac{2.60}{28.00} = 9.2\%$$

Moreover, the ratio of energy used to produce a bead compared with energy used to produce all of the microstructural changes is

$$F3 = \frac{\text{Energy used to produce a bead}}{\text{Energy used to create all of the microstructural changes}} = \frac{1.24}{2.6} = 47.7\%$$

From the second equation, this means only approximate 9.2% electricity is used to create observable microstructural changes. Additionally, from the literature in literature review section 2, it is known that absorptivity of titanium material is about 43% for the liquid titanium at the melting point. So, with LHW process, at least 43% (1.91kW) of

energy delivered to the workpiece (4.46 kW) should be used to create all of the microstructural changes (bead, dilution and HAZ) excluding heat losses. According to result of energy used to create all of the microstructural changes compared to energy delivered to the workpiece, more than 43% of the total energy was used.

4.1.2 Nickel alloy 625 by LHW process

As discussed in section 3.2, one can calculate total energy used to create all microstructural changes in each zone (bead, dilution, and HAZ) by using the equation below which each variable is clarified and investigated as demonstrated in section 3.2. With values obtained from those variables, the total energy used to created observable microstructural changes (bead, dilution, and HAZ) or ΔE_{used} is equivalent to;

$$\Delta E_{used} = \Delta E_{bead} + \Delta E_{dilution} + \Delta E_{HAZ}$$

$$= [\rho * A_b * v_t * \Delta H_{SHL}] + [\rho * A_d * v_t * \Delta H_{SHL}] + [\rho * A_{HAZ} * v_t * \Delta H_{HAZ}^{eff}]$$

$$= [(A_b + A_d) * \Delta H_{SHL} + A_{HAZ} * \Delta H_{HAZ}^{eff}]\rho * v_t$$

$$= \left[(14.2 + 3.0)(mm^2) \cdot 1,100 \left(\frac{kJ}{kg}\right) + 5.0(mm^2) \cdot 550 \left(\frac{kJ}{kg}\right)\right]$$

$$\cdot \left(8,440 \frac{kg}{m^3}\right) \cdot 11 \left(\frac{mm}{s}\right) \cdot 10^{-9} \left(\frac{m^3}{mm^3}\right)$$

$$= [(18,920 + 2,750)] \cdot (8,440) \cdot (11) \cdot (10^{-9}) \approx 2.0 \ kW$$

In conclusion, the total energy that was used to create an entire microstructural changes are 2.00 kW.

In addition, if each portion is separated, the energy used to generate the bead, dilution and HAZ is 1.45 kW (72.5%), 0.30 kW (15%), and 0.25 kW (12.5%) as can be written down below.

$$\Delta E_{used} = \Delta E_{bead} + \Delta E_{dilution} + \Delta E_{HAZ} + \Delta E_{Rad}$$

$$\Delta E_{bead} = 1.45 \text{ kW}$$

$$\Delta E_{dilution} = 0.30 \text{ } kW$$

$$\Delta E_{HAZ} = 0.25 \text{ } kW$$

With the results above, there are a couple of different ratios that are informative. The first is the ratio of energy used to produce the bead to the electricity from wall plug directed to the workpiece:

$$F1 = \frac{\text{Energy used to produce a bead}}{\text{Electricity converted from wall plug to workpiece}} = \frac{1.45}{28.00} \approx 5.1\%$$

In addition, the ratio of energy used to produce all of the microstructural changes to the electricity of both laser and power supply directed from wall plug to the workpiece is

$$F2 = \frac{\text{Energy used to produce a bead}}{\text{Electricity converted from wall plug to the workpiece}} = \frac{2.00}{28.00} \approx 7.1\%$$

Moreover, the ratio of energy used to produce a bead compared with energy

used to produce all of the microstructural changes is

$$F3 = \frac{\text{Energy used to produce a bead}}{\text{Energy used to create all of the microstructural changes}} = \frac{1.45}{2.0} \approx 72.5\%$$

This means only approximate 7.1% electricity is used to create observable

microstructural changes.

4.2 Microstructural investigation

4.2.1 Ti-6Al-4V by LHW process [152, 153]

As discussed in experimental method (in section 3) about grain size

measurement, entries are labeled by layer as a measure of position away from the

substrate. The first is adjacent to the substrate, and the sixth is the last deposited.

Measurements were repeated within each layer to assess reproducibility in both

longitudinal and transverse directions.

<u>**Transverse cross-sectional direction**</u>

Bead type / Bead number	length of line measurement (Micron)	Boundary passed	Grain size (Micron)		
3rd layer bead (0.3 inch from substrate) (Transverse)	2371	5	474		
	2402	5	480		
	2306	4	576		
	2309	4	577	Average grain size (Micron)	527
4th layer bead (0.4 inch from substrate) (Transverse)	2337	5	467		

	2106	4	526		
	2409	4	602		
	2316	4	579	**Average grain size (Micron)**	**543**
5th layer bead (0.5 inch from substrate) (Transverse)	2393	5	478		
	2320	4	580		
	2189	4	547		
	2397	5	479	**Average grain size (Micron)**	**521**
6th layer bead (0.6 inch from substrate) (Transverse)	2264	4	566		
	2281	5	456		
	2429	5	485		
	2240	4	560	**Average grain size (Micron)**	**517**
Stringer bead No.8 - 25x (0.1 inch from substrate) (Transverse)	2336	11	212		
	2362	10	236		
	2417	8	302		
	2316	9	257	**Average grain size (Micron)**	**252**
Stringer bead No.9 - 25x (0.1 inch from substrate) (Transverse)	2407	9	267		
	2240	8	280		
	2369	8	296		
	2130	7	304	**Average grain size (Micron)**	**287**
Weave bead - 25x (Transverse)	2330	6	388		
	2287	5	457		
	2323	5	464		
	2018	5	403	**Average grain size (Micron)**	**428**

Table 4.2.1.1 Grain size measurement of Ti-6Al-4V specimen in transverse cross-sectional direction

Longitudinal cross-sectional direction

Bead type / Bead number	length of line measurement (Micron)	Boundary passed	Grain size (Micron)		
3rd layer bead (longitudinal)	2114	7	302		

	2330	8	291		
	2185	7	312		
	2421	8	303	**Average grain size (Micron)**	**302**
4th layer bead (longitudinal)	2242	6	374		
	2257	6	376		
	2330	7	333		
	2216	6	369	**Average grain size (Micron)**	**363**
5th layer bead (longitudinal)	2107	5	421		
	2374	6	396		
	2296	5	459		
	2254	5	451	**Average grain size (Micron)**	**431**
6th (sixth) layer bead (longitudinal)	2380	5	476		
	2300	5	460		
	2420	5	484		
	2500	4	625	**Average grain size (Micron)**	**511**
Stringer bead no.8 -25x (longitudinal)	2460	9	273		
	2250	8	281		
	1890	7	270		
	2230	8	279	**Average grain size (Micron)**	**275**
Stringer bead No.9 - 25x (longitudinal)	2322	8	290		
	2308	8	289		
	2530	9	281		
	2550	9	283	**Average grain size (Micron)**	**285**
Weave bead - 25x (longitudinal)	1890	5	378		
	2550	7	364		
	2230	6	372		
	2180	6	363	**Average grain size (Micron)**	**369**

Table 4.2.1.2 Grain size measurement of Ti-6Al-4V specimen in longitudinal cross-sectional direction

Comparing the results of these two tables, one can conclude that there is no

significant difference between transverse grain sizes for each, whereas there is a

systematic trend in the longitudinal grain size. The weaves yielded a transverse grain

size (420 micron) that is roughly 90% of the grain size of the multilayers (460 micron) and a longitudinal weave grain size (369 micron) that is approximately the average of the four layers in the multilayer (363 micron) of the similar longitudinal section.

For the single bead stringers, the transverse and longitudinal grain sizes were similar and very close to 50% of that observed in the multilayers. To illustrate a clearer grain size measurement results, graphical representations of both directions are demonstrated below.

Grain size measurement (Longitudinal direction)

Legend:
- ☐ Weave bead - 25x (Longitudinal)
- ☐ 6th layer bead (Longitudinal)
- ☐ 5th layer bead (Longitudinal)
- ☐ 4th layer bead (Longitudinal)
- ☐ 3rd layer bead (Longitudinal)
- ■ Stringer bead no.9 - 25x (longitudinal)
- ■ Stringer bead no.8 - 25x (Longitudinal)

X-axis: Average Grain size (micron)
Y-axis: Type of weld bead
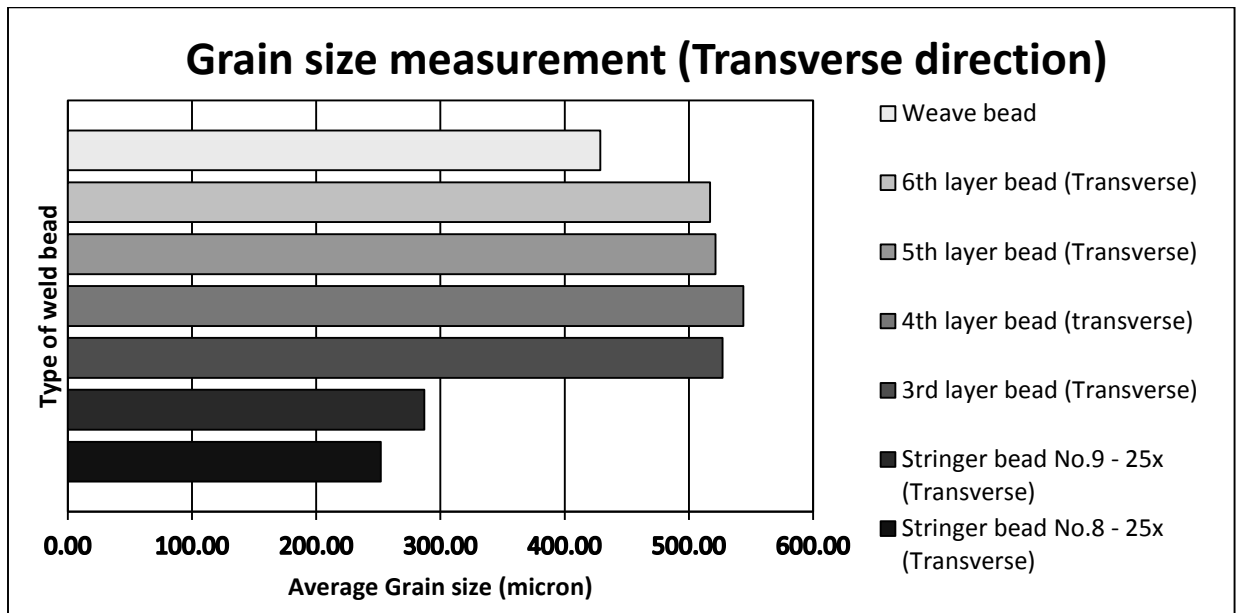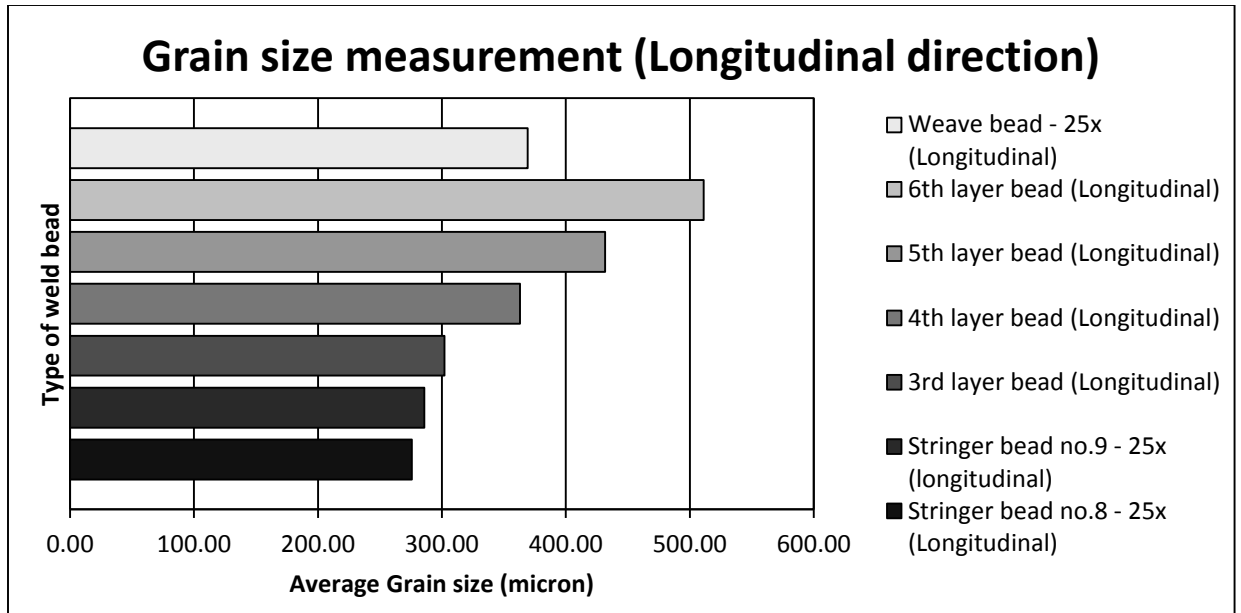
Figure 4.2.1.1: Graphical representation showing grain size measurement of both directions (Top) Transverse directions (Bottom) Longitudinal directions

Apart from the sixth layer build-up, another build-up which is called a "pillar" of Ti-6Al-4V was constructed by the same LHW process. The above systematic results compare well with the typical grain sizes observed at different locations in a large pillar specimen that is 23 layers high from its substrate which a 50 mm high parallelepiped was obtained by machined. Two figures below demonstrate before and after of the pillar build-up.

Figure 4.2.1.2: As-deposited Ti-6Al-4V pillar build created by LHW process (Left) showing overall of the part, (Right-top) and (Right-bottom) showing crack occurred during the process
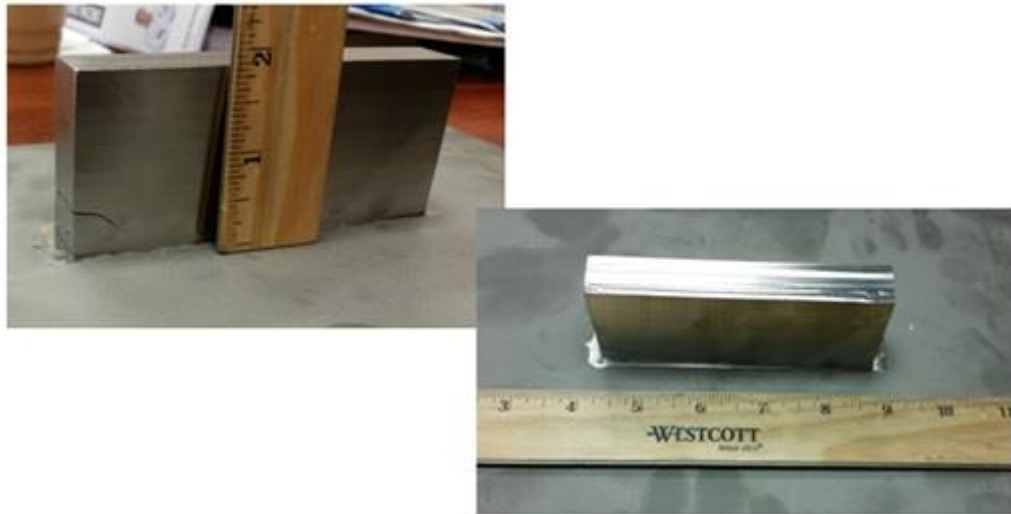
Figure 4.2.1.3: Ti-6Al-4V pillar build created by LHW process after bring machined (Left) showing height of the pillar at 1.96 inch, (Right) demonstrating approximately 4.5 inch after being machined

According to figure 4.2.1.4, it shows the cut plan after machining titanium pillar build-up with the specimens used for microstructural analysis in green and labeled with a numbered code. Each M1-M6 position corresponds to different positions. Specifically, M2 and M6 intersect the substrate at the lower third of the build-up, whereas M1 and M5 correspond to the upper half. Symbols using in this plan will be related in the result table below.
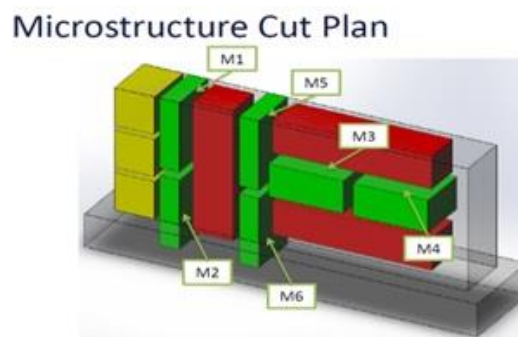
Figure 4.2.1.4: Ti-6Al-4V pillar build-up (50mm x 150mm x 25 mm in size) which was cut as shown to investigate microstructure and columnar grain size in transverse direction

It is therefore expected that the grain size observed in M2 and M6 should be closely correlated to that observed in the 6 layer specimen discussed above since the heights of both cases are relatively similar to each other. This is the case as can be seen by comparing the measurements from M2 and M6, given in the table in table 4.2.1.3 below against the values in table 4.2.1.1. Both grain sizes are just in excess of 0.5 mm. (Note, these are a factor of 10 smaller than for the e-beam specimen in figure. 3.2.2.2). One implication of this is that the thermal load associated with the deposition of more than 15 additional layers was insufficient to allow changes in grain size structure associated with the solidification.

The table below demonstrates grain size measurement from the pillar build-up part categorizing M2 and M6 as representatives of lower region and M5 as upper region of the pillar build-up

Table 4.2.1.3: The table above showing average grain size of Ti-6Al-4V pillar build up specifically from M2, M5, and M6 parts of the build-up schematic above. The first four rows demonstrates the M2 and M6 parts which are located at the bottom of the pillar build-up while the second last two rows of M5 part which is located at the top of the pillar build-up

Bead type / Bead number	Length of line measurement (mm)	Boundary	Grain size (mm)	Grain size (micron)
Pillar M2 - 100x	2.5	5	0.5	500
Pillar M2 - 100x	2.56	5	0.51	512
Pillar M6 - 100x	2.77	5	0.54	540
Pillar M6 - 100x	2.66	5	0.53	532
Pillar M5 - 100x	2.67	4	0.67	667
Pillar M5 - 100x	2.7	4	0.68	675

The results obtained from the upper region of the pillar specimen are significantly coarser (roughly 25%, 670 versus 540 microns for the averages of M6 and M5 respectively). This is modestly inconsistent with the transverse grain size results that were obtained for the 6 layer specimen (see Fig. 4.2.1.1) which had suggest no dependence on layer position for transverse. It is, however, still consistent with a weak dependence relative that observed for the longitudinal grain size.

Furthermore, another test part with features shown below was created with LHW and laser powder bed processes to compare and benchmark against each other. The illustration and welding condition titled below demonstrates the finished test part with features of LHW process.

Fig 4.2.1.5 the demonstration test part created by LHW process with wire size 0.045 inch, laser power at 6000 W, wire feed speed at 325 inch/minute, travel speed at 60 inch/minute with argon chamber as a function of gas shielding.
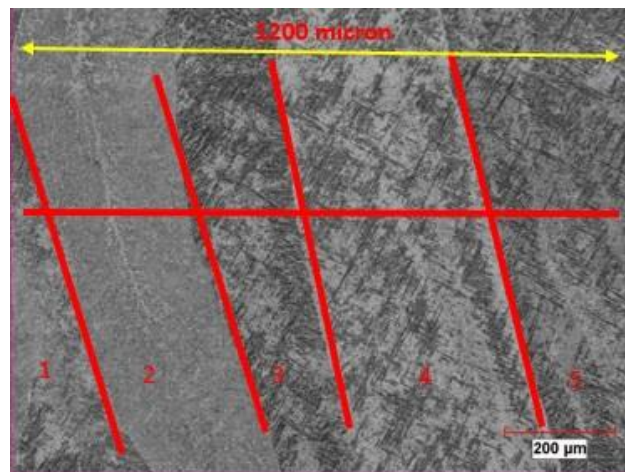
Figure 4.2.1.6 100x magnification grain size picture of Ti-6Al-4V created by LHW process

According to figure 4.2.1.6 above, with the line intercepted method, it is found that grain size of the sample part created by LHW process is about 240 micron (1200/5).

Bead type / Bead number	Length of line measurement (mm)	Boundary	Grain size (mm)	Grain size (micron)
Demonstration part (LHW process)	1,200	5	0.24	240

4.2.2 Ti-6Al-4V by laser powder bed process

Figure 4.2.2.1: A schematic cutting plan of titanium build-up (rp+m demonstration part identifying test coupon location (A, B, C, D, E, F, and G). The part was made by EOS laser powder bed machine. Power used in this case was 3,600 W, build rate is 3.75 mm^3/s, laser type is Yb-fiber laser at 200 W and the machine model is the EOSINT M 280 (Direct Metal Laser Sintering (DMLS) process)

After the titanium build-up was made by EOS powder-bed process and rp+m company, the part as shown in figure 4.2.2.1 above was cut up, etched, polished, and mounted to investigate microstructure of the part. Test coupon locations (A, B, C, D, E, F, and G) are identified as can be seen in the figure 4.2.2.1 to perform grain size measurement, chemistry analysis, and mechanical properties test.

To benchmark against the similar part manufactured by the LHW process in

figure 4.2.1.5, grain size measurement for figure 4.2.2.1 had been executed and its

result is shown below.
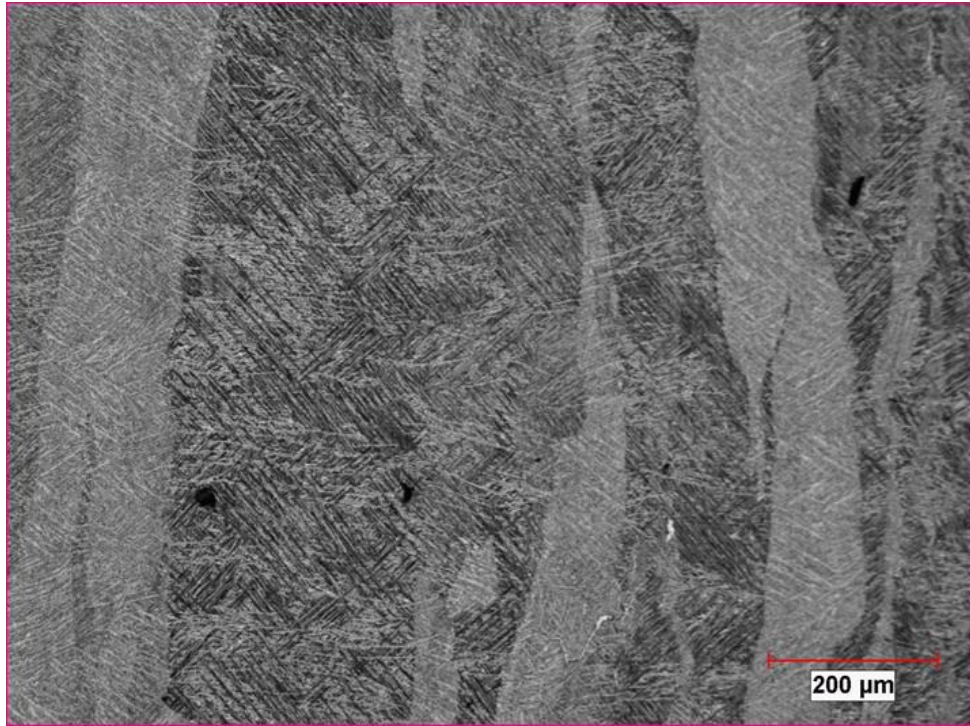
Figure 4.2.2.2 100x magnification grain size picture of Ti-6Al-4V created by a laser powder bed process

Specifically to grain size measurement, the expectation of result is to see similar

grain size along layers of the build-up. In other words, similar grain size of the upper and

lower region of the same part are anticipated to be similar. The grain size is really the

width of columnar grain colonies in a cross-sectional image of the build-up. The 100x

magnification photos of the part obtained from optical microscopy were selected to

measure grain size as grains and grain boundaries are obvious to count and calculate. To

obtain the average columnar grain size, the standard "line intercept method" was used

which is similar to the one created by the LHW process.
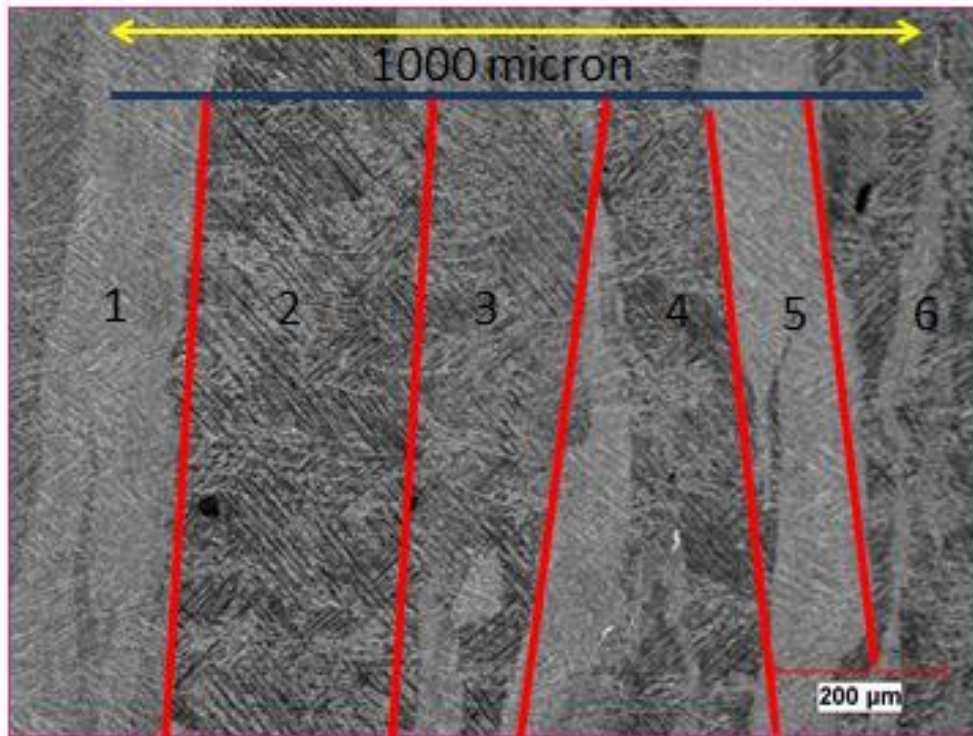
Figure 4.2.2.3: Similar picture to figure 4.2.2.2 showing how to use line intercept method to measure grain size measurement. In each boundary (red line), it shows a major phase that first formed and resolidified.

From the figure 4.2.2.3, the blue line is equivalent to 1000 micron and the red lines representing each grain size are roughly 6 in this case. Thus, one can conclude that the grain size of the figure 4.2.2.3 using line-intercept method is approximately 1000/6 or 160 micron.

Bead type / Bead number	Length of line measurement (mm)	Boundary	Grain size (mm)	Grain size (micron)
Demonstration part (DMLS process)	1,000	6	0.16	160

One important consequence of obtaining the fine grain size is that it allows the use of ultrasound to inspect and investigate the test parts created by both processes.

4.3 Mechanical properties

It is essential for this project to investigate mechanical properties of parts created by the LHW process to see whether the parts can be used and reach the standard of real-world applications or not. The parts created by the LHW process are also benchmarked against those manufactured by the laser powder bed process and an ASTM F 136 standard of Ti-6Al-4V.

4.3.1 Ti-6Al-4V test part

For specimens of Ti-6Al-4V material, the test part shown below with several features had been cut and machined to prepare for mechanical properties testing. Two similar test parts fabricated from the LHW process and the laser powder-bed process were inspected by Alcoa Titanium & Engineering Products.
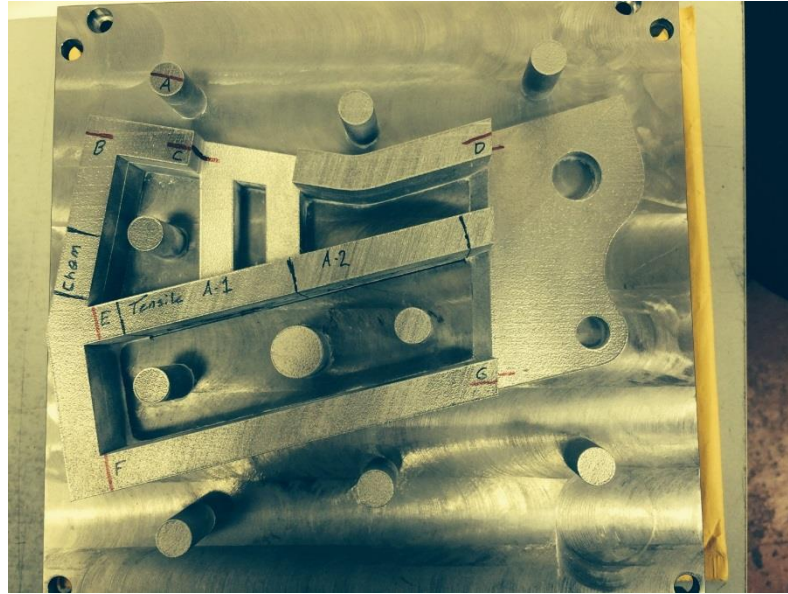
Fig 4.3.1.1 Test part of Ti-6Al-4V created by the laser powder bed process and cross-sectioned to measure mechanical properties as shown in coupon locations of A1, A2, and A3 and of A-F for chemistry and microstructure investigations. Red lines indicate the place of examination for microstructure specimens

Fig 4.3.1.2 Test part of Ti-6Al-4V created by the LHW process and cross-sectioned to measure mechanical properties, chemistry, microstructures as shown in coupon locations. The part was able to be manufactured on both sides. White lines indicate the place of examination for microstructure specimens. (Left) Side A and (Right) Side B

Before performing mechanical testing, the samples were stress-relieved at 790C (1450 F) for two hours followed by air cool and were surface-finished. The table below shows ultimate tensile strength (UTS), 0.2% yield strength (YS), elongation (EL), and reduction of area (RA) of the tensile.

Tensile test results[2]

Table 4.3.1.1 A comparison table showing mechanical properties of test parts fabricated by powder bed and LHW processes with Ti-6Al-4V
- **LHW = Demonstration part made by Lincoln Electric using LHW process**
- **EOS = Demonstration part made in EOS laser powder bed machine**
- **ASTM F136 standard = Ti-6Al-4V**

---

[2] Ernie Crist is a director of Process and Product Development Advanced Innovation & Technology at Alcoa Titanium & Engineered Products. He and his team help provided tensile and mechanical tests and results of this project by using equipment at the company's facilities.

Number	Sample	UTS, MPa (ksi)	0.2% YS, MPa (ksi)	EL, %	RA, %
1	EOS #1	1,025 MPa (148.7 ksi)	935 MPa (135.7 ksi)	13	47
2	EOS #2	1,027 MPa (149.0 ksi)	935 MPa (135.7 ksi)	13	44
3	EOS #3	1,021 MPa (148.2 ksi)	931 MPa (135.1 ksi)	11	42
4	LHW #1	1,161 MPa (168.5 ksi)	1,085 MPa (157.4 ksi)	5	9
5	LHW #2	1,149 MPa (166.7 ksi)	1,079 MPa (156.6 ksi)	2	6.5
6	LHW #3	1,119 Mpa (162.4 ksi)	1,102 MPa (159.9 ksi)	3	1.1
7	ASTM F136	950 MPa (137 ksi)	880 MPa (120 ksi)	10	20

As demonstrated in the table above, ultimate tensile strength (UTS), yield strength (YS), and percent of elongation are demonstrated for test parts fabricated by powder bed process with an EOS machine (Row 1-3), LHW process (Row 4-6), and a Ti-6Al-4V for ASTM F136 standard (the last row).

In terms of UTS and YS, productions from both processes were able to achieve higher value compared to the ASTM F136 standard of Ti-6Al-4V. Nevertheless, for elongation (ductility), powder bed process demonstrated higher elongation while LHW process provided less elongation regarding to the ASTM F136 standard of Ti-6Al-4V value. These results directly affect to properties of these parts and lead us to believe that it is related to a cracking problem in the part manufactured by the LHW process which will be discussed in Section 5 (discussion).

In the chemistry result, some of test parts used LHW process demonstrates higher oxygen (>0.20%) and nitrogen (>0.05%) contents which is tabulated and

discussed in the next section. The chemistry result confirms consistently with results from mechanical properties indicating effect and influence of containing high interstitial oxygen and nitrogen contents in LHW test parts compared to standard of ASTM F136.

4.4 Chemistry analysis

4.4.1 Ti-6Al-4V[3]

Chemical analysis of test parts created by LHW process is definitely one of the quality standards that can be used to evaluate quality of test parts. As briefly discussed earlier, an excessive amount of nitrogen and oxygen contents can negatively affect to desired mechanical properties such as tensile strength and ductility and cause defects such as cracking. According to ASTM F136 standard of Ti-6Al-4V used, limitation of oxygen content should be less than 0.2% and nitrogen should be less than 0.05% of the total chemical composition of the Ti-6Al-4V specimen.

As a result demonstrated below, chemical composition results are shown for test parts created by powder bed process with EOS machine (EOS) and laser-hot wire process (LHW).

Table 4.4.1.1: Chemistry results showing oxygen and nitrogen contents in the Ti-6Al-4V test parts created by laser powder bed process (EOS) and laser-hot wire process (LHW)[3]

- **rp+m = Demonstration part made in EOS laser powder bed machine**
- **LHW = Demonstration part made by Lincoln Electric using laser hot-wire process**
- **ASTM F136 standard= Ti-6Al-4V**

Number	Sample location	Content of oxygen (%)	Content of nitrogen (%)
1	EOS #1	0.148	0.010
2	EOS #2	0.144	0.012
3	LHW #2	0.196	0.124
4	LHW #4	0.261	0.162
5	LHW #5	0.268	0.167
6	Ti-6Al-4V	0.20%	0.05%

On one hand, for test part fabricated by EOS machine, the process and machine were able to constantly maintain level of oxygen and nitrogen to meet the standard requirement as shown at the top two rows of the table above (EOS#1 and EOS#2). On the other hand, for test part fabricated by LHW process, the contents of oxygen and nitrogen still needed to improve obviously since they were higher than the standard limitation (last row). At the last row of the table, it indicates the ASTM F136 standard of oxygen and nitrogen for Ti-6Al-4V material.

Apart from the previous specimen, simply "E" and "Pi" shaped build-ups were created to assess chemical composition also. The objective was to investigate whether or not oxygen and nitrogen composition were too excessive in these simple specimens or not.
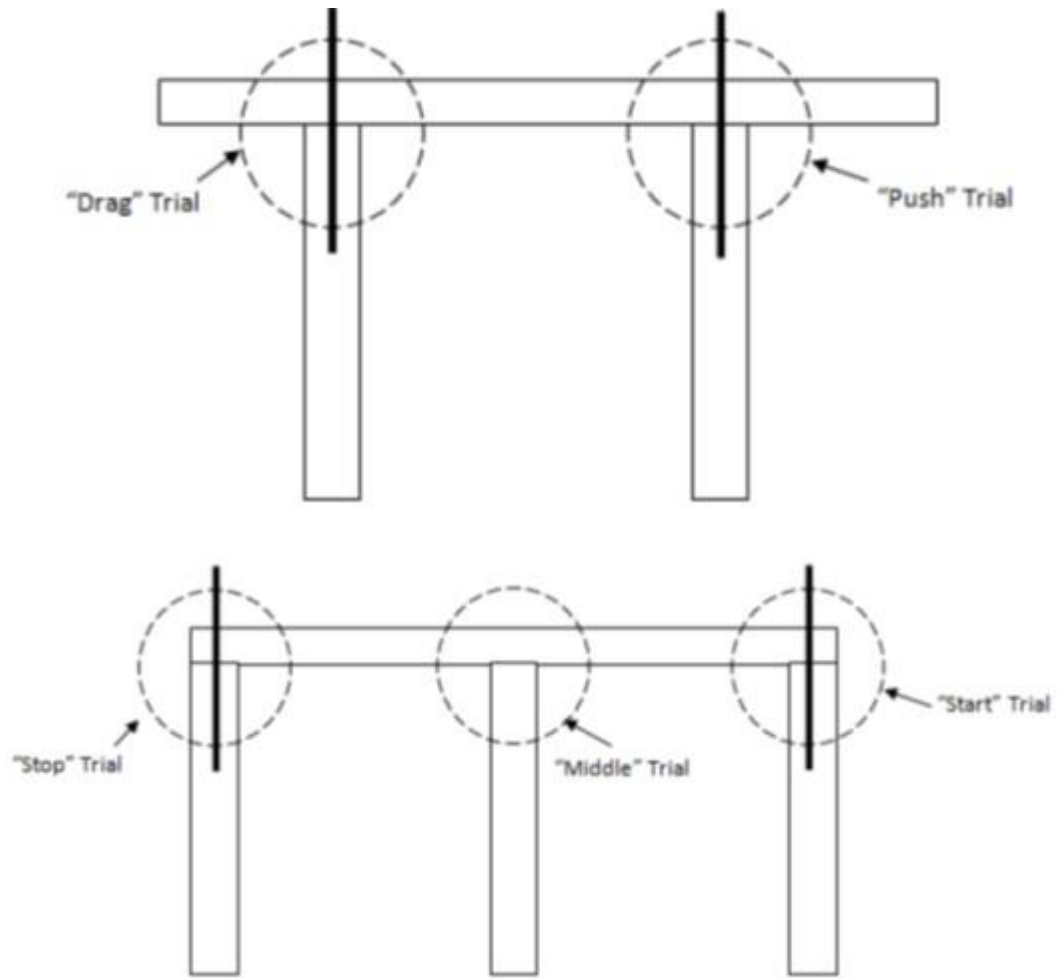
Figure 4.4.1.1 Microstructure cutting plan of (Top) "E" shaped build up (Bottom) "Pi" shaped build up

As can be seen above, for "Pi" shaped build up, 2 different welding direction were used in the specimen as can be called "Drag" and "Push" method. With drag method, after creating a long weld bead in horizontal as a first pass, the next weld bead will start from the intersection between the first and second weld bead as illustrated in figure 4.4.1 on top left picture. On the other hand, push method does oppositely by creating or pushing a second bead from blank space to finish at the intersection between the first and the second weld bead created. Schematic of drag and push methods is shown

below.
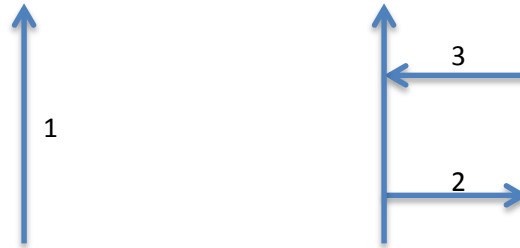
Figure 4.4.1.2 Demonstration of drag and push modes (2) drag mode (3) push mode

With that information of the two build-ups, chemistry analysis had been

completed at each intersection location, as shown below.

ID	O_2 #1	O_2 #2	O_2 #3	O_2 Avg	N_2 #1	N_2 #2	N_2 #3	N_2 Avg
Pi-Drag	0.239	0.183	0.215	0.212	0.135	0.084	0.149	0.123
Pi-Push	0.23	0.225		0.228	0.008	0.089		0.089
E-Stop (drag)	0.244	0.264		0.254	0.126	0.137		0.132
E-Middle (drag)	0.304	0.23	0.219	0.251	0.243	0.095	0.093	0.144
E-Start (drag)	0.165	0.253	0.277	0.232	0.037	0.13	0.228	0.132

Table 4.4.1.2 Oxygen and nitrogen content (wt.%) near intersections in the "E" and "Pi" build-ups.[3]

Several similar analyses had been taken for both oxygen and nitrogen content

measurement to ensure consistency. In average, both contents were still higher than

the standard limitation. As can be seen in the table 4.4.1.2, in Pi and E sample of this

experiment, push method is able to provide lower nitrogen content and comparable

oxygen content compared to drag method. Although extra experiments should be

conducted in the future to supportively confirm that push method can provide lower

interstitial contents, CAD or other AM designers (CAD-to-path designer) can use this

information to get benefits from design phase to improve properties of manufactured

parts. For instance, with LHW process, designers and operators can design their AM

parts to help create a way using push method to build the parts and get desired features

and properties.

Moreover, a single layer of weld bead (stringer) was created to compare

chemical composition with and without trailing gas shielding. As a result shown below, it

was clear that trailing gas shielding set up with a welding nozzle during the process does

assist the part to collect less contents of both nitrogen and oxygen. This result is helpful

in creating next specimens in reducing cracking susceptibility problem.

Standard		Trailing gas shielding	
Oxygen	0.192	Oxygen	0.186
Nitrogen	0.104	Nitrogen	0.053

Table 4.4.1.3 Comparison of oxygen and nitrogen contents (Left) without trailing gas shielding (Right) with trailing gas shielding

4.4.2 Nickel Alloy 625

For nickel alloy 625, chemical analysis was conducted to investigate alternatives

in using shielding gas in the LHW process. In this experiment, both stringer bead and

weave specimens were created by using nitrogen, air as well as argon shielding gas to compare contamination contents in each shielding gas. There are two contents as oxygen and nitrogen that was determined and tabulated below.

Shielding gas	Oxygen content	Nitrogen content
Argon	0.040	0.009
Nitrogen	0.049	0.015
Air	0.066	0.014

Table 4.4.2 Oxygen and nitrogen contents in nickel alloy 625 samples

As a result, argon shielding gas performance is shown to be better than the other choices as the specimen contains less oxygen and nitrogen in the interstitial site as contamination. Certainly, this result confirms that argon shielding gas is efficient and suitable to use during the process.

4.5 Flaws and defects

Currently, every additive manufacturing process has its own microstructural and defect problems depending on their characteristics, surrounding environment, and parameters used during each process. Certainly, this section will show the result in terms of defects that are obtained for test parts manufactured by both powder bed and LHW additive processes.

4.5.1 Ti-6Al-4V

4.5.1.1 LHW process

In terms of defects for LHW process, cracking problem is also found which is under assumption of excessive nitrogen and oxygen contents in the part's interstitial site that cause the cracking. This proves consistently with chemistry and mechanical testing that will be discussed in section 4.5 and 4.6.
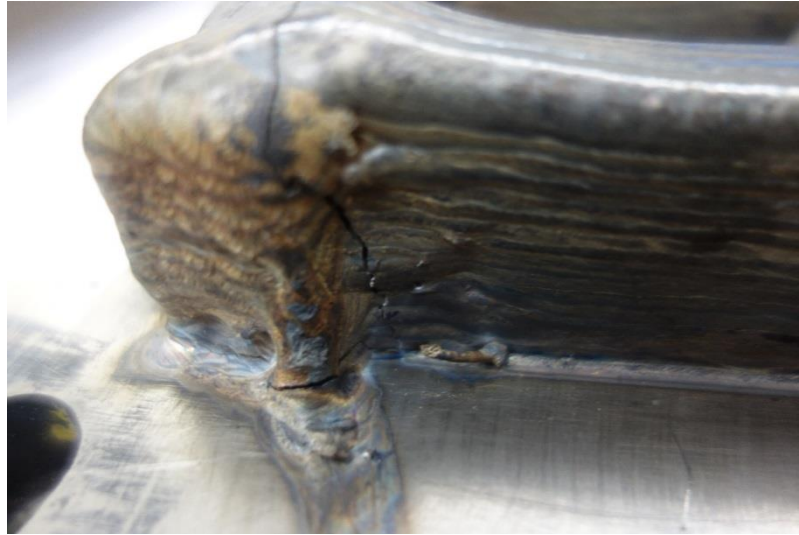
Fig 4.5.1.1.1. Cracking problems shown in the test part using LHW process
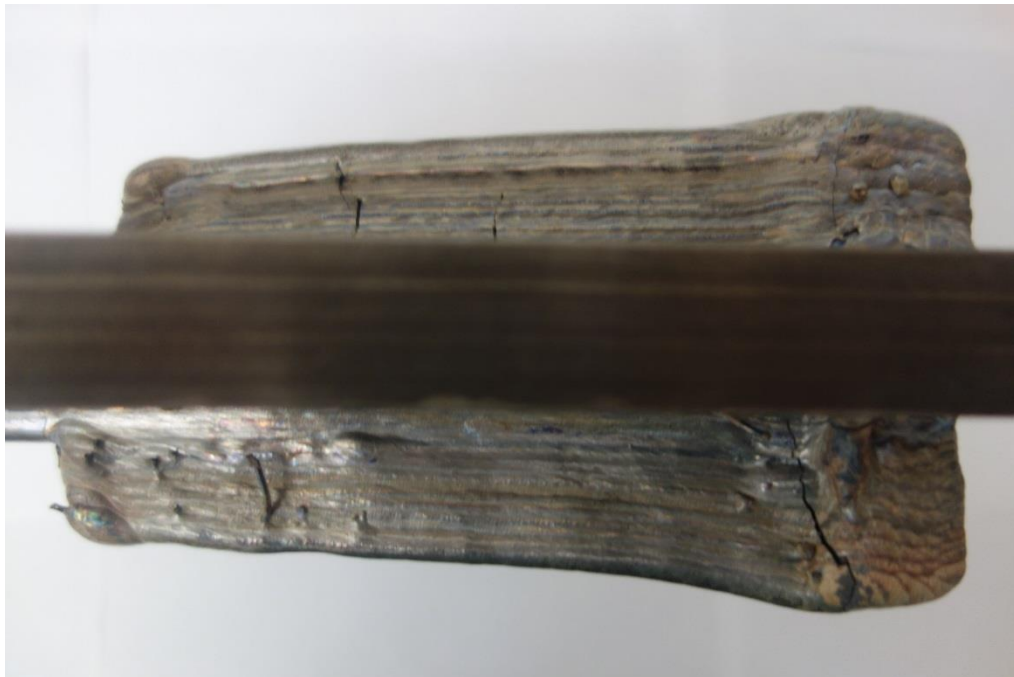
Fig 4.5.1.1.2 Cracking problems on both sides

Additionally, localized lack of fusion was also found in microstructure of the part built by

LHW.
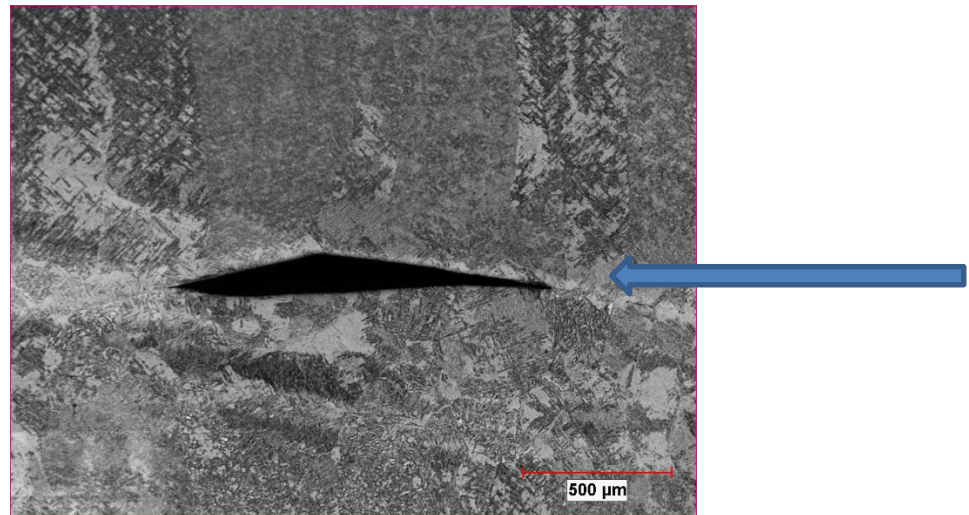
Fig 4.5.1.1.3 lack of fusion defect is shown in microstructure of demonstration part built by the LHW

process with laser power at 6,000 W, wire feed speed at 325 inch/min, travel speed at 60 inch/min and

hot wire power at 830 W

Apart from the previous specimen that was created on both sides of the

substrate, with "E" shaped build up, cracking was also seen as it was cut up to see cross-

sectional microstructure. The location of the crack and high magnification focusing at

the crack are shown below.
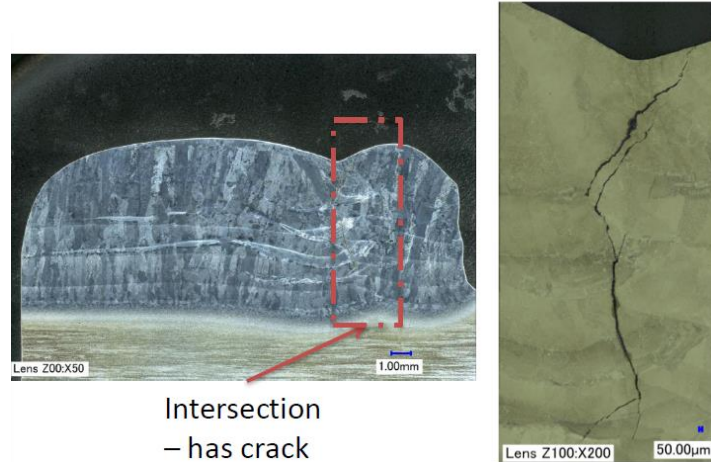
Figure 4.5.1.1.4 (Left) Longitudinal cross-section of an intersection in the E-shaped build-up; (Right) higher magnification image of the intersection showing the crack

4.5.1.2 Laser powder bed process

For the test part using powder bed process, after finishing on the first side, the part is discovered to have peel-off delamination at the bottom (arrowed as blue) between the part and the substrate. This happened due to high thermal stress and high temperature during the process. This confirms by temperature recorded at 80 Celsius degree at the build plate. The original plan was to attach the build-up with the substrate on both sides. However, it was not possible to create on the second sides since the peeled-off part was slammed by the recoater arm(powder plowder) Additionally, the technical issue from the machine reflected to mis-registration during the process which can be noticed as a line in about the middle of the part as arrowed in red.
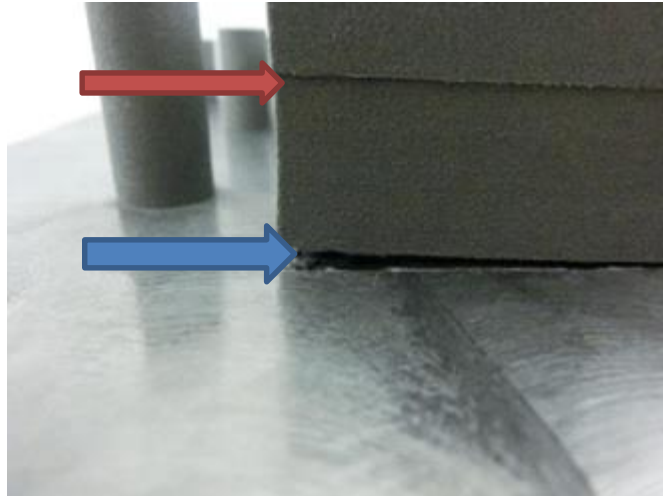
Figure 4.5.1.2.1. Peel-off delamination between Ti-6Al-4V substrate and added part due to high thermal stress marked as blue arrow and mis-registration marked as red arrow

With the same reason of high thermal stress created, it also caused the substrate to get warped or have an evidence of plate curvature. This lifting up eventually affected the recoater arm to jam.

Figure 4.5.1.2.2. Substrate warpage occurred during powder bed process due to high thermal stress as indicated by blue arrow
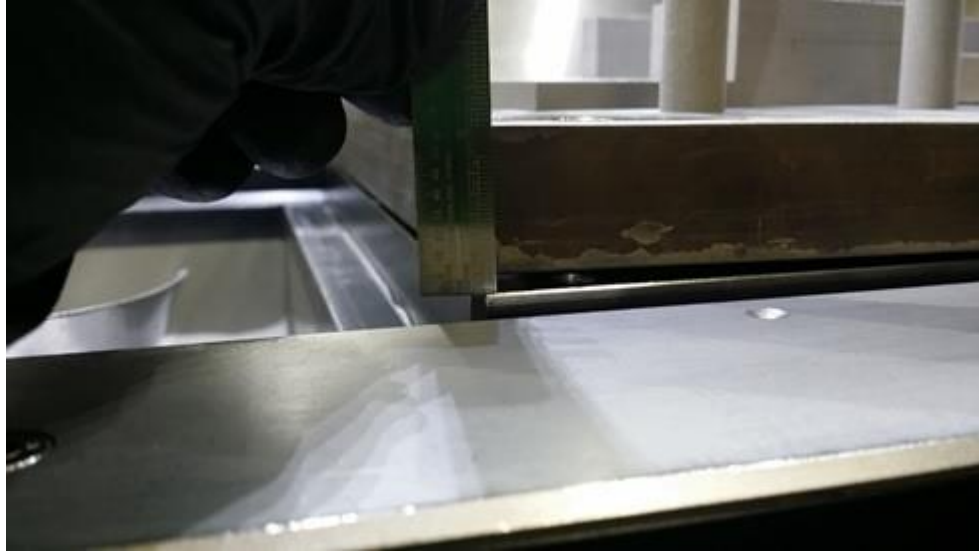
Figure 4.5.1.2.3. The substrate was uplifted to 6 mm (1/4 inch)

After the substrate warpage occurred, it was unable to build the part on the other side as the original plan was set because the machine could not distribute metal powder during the process like previous side (recoater arm jam). This prevention causes the process to stop, otherwise more damages could occur.

Figure 4.5.1.2.4 head crash due to substrate warpage during an attempt to build on the other side (after finishing the build-up on first side)
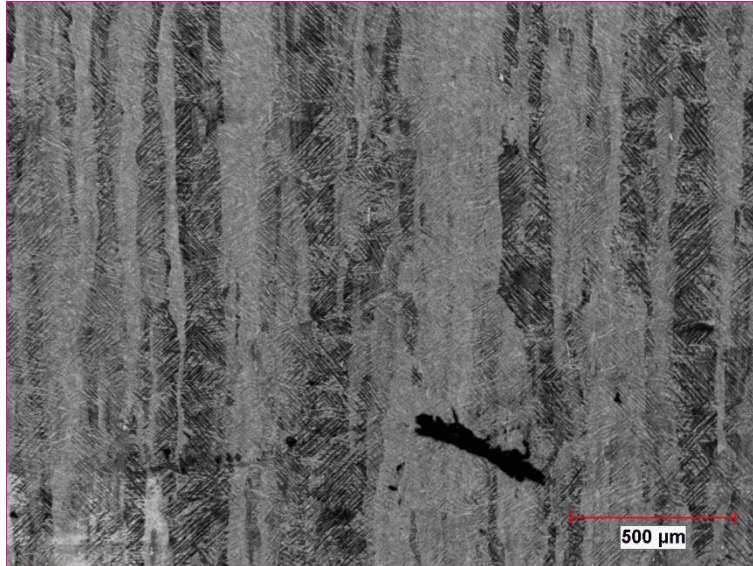
Figure 4.5.1.2.5 porosity is shown in microstructure of specimen built by the laser powder bed process

Moreover, as can be seen above from the micrograph, porosity defects were also found in the case of Ti-6Al-4V specimen by using laser powder bed process even not a lot of them has been found.

5 Discussion

5 .1 Energy analysis discussion

5.1.1 Ti-6Al-4V by LHW process

From the result of energy calculation in section 4, it is found that energy used to produce the bead to the electricity converted from wall plug to workpiece equals to 4.4%. In addition, the ratio of energy used to produce all of the microstructural changes to the electricity of both laser and power supply directed from wall plug to the workpiece is about 9.2%. Moreover, the ratio of energy used to produce a bead compared with energy used to produce all of the microstructural changes is 47.7%

This means only approximate 4.4% of the entire electricity converted from wall plug to workpiece is used to produce a bead (create a real product). The balance (95.6%) that is the energy not used to produce a bead is a combination of: i) heat lost from the wire to the atmosphere as it is being fed; ii) the energy in the reflected fraction of the laser beam; iii) energy used to melt the pre-existing substrate (dilution); iv) conduction in the substrate; and v) convective losses from the substrate to the atmosphere; vi) wall plug efficiency of the laser supply is only 30% (from wall-plug to workpiece). Taken together these are 95.6% of the total energy supplied to the workpiece.

As can be noticed from the results, some portion of energy delivered to the workpiece was lost. Even though this portion is small, it is worth to take a look and estimate how much energy loss occurred during the process. Therefore, in terms of completeness of energy analysis, energy loss calculation was also performed. Mainly, convective conductive and radiative losses are considered as heat losses [165] and conducted to compare with the entire energy used to melt metal in this case.

So, heat transfer from a surface by convection and radiation can be done by the equations below [166, 167, and 168]:

Convective loss = $Q_{conv} = h(T_s - T_e)$

Radiative loss = $Q_{rad} = \in \alpha \, (T_s^4 - T_e^4)$

Each nomenclature is defined as follows:

Q_{rad} – Heat loss from radiation

Q_{cond} – Heat loss from conduction

h – Heat transfer coefficient ($60 \frac{W}{m^2 K}$ $when$ $\in$ $= 0.2$)

T_s - Temperature at surface of materials

T_e - Ambient temperature of surroundings

$\in$ - Emissivity coefficient (0.19 for Titanium) [154]

α – Stefan's constant = $5.67 \; x \; 10^{-8}$
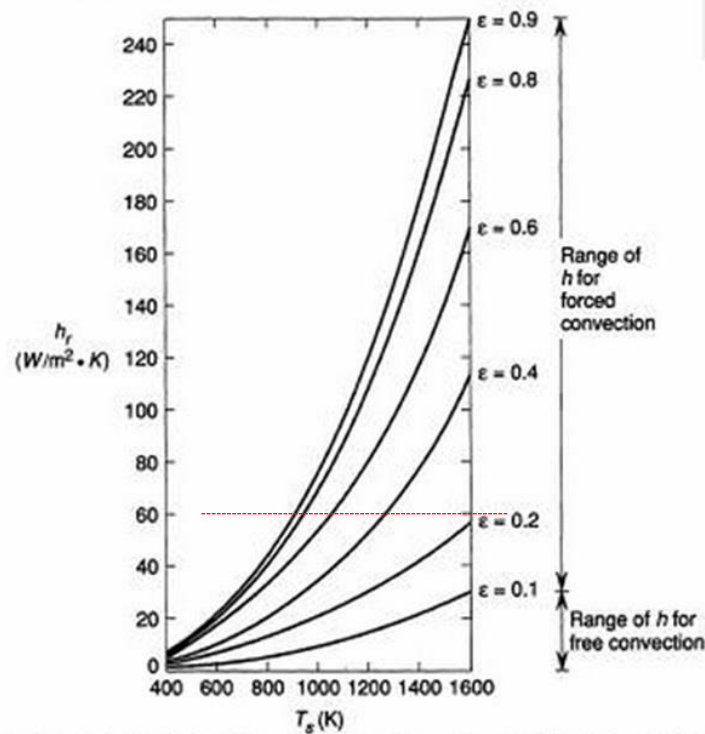
Figure 5.1.1.1 Variation, with surface temperature and emissivity, of the radiation heat transfer coefficient for emission of radiation to surroundings at 298K. Red dashed line shows radiation heat transfer coefficient of titanium material [154].

For temperature at the titanium surface (T_s) in this case, it is assumed to include superheat temperature at 2,000 C (2,273 K). One can find convective, radiative and conductive losses from referring to the graphical representation and equations above as

156

follows:

$$Q_{conv} = h(T_s - T_e)$$

$$= 60(\frac{W}{m^2 K}) \ x \ (2{,}273 - 300)K$$

$$= 118{,}380 \ (\frac{W}{m^2})$$

So, heat of convective loss during the process is $118.380 \ (\frac{W}{m^2})$

Therefore, after getting amount of heat loss from convection as shown above, one can calculate the energy loss from convection by performing multiplication each heat loss and approximate area of weld area at peak temperature during the LHW process
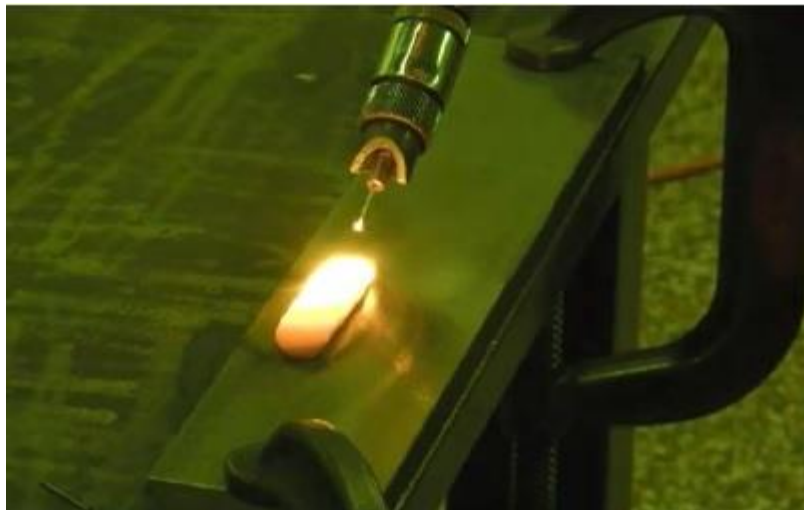
Figure 5.1.1.2. Weld bead created by the LHW process showing approximate area at peak temperature which can be estimated from the area of light shining of the whole weld bead

$$\Delta E_{conv} = bead \ area \ of \ peak \ temperature * Q_{rad}$$

$$\Delta E_{conv} = 300 \ mm^2 \ * 10^{-6} * 118{,}380 \ \frac{W}{m^2}$$

$$\approx 36 \ W \ or \ J/s$$

Therefore, energy loss for convection is equivalent to $36 \ W$

Secondly, to calculate radiative loss, the equation below is used:

$$Q_{rad} = \ \in \alpha \ (T_s^4 \ - \ T_e^4)$$

$$= (0.19) \left(5.67 \ x \ 10^{-8} \ \frac{W}{m^2 \ k^4}\right) (2{,}273^4 - 300^4)K$$

$$= 287{,}476 \frac{W}{m^2}$$

So, heat of radiative loss during the process is equivalent to $287{,}476 \frac{W}{m^2}$.

With the same idea of finding energy loss in convection loss, one can find energy

loss of radiation by

$$\Delta E_{rad} = bead \ area \ of \ peak \ temperature \ * \ Q_{rad}$$

$$\Delta E_{rad} = 300 \ mm^2 \ * 10^{-6} * 287{,}476 \ \frac{W}{m^2}$$

$$\approx \ 86 \ W \ or \ J/s$$

Therefore, energy loss for convection is equivalent to $86 \ W$

Currently, if values of energy used to create all microstructural changes were to

separated, 3 zones would be shown as follows:

$$\Delta E_{bead} = 1.24 \ kW$$

$$\Delta E_{dilution} = 0.84 \ kW$$

$$\Delta E_{HAZ} = 0.51 \ kW$$

And from energy lost calculation above, one can conclude that:

$\Delta E_{Conv} = 0.036 \ kW$

$\Delta E_{Rad} = 0.086 \ kW$

These convective and radiative losses are relatively low compared to other losses in the system such as the energy in the reflected fraction of the laser beam (about 57% reflection) and wall plug efficiency of the laser supply which is only 30% from wall-plug to workpiece.

Moreover, to cross-check with titanium absorptivity at 43% approximately as reported by Xie and A. Kar (1999), knowing from experiment using LHW process to create the demonstration test part:

Surface area (front, side, and back) of the demonstration test part $\approx$ 0.25 m^2

Q = 4.46 kW = 4460 W

And according to figure 5.1.13 and figure 5.1.1.4 below, average temperature of each layer deposited in LHW process derived from thermocouple is about 300 C
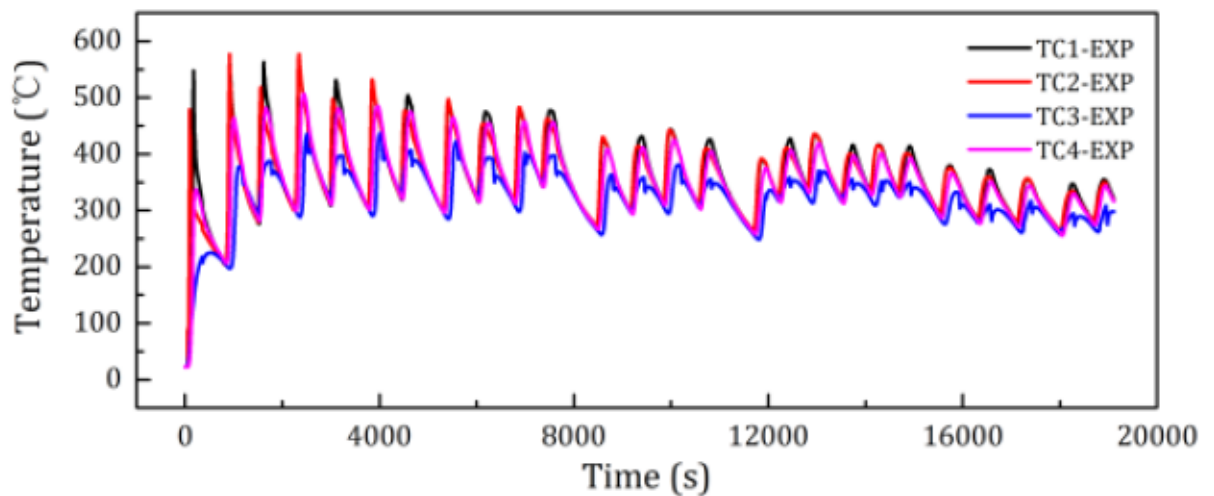
Figure 5.1.1.3: Temperature variation curves by thermocouples was set-up under substrate during LHW process. Each peak represents each layer when the laser travels through the area on the top of thermocouple [183]
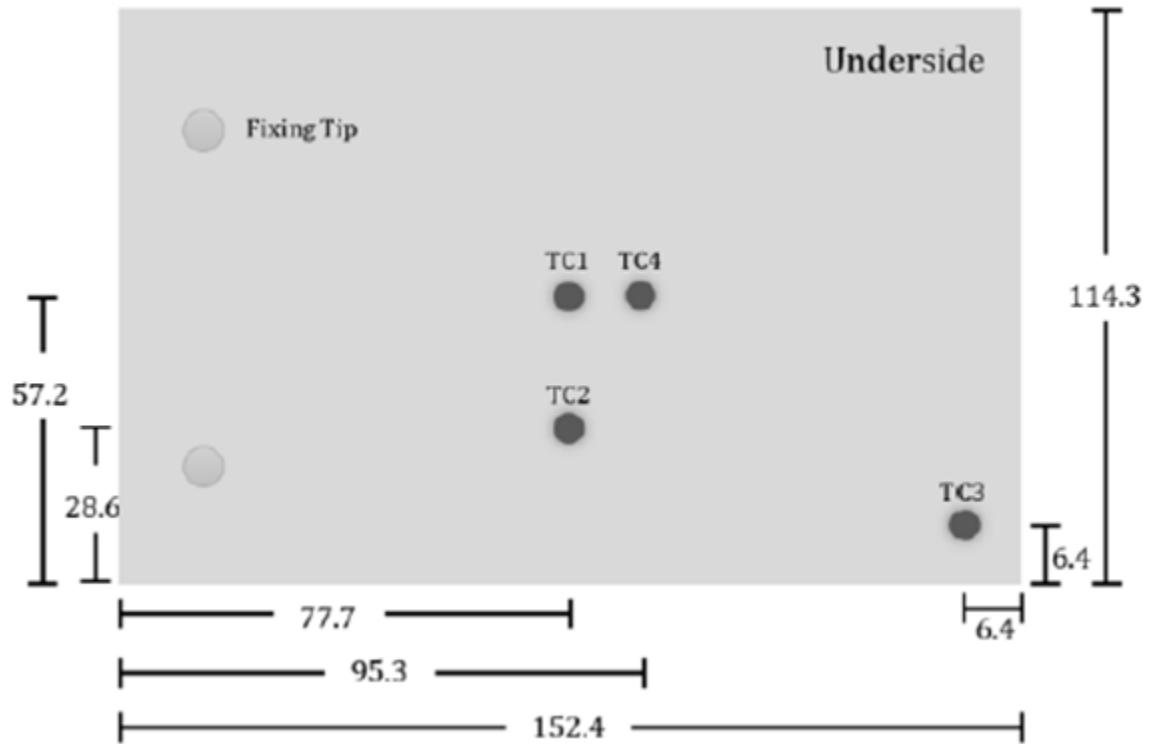
Figure 5.1.1.4: Position of thermocouple in substrate of LHW process (unit: mm). Label of TC1 – TC4 represent each thermocouple set up in different position. This schematic can be used to relate with graphical representation in figure 5.1.1.3. [183]

Therefore, one can estimate heat transfer coefficient being used in the process by

$$Q = h(T_s - T_e)\text{A}$$

4,460 W = h * (598 K – 298 K) * (0.25 m²)

h ≈ 60 W/m²K

This result is similarly related to figure 5.1.1.1 where heat transfer coefficient of titanium material is about $60 \frac{W}{m^2 K}$. This heat transfer coefficient demonstrates approximate heat distributed around the substrate and the part during the process. Therefore, one can conclude that this value of heat transfer coefficient was used to affect temperature change (in figure 5.1.1.3) during the process. Also, since it is consistent to result in figure 5.1.1.1, it demonstrates that absorptivity at about 43% for titanium when radiating by laser at melting point is about reasonable in this case.

5.1.2 Benchmarking with Ti-6Al-4V with laser powder bed process

To further evaluate energy efficiency of the LHW process, one way that is valid to do is to benchmark against other related additive manufacturing process whether an advantage in terms of energy efficiency still exists or not.

Therefore, an energy efficiency benchmark between the LHW process and laser powder bed process was performed. Since the laser powder bed process is one of the mainly additive manufacturing process in powder-based, it is a good indicator to compare with the wire-based laser hot wire process. Firstly, the total added embodied energy (the total energy consumed by the entire process) is calculated as follows:
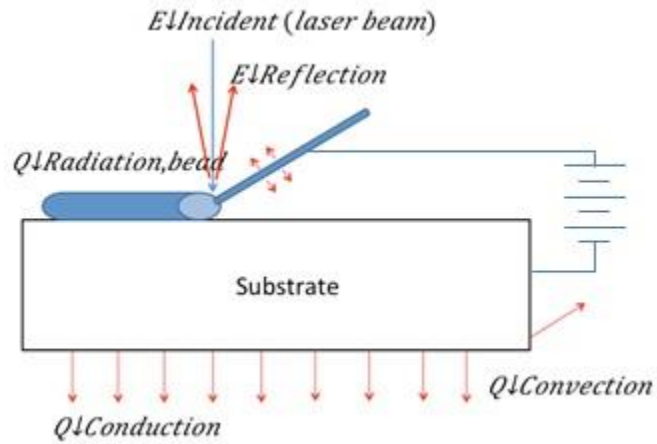
Figure 5.1.2.1 Schematic of LHW process showing heat inputs and losses

There are two heat energy sources that is used in the LHW process which are

    1. Electricity used by laser - According to [155 and 156], laser beam

absorption rate for titanium is about 30% and the laser power used is 8,000 kW.

So, the total electricity used by laser equals to

    $\approx$ (1/0.3)*8,000 $\approx$ 27,000 W

    2. Electricity used in hot wire – This energy is supplied by the welding

power supply to resistively pre-heat the wire before feeding to be melted by

laser during the LHW process which equals to

    $\approx$ 1,000 W

Then, volume added to part per unit time is estimated by performing a

multiplication of wire feed rate and wire cross-sectional area and is shown as

follows:

    $\approx$ (wire feed rate)*(wire cross-sectional area)

    $\approx$ (300 in/min)*(π*(0.045in/2)^2)

≈ 0.48 in³/min ≈ 0.008 in³/s

≈ 130 mm³/s

So, one can find the total added embodied energy by calculating a division of the total electricity used and volume added to part per unit time which is equivalent to

≈ 28,000/130 ≈ 215 J/mm³

Secondly, the same calculation was accomplished to obtain the total added embodied energy for the EOS powder bed process. According to datasheets of EOSINT M 280 machine and EOS titanium powder, it was known that power used to create the demonstration part is 3,600 W and build rate is 3.75 mm³/s.
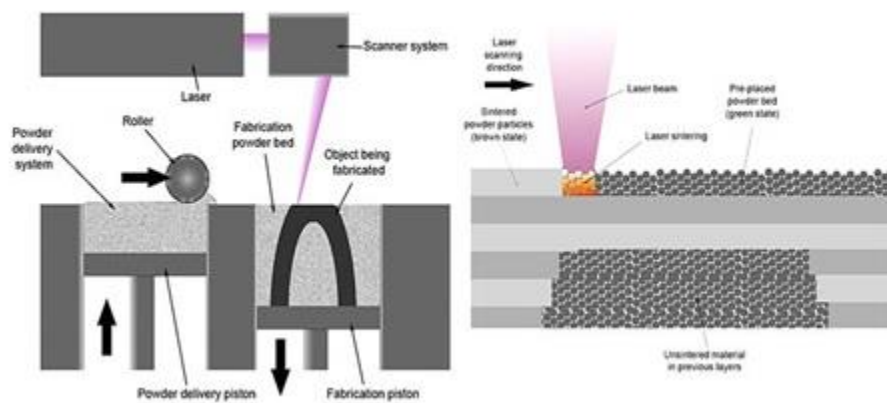
Figure 5.1.2.2 Schematic of laser powder bed process

Therefore, the added embodied energy ≈ 3,600/3.75 ≈ 950 J/mm³

As a result of these two processes, EOS machine will use 950/215 or

approximately four and a half times as much energy used to manufacture the same volume of a part. This implies that energy used to build a deposit in the similar volume is more efficient in the LHW process. In addition to this outcome, it is relatively consistent to other literature that demonstrates higher energy used with the similar laser powder bed process [157].

5.1.3 Nickel alloy 625 by LHW process

5.1.3.1 Energy lost calculation

From the result of energy calculation in section 4, it is found that energy used to produce the bead to the electricity converted from wall plug to workpiece equals to 5.1%. In addition, the ratio of energy used to produce all of the microstructural changes to the electricity of both laser and power supply directed from wall plug to the workpiece is about 7.1%. Moreover, the ratio of energy used to produce a bead compared with energy used to produce all of the microstructural changes is 72.5%

This means only approximate 5.1% of the entire electricity converted from wall plug to workpiece is used to produce a bead (create a real product). The balance (94.9%) that is the energy not used to produce a bead is a combination of: i) heat lost from the wire to the atmosphere as it is being fed; ii) the energy in the reflected fraction of the laser beam; iii) energy used to melt the pre-existing substrate (dilution); iv) conduction in the substrate; and v) convective losses from the substrate to the atmosphere; vi) wall plug efficiency of the laser supply is only 30% (from wall-plug to workpiece). Taken together these are 94.9% of the total energy supplied to the workpiece.

As can be noticed from the results, some portion of energy delivered to the workpiece was lost. Thus, energy loss calculation was also performed. Mainly, convective conductive and radiative losses are estimated.

So, heat transfer from a surface by convection and radiation can be done by the equations below [158, 159, and 160]:

Convective loss = $Q_{conv} = h(T_s - T_e)$

Radiative loss = $Q_{rad} = \in \alpha (T_s^4 - T_e^4)$

Emissivity for nickel = 0.07 [161]

Heat coefficient = $30 \frac{W}{m^2 K}$

Since melting temperature of nickel material (1455 C) is lower than that of titanium (1668 C), superheat temperature or peak temperature at the material surface is reduced in this calculation accordingly to 1800 C (2073 K). With similar nomenclatures and equation details explained in titanium case, the result of each loss is as follows:

$$Q_{conv} = h(T_s - T_e)$$

$$= 30(\frac{W}{m^2 K}) \; x \; (2,073 - 300)K$$

$$= 53,190 \; (\frac{W}{m^2})$$

So, heat of convective loss during the process is $53,190 \; (\frac{W}{m^2})$

$$\Delta E_{conv} = bead \; area \; of \; peak \; temperature * Q_{rad}$$

$$\Delta E_{conv} = 300\ mm^2\ *10^{-6}*53{,}190\ \frac{W}{m^2}$$

$$\approx 16\ W\ or\ J/s$$

Therefore, energy loss for convection is equivalent to $16\ W$

Secondly, to calculate radiative loss, the equation below is used:

$$Q_{rad} = \in \alpha\ (T_s^4 - T_e^4)$$

$$= (0.07)\left(5.67\ x\ 10^{-8}\ \frac{W}{m^2\ k^4}\right)(2{,}073^4 - 300^4)K$$

$$= 73{,}263\ \frac{W}{m^2}$$

So, heat of radiative loss during the process is approximately equivalent to $73{,}263\ \frac{W}{m^2}$.

With the same idea of finding energy loss in convection loss, one can find energy loss of radiation by

$$\Delta E_{rad} = bead\ area\ of\ peak\ temperature\ *\ Q_{rad}$$

$$\Delta E_{rad} = 300\ mm^2\ *10^{-6}*73{,}263\ \frac{W}{m^2}$$

$$\approx 21\ W\ or\ J/s$$

Therefore, energy loss for convection is equivalent to $21\ W$

Compared the value of energy loss from convection, radiation, and conduction to each energy used to create bead, dilution, and HAZ,

$$\Delta E_{bead} = 1.45\ kW$$

$$\Delta E_{dilution} = 0.30\ kW$$

$$\Delta E_{HAZ} = 0.25\ kW$$

And in terms of energy losses:

$$\Delta E_{Conv} = 0.01 \; kW$$

$$\Delta E_{Rad} = 0.02 \; kW$$

Although with these two energy losses seem not high. However, if including laser wall plug efficiency and reflectivity of titanium material, only 7.1% was used to create observable microstructural changes.

5.1.3.2 P-V mapping study

Furthermore, the p-v mapping study of nickel alloy 625 cladding with LHW was completed. Dilution and bead profile of cladding are strongly relevant to laser power, hot wire power, travel speed, and welding patterns (Stringer and weave patterns).

For stringer welding pattern, in case of laser and wire travel in a single straight direction, the amount of the dilution was found to rely on laser power, hot wire power (electrical source), and also travel speed as shown in Figure 5.1.3.1.
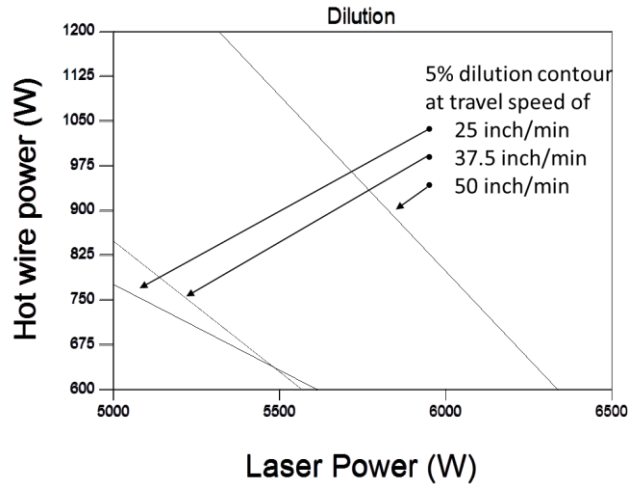
Figure 5.1.3.2.1 Laser and hot wire power space to obtain Inconel 625 overlays with <5% dilution at various travel speeds [4]

On the other hand, for weave pattern, this is where laser and wire were directed in oscillate perpendicular pattern to the travel direction. Thus, dilution for weave pattern was discovered to depend on amplitude, laser power, and hot wire power, as shown in Figure 5.1.3.2.1.
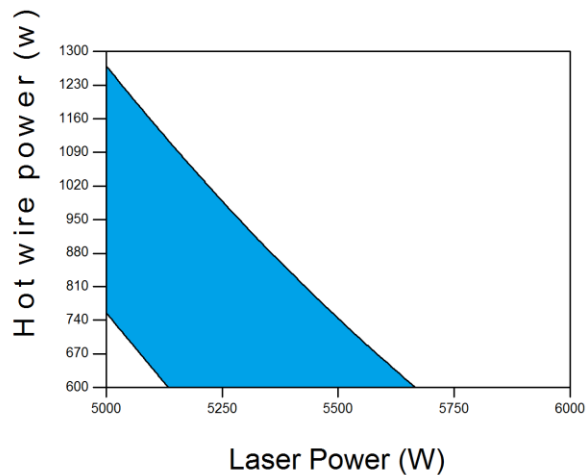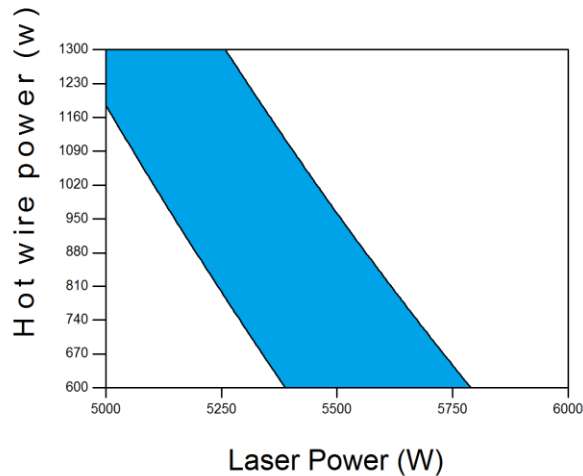
Figure 5.1.3.1.2 Laser and hot wire power range (filled in blue) to obtain nickel alloy 625 overlays with <5% dilution at (Top) 6mm and (Bottom) 12 mm weave amplitudes, respectively

The two graphical representation above shows consistent result for welding parameters that influence to dilution percentage. As can be seen above, to accomplish less than five percent dilution in weave pattern in nickel alloy 625, an appropriate range of hot wire power and laser power needs to be used according to the results of the above experiment. The blue range that shows in the figure 5.1.3.1.2 demonstrates a good range to use these two powers in order to get low dilution (<5%) at 6 mm and 12 mm respectively.   Compared these two pictures, one can conclude that, with wider weave, more energy of laser and hot wire powers can be used to achieve similarly low dilution. As in the 12 mm weave graphical representation, laser power can be used up to roughly 5,750 W and hot wire power can be used up to 1,300 W while at the 6 mm weave, less of two power sources were applied to get low dilution.

5.2 Grain size measurement

5.2.1 Ti-6Al-4V

After grain size measurement of both LHW and laser powder bed processes have been performed. According to the results from section 4, it is found that the average columnar grain size of the test part created by LHW process (roughly 240 micron) is bigger than that created by EOS machine (approximately 160 micron). This is simply because power input used by the LHW process (6,000 kW) is higher than that of the laser powder bed process with EOS machine (3,200 kW). From this research, this implies that the higher heat input utilized, the bigger grain size will be. This result is relatively consistent to Muthupandi (2003) [162].

Furthermore, as stated before, very limited grain growth or grain coarsening is preferred for a better mechanical properties of the structure and it also decreases the probability of internal strength-limiting structural defects [163, 164]. Specifically to this research, this concept of grain growth has been applied also. A series of upper, middle, and lower micrographs of both process are organized and compared to investigate whether there is any significant grain growth in the specimens or not. So, a series below demonstrate top, middle, and low level of microstructure of the test part by the LHW process.
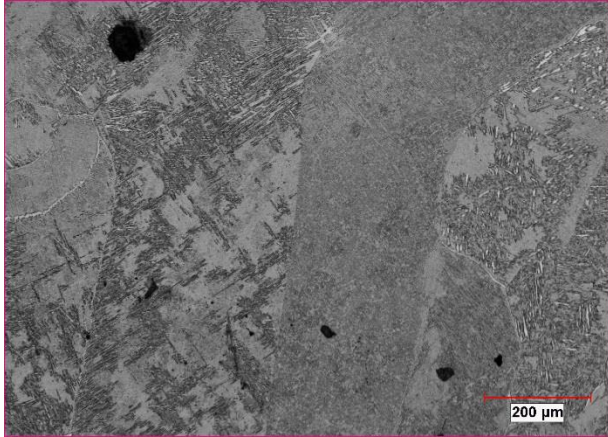
Top area of the part
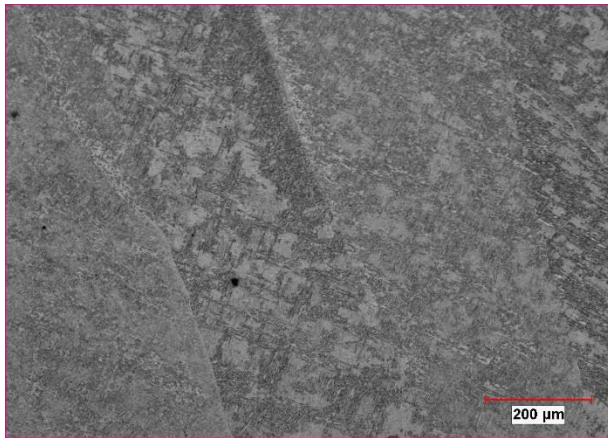
Middle area of the part
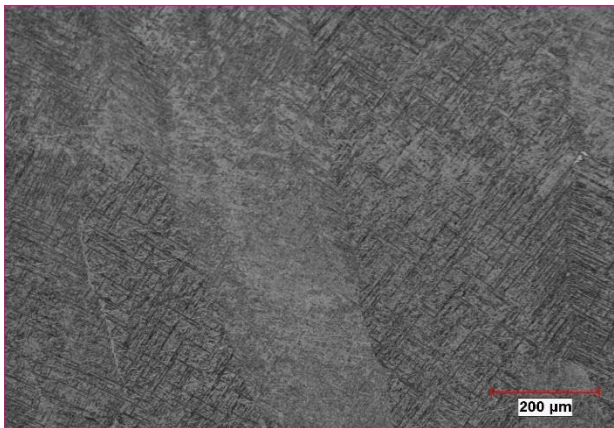
Bottom area of the part

Figure 5.2.2.1. Microstructural pictures showing top, middle, and bottom areas of the LHW demonstration part which have similar columnar grain size (240 micron)

Also, another series below demonstrate top, middle, and low level of

microstructure of the test part by the laser powder bed process.
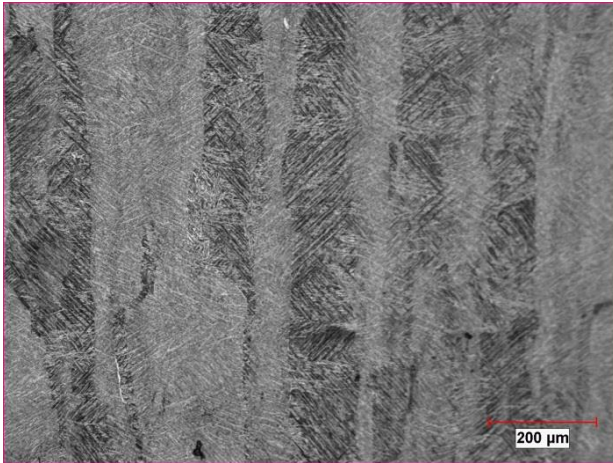
Top area of the part
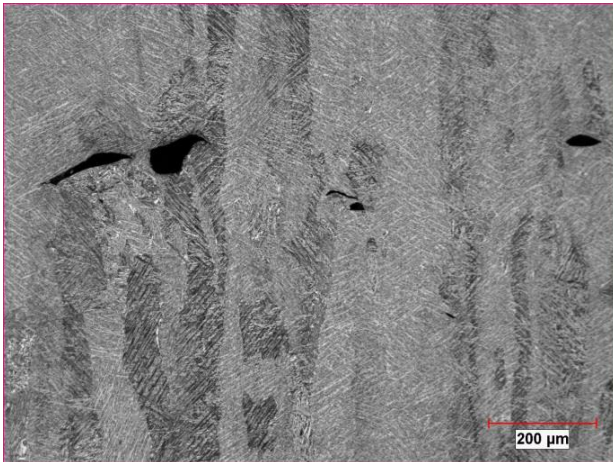
Middle area of the part
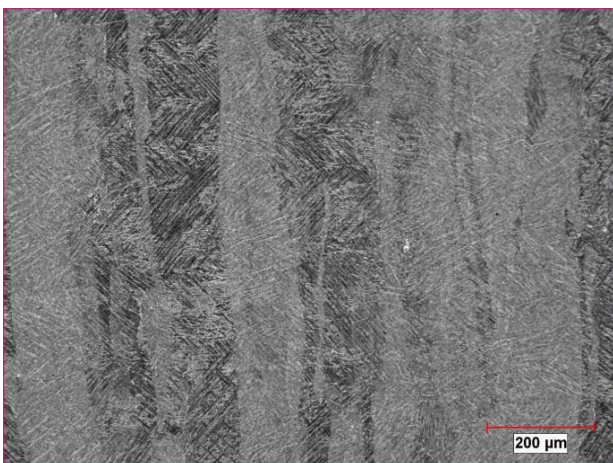
Bottom of the part

Figure 5.2.2.2: three microstructural pictures showing top, middle, and bottom areas of the EOS demonstration part which have similar columnar grain size (160 micron)

From the figure 5.2.2.1, figure 5.2.2.2 and the result of grain size measurement, it was found that there is no significant columnar grain growth between top, middle, and bottom part of the cross-sectional test part created by both processes. According to the concept of grain growth, this result is satisfactory and also provides an opportunity for the specimens to obtain good mechanical properties. The term of good mechanical properties imply that the mechanical properties of the specimen are comparable to those of the base metal. This is because grain size is similarly equivalent regardless of any positions on the test part.

5.3 Mechanical properties

5.3.1 Ti-6Al-4V

As demonstrated in the result section of mechanical properties, both processes are achievable in yield strength and ultimate tensile strength compared to the Ti-6Al-4V ASTM F136 standard. However, elongation of specimens built by LHW process showed less value than the standard. With these results, even though they showed strongly good mechanical properties in strength, they lead and consistently confirm cracking problems occurred in the specimen. From these literature [165, 166, 167], they all have evidences to support that more oxygen content strongly influences microstructural and mechanical properties of titanium alloy material. This is because more oxygen content in the interstitial site help accomplish desired strength and fatigue performance [168]. Nevertheless, this result comes with the expense of low ductility of the beta alloy causing more brittleness even post heat treatment is applied.

Since there is a large volume fraction of the alpha phase compared to beta phase in Ti-6Al-4V, it is believed to be dominantly responsible for final mechanical properties in the material such as age-hardening of Ti-6Al-4V is presumed to alter by microstructural changes in the alpha phase [169-171]. However, some other literature demonstrated that beta phase also influences to microstructure and mechanical properties as well [172]. Thus, as Ti-6Al-4V is a two phase alpha-beta titanium alloy that is close to alpha side, the material will certainly get effect from oxygen as it is an alpha-stabilizing element even a small portion of oxygen has been added.

In increasing oxygen content, the phase ratio changes toward more alpha and influence the transus temperature between alpha and beta to be raising up. Since oxygen elements are small, they can contaminate the titanium alloy by locating on interstitial sites in the crystal lattice and prohibit the movement of dislocations. Thereby, the oxygen elements help increase strength and hardness at the expense of more embrittlement and less ductility [167]. The graphical representation below show a result of higher hardness when more oxygen weight percent is high.
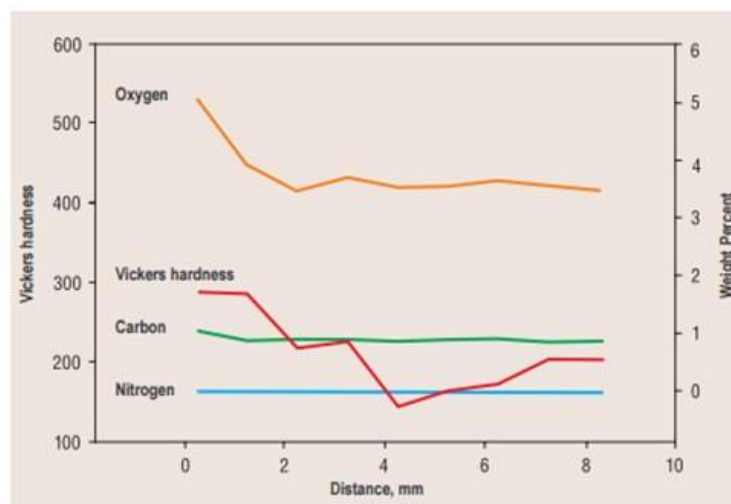
Figure 5.3.1 Vickers hardness and impurity content profiles down the centerline (from top (0 mm) to bottom) of titanium alloy weld [173]

According to [173], a specimen that contains high oxygen weld (0.437 wt%) demonstrates cracks from the bend test and Vickers microhardness indentations which does not occur in low oxygen weld specimen. Moreover, as can be seen below, the table shows that high oxygen weld tends to have lower bend strength. This is relatively correlated to our mechanical result where strength increases at the expense of ductility.

Impurity content (wt%)	Low oxygen weld	High oxygen weld
Oxygen	0.19	0.437
Nitrogen	0.05	0.392
Bend strength, MPa (ksi)	73.3 (10.6)	27.5 (4.0)

Table 5.3.1 Properties of titanium weld for low and high oxygen content [173]

Furthermore, as [174] discussed, when titanium alloy is exposed to air and moisture at temperatures exceeding 500 C (930 F), it will start to pick up oxygen, nitrogen, carbon and also hydrogen. These small atoms in the interstitial site located between titanium atoms and inhibit plastic deformation. Then, it cause increasing strength and decreasing ductility. If high contamination occurs, cracking can ensue from the stresses formed during welding processes especially with the alpha phase titanium alloy [174].

Moving to preliminary solutions to help avoid contamination cracking, minimizing exposure of molten pool and the heated weld region is appropriate to

execute and can be done by supplying enough inert gas shielding to the torch, weld

pool, and back of the joint and also degreasing the joint prior to welding if needed.

5.4 Chemical analysis

5.4.1 Ti-6Al-4V

This section is significantly related to the previous section (mechanical

properties) in terms of showing cracking in Ti-6Al-4V material. As being illustrated in the

chemistry results, oxygen concentration was found to be more than acceptable rate in

cracking build-up of Ti-6Al-4V.

From the result, compared bulk section to near intersects and surfaces section,

there is a slight difference of both oxygen and nitrogen concentration between these

two sections. As can be seen below, oxygen and nitrogen contents have been found

more near intersects and surfaces of the part compared to bulk section.
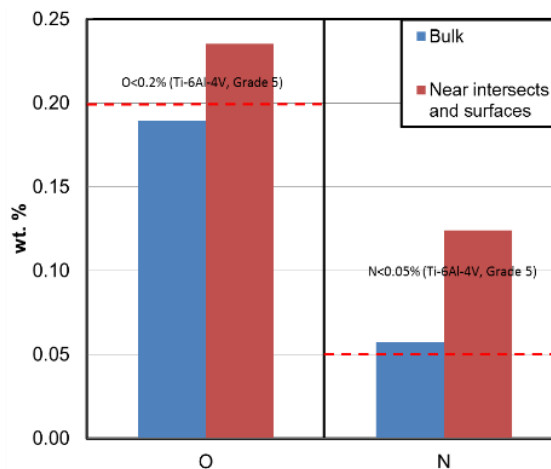
Figure 5.4.1: Average oxygen and nitrogen contents measure from Ti-6Al-4V LHW test part (Blue) bulk

section (Red) near intersects and surfaces section

Table 5.4.1: table below showing numerical value of average oxygen and nitrogen contents of bulk and near intersects and surfaces area of Ti-6Al-4V part with LHW process

Interstitial contents	ASTM F136 standard	Bulk area	Near intersects and surfaces area
Oxygen	0.20%	0.18	0.24
Nitrogen	0.05%	0.06	0.13

This is because, during the process at the temperatures higher than 550 C, the titanium build-up starts to pick up surrounding contamination (including oxygen and nitrogen) and the first place to pick those up is at the top of the weld metal pass. This clearly can be observed as the color of the surface turns to yellow from silvery. It can also be seen in microstructure [190]. Additionally, near intersects or between layers, sometimes other technical problems with laser hot wire process can interrupt process leading the part to pick up more contamination during fixing.

For instance, at the beginning of building up a layer, as known that in LHW process uses electricity to heat up wire and laser as two main heat sources, running the wire and laser at the same time can cause the wire to not completely melt and leave a twist of the wire on the surface. This problem sometimes forces the process to stop and needs to open an argon chamber that is already covered with argon gas. After the part is exposed to surrounding while it is still at high temperature, more contamination can be occurred. So, the solution that was used in this experiment is to run and start moving the laser first at approximately a quarter of an inch and then followed by run the wire.

This way the laser have time to create a melted weld pool for the wire to be fed in at the start point and allow the wire to be entirely melted. This techniques was also applied at the end of each layer by stopping the wire first then followed by laser.

Moreover, with titanium that is sensitive at high temperature, using too high laser power/resistively heated wire power can cause the melt pool during the build unstable. Meaning that melted titanium tends to get away from the weld puddle due to a small surface tension instead of maintaining itself in the weld puddle, re-solidifying, and cooling off. With this abnormal situation, unstable melt pool is able to cause arcing during the process and then lead to a colloquialism called "noodling" where a part of unmelted wire is stuck on the surface of the build-up layer because wire gets pushed back from the unstable melt pool and cannot be melted by the time laser was radiated. This certainly can affect desired mechanical properties and can lead to welding defects which will be discussed in the next section. From this experiment, titanium is found to have low range of laser and hot wire power to operate during the process in order to control stability in the weld melt pool.
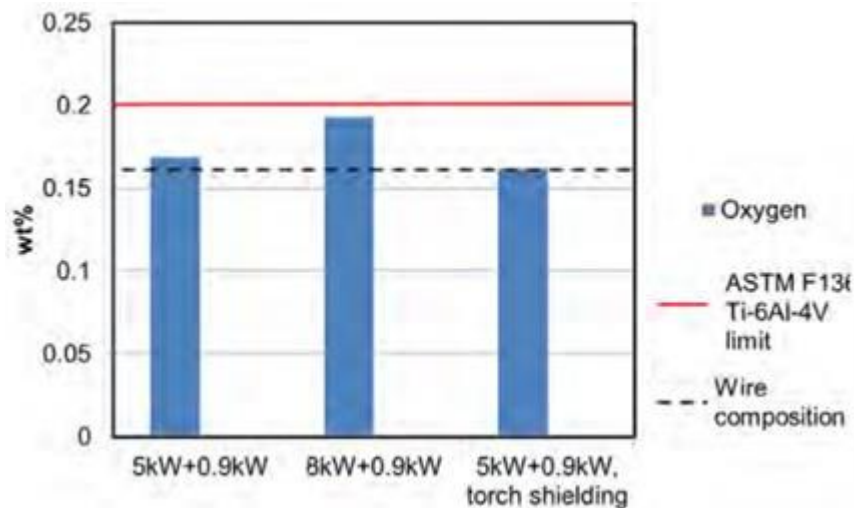
Figure 5.4.2: Oxygen contents in LHW test part using argon chamber and (left and center) without torch shielding and (Right) with torch shielding
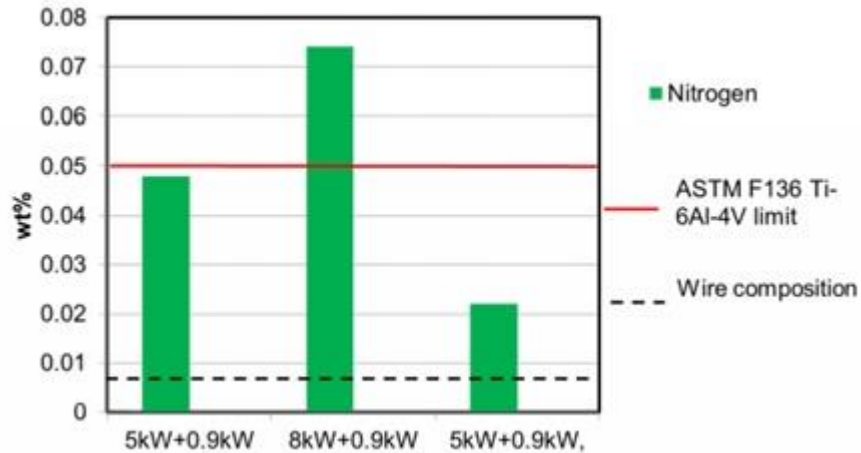
Figure 5.4.3: Nitrogen contents in LHW test part and (left and center) without torch shielding and (Right) with torch shielding

Furthermore, as shown in figure 5.4.2 and figure 5.4.3, average result of oxygen and nitrogen concentrations demonstrate that with torch shielding used during the LHW process, less contamination can be gained which also affects to better mechanical properties and likely less cracking.

Another interesting point from these two figures is they show that using higher laser power from 5 kW to 8 kW influences the Ti-6Al-4V specimens to pick up more oxygen and nitrogen concentrations. This result is consistent to what has been discussed in the previous section (Section 5.3) where unstable weld pool can lead to arcing, a part of wire stuck on the surface and also worse mechanical properties. In addition to the unstable weld pool issue, there is a literature by X. Cao et al. (2005) [175] states that high beam laser power (at 6 kW) led to more spattering and less weld quality compared

to a lower laser power. According to the idea summarizing in the previous section, the

unstable weld pool due to spattering, can leave the wire unmelted and create arcing.

This arcing then blows argon gas surrounding away permitting more oxygen

concentration to get into the titanium lattice. Eventually, high oxygen concentration

leads to poor mechanical properties including cracking problems [176].

5.5 Flaws and defects

5.5.1 Laser powder bed process
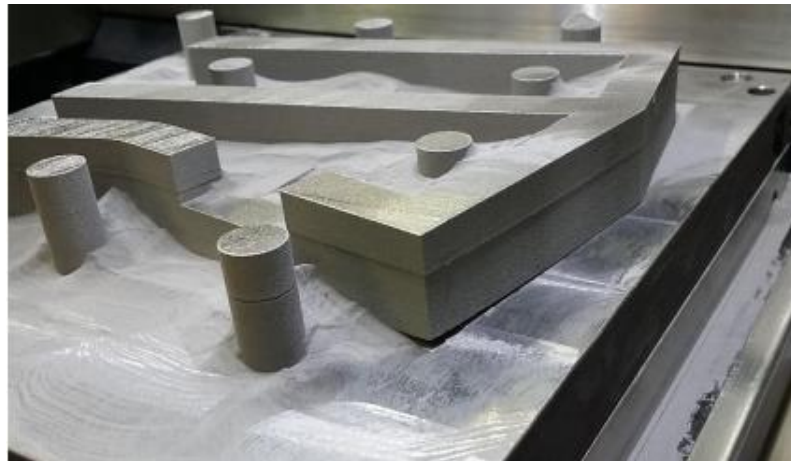
Figure 5.5.1.1 Ti-6Al-4V build-up lifted off from its substrate approximately 0.25 inch

Due to high temperatures (80 degrees Celsius recorded at the build plate), heat

transfer, and stresses during welding, part started to lift up off the build plate more

noticeable in the front right hand section. The lifting up eventually caused the recoater

arm to jam. During the recovery process, the temperature of the part dropped back

down to normal build plate temperature of 35 degrees Celsius causing a noticeable

deformation /stepping effect.

The first build and chamber were completely cleaned. The build plate was

prepared for removal. Upon removing the build plate mounting bolts it was noticed the

build plate was warped up approximately .250" due to high temperatures, heat transfer,

and stresses during welding the first build.

The build plate was flipped completely over and calibrated to begin the second

build. The plate was leveled as best as it could be considering the amount of warping

from the first build. The second build was started and within a couple layers the welds

looks much worse because of the un-level build plate. The trapped oxygen under the

flipped over build plate caused the oxygen level to rise above the programmed safety

level and caused an error during the weld and the build could not be resumed.
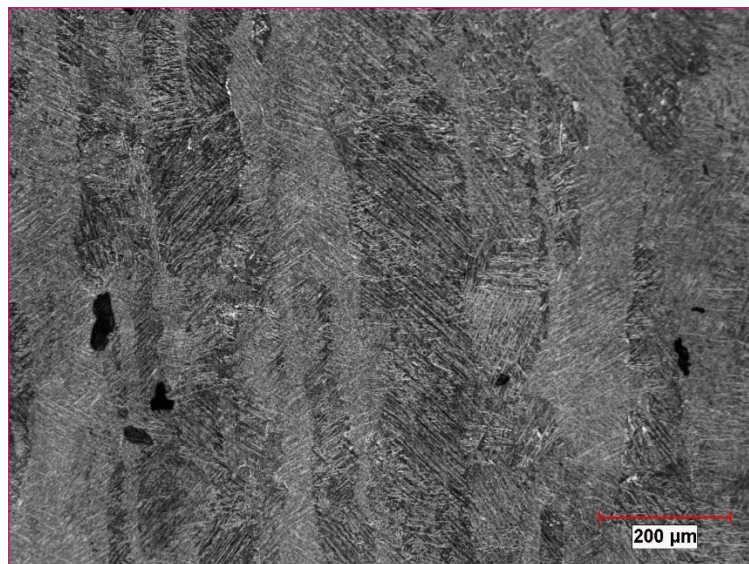
Figure 5.5.1.2: lack of fusion between layers of the titanium demonstration part made by EOS machine

Furthermore, as shown in figure 5.5.1.2, in some area of the part, such as areas in between boundaries of two weld layers, suspected lack of fusion in weld joints were discovered. From the result of the experiment, even there were not a lot of them occurred, laser power and scan speed are main welding parameters that need to be optimized to solve lack of fusion problem [177, 178]. In this case, it could be too low laser power was used, so the material was not completely melted when stacking up in previous layer.

5.5.2 Flaws and defects of test part created by LHW process

5.5.2.1 Oxidation effect

In Ti-6Al-4V, as discussed in the result of Ti-6Al-4V specimen, it was found that cracking occurred during the process was from too much oxygen and nitrogen in the interstitial site of the specimen. This confirmed by the result of chemical analysis as shown in the section 5.4.1. In this section, more discussion about this issue will be provided.

As well-known from the result, titanium is easy to combine with oxygen. When the temperature is above 540-800 C, it tends to form titanium oxide because the surrounding environment can penetrate into the surface of titanium alloy. This happened also in this experiment during Ti-6Al-4V LHW process. In determining oxide layer preliminarily, other than performing chemical analysis, surface discoloration is an excellent alternative to provide a good indicator of the degree of atmospheric contamination.

182

Figure 5.5.2.1.1 Titanium weldability color chart from (1) which is the best to (8) which is the worst in terms of good mechanical properties (less oxide layers) [64]

A shown above, according to [179-181], there are several colors in titanium welding that can be found based on contents of oxide layers attached in titanium alloy welds. Under perfect shielding conditions, appearance of the weld should be bright and silvery in color as can be seen in number one on the very top left of figure 5.7.2.1. Besides, it is normal to see-discoloration at the outer edges of the weld (HAZ) in both cases from number 1-8. However, it is not as significant as discoloration at titanium weld bead itself [180]. In the figure 5.7.2.1, oxide layers or contamination increases as the labeled number increases. So, it is clear to see that as contamination augments, the color changes from silver to a light straw color, then dark straw, dark blue, light blue, grey and eventually a powdery white.

According to this [179-180], the light (2) and dark straw (3) contains light

contamination which is still acceptable. Dark blue (4) contains more contamination and

maybe acceptable depending on service operations and conditions. Other than that,

they are hardly acceptable since they have too much contamination. This is just only

single-pass welds. In addition to multi-pass welds, the contamination can influent any

subsequent welds, so more inspections of each pass should be investigated.
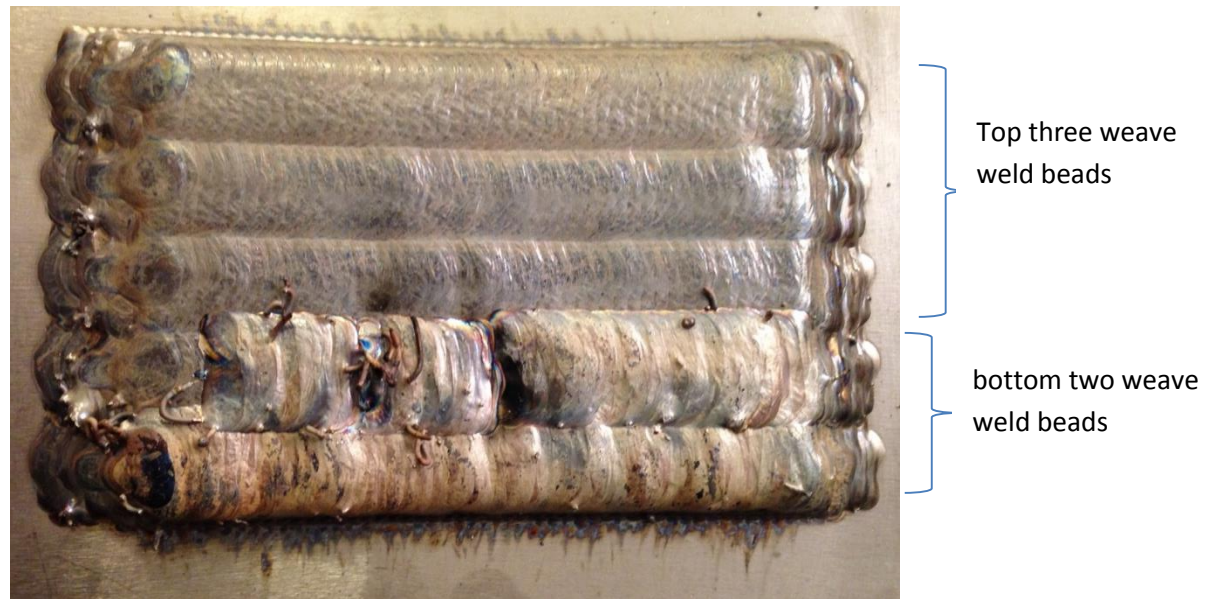
Figure 5.5.2.1.2 Ti-6Al-4V build-up created by LHW process showing first top three layers with silvery

and bright appearance while the two bottom layers are more in powdery white indicating more oxide

susceptibility. In this case, laser power equals to 5,500 W, hot wire power equals 400 W, wire feed

speed equals to 260 inch per min, and travel speed equals to 8 inch/min at 1.7 Hz for frequency of the

weave and weaving amplitude is 11mm.

With this discoloration theory, if it were to apply in this experiment where Ti-

6lAl-4V specimen was built by the LHW process, one can find that the theory does make

sense in this case. As shown in figure 5.7.2.2, the top three weave beads which was

shielding in argon gas during each weld pass demonstrated bright and silvery appearance in their weld beads whilst the bottom two weave beads showed their appearances more into powdery white. Even the similar gas shielding and surrounding environment were used, the bottom two weave beads did not get covered from argon gas shielding long enough. With the theory, one can preliminarily suggests that titanium oxide layers are formed in surface of the bottom two weave beads more than the top three weave beads based on the surface discoloration discussed. Although, this methodology is proved to be accurate at some level. More consistent analysis, such as chemical or mechanical testing, are still required to confirm about oxidation formed in titanium welds.

Regarding with the cracking issue, mechanical properties investigation was also conducted to check consistency with the discoloration theory. According to [182], when a thin layer of hard and brittle titanium oxide is formed, the titanium alloy specimen shows excellent yield and tensile strength at the expense of more brittleness (less elongation). This effect can decrease the corrosion resistance of titanium alloy [182]. When low brittleness is exposed to the highly focused laser beam during welding, tension forces of the laser can create the formation of cracking.

During the process, when the laser beam moves ahead, the surface is subjected to a rapid cooling process from the heat conduction and the cooling of gas flow effect. This forms a quenching effect and makes the surface cool down quicker than the matrix material. This brings to tension stress occurred and when it goes over the yield stress, cracks can be formed since titanium oxides support more brittleness [182].This is

obvious to mechanical result shown in section 4.3.1 where specimen of Ti-6Al-4V created by the LHW process shows higher strength and lower ductility compared to the ASTM F136 standard of Ti-6A-4V.

Furthermore, with the part shown below, there was an accomplishment to build Ti-6Al-4V build-up on both sides and maintain the substrate to be flat after the LHW process. This is because a balance of high thermal stress was maintained during the build. The key way that was used is to build and flip the substrate every other 2 layers from one side to the other side. In other words, first two layers are being built on one side, the substrate got flipped, and then the next two layers are being built on the other sides. The strategy was remain using until the part is done successfully. Nevertheless, some cracks on both sides of substrate were still found due to high content of oxygen and nitrogen which were discussed in 5.3 (mechanical properties) and 5.4 (chemical analysis). Additionally, these cracks all seemed to appear at either the intersection of passes or at the stop point of a weld. It is possible that the cracks formed due to the slower travel speed and increased heat, which caused an increase in the residual stress at those points.
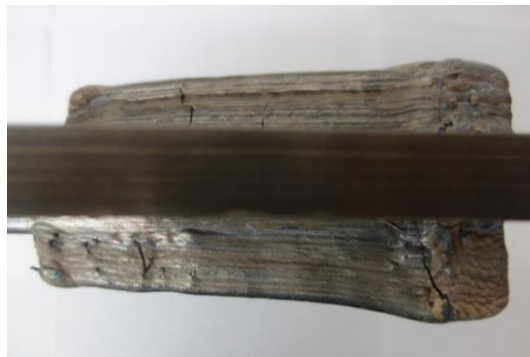
Figure 5.5.2.1.3: the test part showing both sides of build-up created by LHW process with flat substrate

6 Conclusions

With all of constructive results and discussions on this project, there are several main conclusions that should be drawn to help reader understand and take profits from reading the thesis. They are summarized as follows:

1. Regarding to Ti-6Al-4V material, either Laser hot wire or laser powder bed processes, they both provide imperfect part and contain their own problems developed during/after each process. On one hand, for LHW process, it seems to contain too high interstitial content of oxygen and nitrogen. This confirms by chemical analysis and mechanical properties testing and it is a main reason for cracking in the LHW process. The preliminary solution is to use gas shielding protection which is argon in this case. A chamber flooded with argon gas for a certain period of time and also trailing gas shielding set up at weld nozzle are applied in building each layer during the process. This solution turns out to a better result of contamination by oxygen and nitrogen. On the other hand, for the laser powder bed process, high thermal stress is a main problem causing distortion of the substrate and peel-off delamination between the part and its substrate. To deal with the problems, a small change in design, such as add a small radius (fillet) to the base of the part or rotate the part in CAD file to not be straight to the recoater blade (avoid slamming between recoater arm and the part), would be helpful not only to help transfer heat but also reduce stress during the process.

187

2. Compared to the powder bed process, the result from this research is demonstrated that the build rate of LHW process is much higher regarding the same volume of a part. Additionally, more energy efficiency can be obtained by the LHW process as well according to the comparison result. In terms of microstructure, both processes provide similarly fine microstructure and comparable mechanical properties.

3. For nickel alloy 625 built by LHW process, the nickel alloy overlays is proved to be acceptable to use under corrosive environment with the standard of ASTM G28. With one and two layers cladding on the substrate with similar composition, the overlays showed a greater result in corrosion rate compared to acceptable rate derived from industry used and other related literature.

7 Future work

Similar to any other projects, there are some room for improvement to be applied regarding to this project in order to obtain better understanding and result which certainly could be useful for any future related projects. Some recommendations are as follows:

1. For Ti-6Al-4V material built by LHW process, contamination of oxygen and nitrogen is believed to be a main reason for cracking in the experimental specimen. More investigations on contamination should be extensively conducted. In this particular research, only one methodology used to measure oxygen and nitrogen level had conducted after the part was completely created and cooled down by cutting up and investigating the specimen's microstructure. Although this methodology is sufficient, investigations during the process would also be helpful for consistent manner of the result. For example, during the process, oxygen content or other compositions can also be roughly measured by the oxygen/other composition meters/sensors or as a proxy of argon gas and air combination to ensure that contamination level is still acceptable based on current welding parameters used.

2. Extended to the first suggestion, apart from composition measurement during the process, it might be valuable to consider measuring temperature of the build-up, in the weld pool, or other positions in surrounding areas. This

189

will help us in recording how much temperature when it goes to the highest peak point in heating up and lowest point in cooling down. Knowing the temperature in each stage can help researcher to define a firmly and consistently strategic plan to obtain a desired result. For example, researcher/operator can specify a certain temperature to cool down and/or set a certain time to wait between each layer. This suggestion should provide more consistency to the part in terms of shape and mechanical properties.

3. For Ti-6Al-4V created by laser powder bed process, high thermal stress due to high temperature seems to be a problem in this case resulting the specimen to be warped and had peel-off delamination between build-up and substrate. In order to gain a success build, not only thermal heat transfer needs to be taken care of but also a good foundation of first few layers built is found to be important. Therefore, in design process, minimizing blunt sharp walls would be better. This will help the recoater arm (powder plowing arm) to plow powder across more smoothly. One way which is usually used to reduce sharp walls is to create a small radius at the base of the part (fillet). This should help transfer heat during the process and reduce stress due to sharp transition as well. With a small change in design process, a successful build-up should be possible to create.

8 Appendices

8.1 Appendix I - Procedure in of LHW process

In the experimental methodology section, all descriptions are made to be understandable and concise enough for readers to understand basic and idea of how to perform experiments in this thesis with LHW process. However, in this appendix, more details will be described thoroughly in order to provide a guideline for those who would like to follow and obtain similar results as shown in this thesis.

In this experiment of LHW process, the laser system isYLS-15000 IPG photonics fiber laser and the robot model is FANUC robot M-710ic-50. Both were used for the entire project in all experiments to fabricate specimens from Ti-6Al-4V and nickel alloy 625 wire created by The Lincoln Electric Company. In laser system, a Yb-fiber laser at 1,070 nm in wavelength was used. Power wave S500 model is welding power supply which was used to pre-heat wire in LHW process. Wire size in both materials is 0.045 inch (1.14mm). Every specimen was fabricated on the fixed table system and built on pre-existing substrate (base metal) by the robot welding machine. In Ti-6Al-4V, substrates used have the same composition to wire. In nickel alloy 625, iron substrates were used.

While programming part is very important in controlling the robot machine to weld, move, and follow orders, this appendix will not specifically talk about programming in details as there are many techniques and knowledge involved which is out of the scope. Besides, welding knowledge and skills are good to have in order to

obtain understanding and more balance in creating AM parts by LHW process. All of AM

parts built by LHW process were fabricated by The Lincoln Electric Company.

In each layer, after finishing the deposit, waiting time is about 5 minutes to let

the deposition cool down. After that, in argon box, argon diffuser was used to diffuse

argon gas at about 5 minutes at 60 cubic feet per hour (CPH) or 1.7 m^3/h. This means

about 10 mins was spent in each layer to wait it cool down and diffuse argon gas to use

in the next layer. Only a processing time of depositing one layer is about 1-2 minutes.
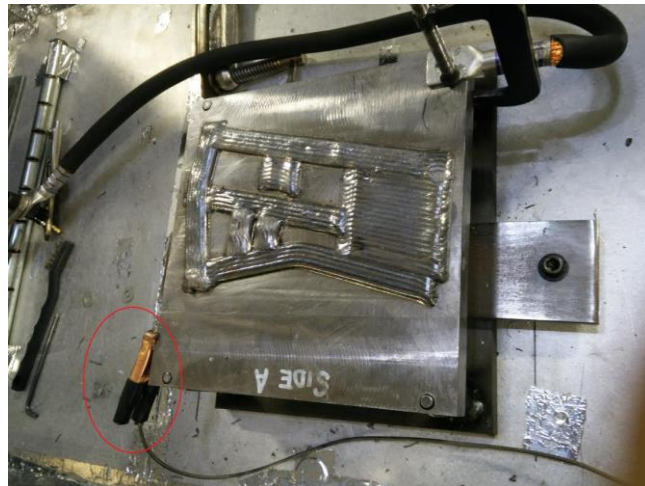
Figure 8.1: A photo of LHW process set-up showing substrate, a part of build-up, argon diffuser, ground cable with clamp, and sensor lead (circled in red and used for monitoring voltage feedback)

For demonstration part with several features on substrate at size 10 inches times

10inches, it took about 40-50 hours to complete the entire part (two-sides build-up). It

would take less than that for just simple build-up or a few layers of stringer bead and/or

weave pattern.

More than 50% of the experimental time were used to wait the material cool

down and argon gas to be ready to cover the build part. Even it slows down the process,

but it is very important to strictly use argon gas to gain less oxygen and nitrogen contents in order to get desired mechanical properties.

8.2 Appendix II – Ultrasonic C-Scans for LHW process

In terms of inspection, ultrasonic test instruments have been selected and used to investigate inside test parts in this project. The ultrasonic instruments use high frequency sound waves to check approximate location of internal structure of the test parts including measuring distance away from its indexing surface (thickness).

To perform non-destructive evaluation (NDE) using ultrasonic instruments, it can be either single active element or two paired elements that transmits and receives high frequency sound waves. There are several kinds of ultrasonic inspections such as A-Scan, B-Scan, and C-Scan.

Specifically in this project, C-scan have been used to inspect internal structure of the build-ups. There are 2 modes that are used which are time of flight (TOF) and amplitude modes. These two modes were used simultaneously to work together and increase efficiency of inspection.

On one hand, the amplitude mode is used to measure reflectivity in all area of the test part by setting a gate to target destination of the sound wave. With this mode, it results reflectivity in all areas and each area is differentiated by different colors. As can be seen below in figure 8.2.1, the color scale is used in this case. On left hand side, red

color tells most reflection while blue color indicates the least reflection.

Figure 8.2.1 Blue-to-red color scale used to indicate depth or percentage of reflectivity in specific area

After getting the reflectivity, the location of biggest reflectivity (Strongest signal or color is red) is then used in time of flight (TOF) mode to further perform analysis. For the TOF mode, it is used to measure distance in a unit of time by counting time from transmitting on the indexing surface until the sound wave gets back to the surface from reflection. In this case, color scale above is applied also. However, it is translated in different meaning although the same color scale is used. In TOF mode, the color scale is utilized to differentiate measured distance by indicating red color as the furthest distance and blue color as the nearest distance regarding to indexing surface.

All works below have been done by Alban Bakia, a senior NDT Level 3 Specialist, who works at Alcoa Titanium & Engineered Products. Therefore, in our case, we started from scanning on the front view of the part as shown below.
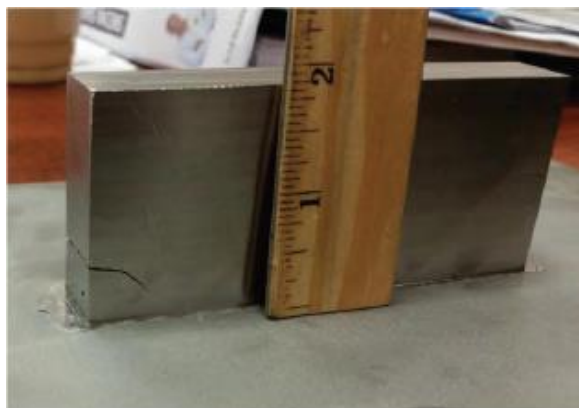
Figure 8.2.2: Ti-6Al-4V massive build-up (nominally 50mm x 150mm x 25 mm from which NDE and mechanical property specimens were taken
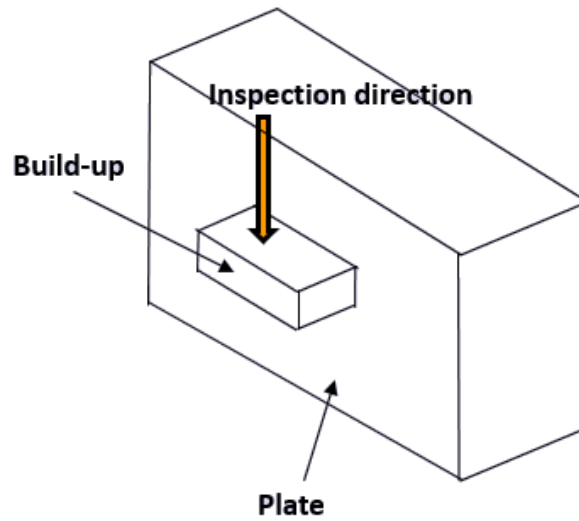
Figure 8.2.3: Schematic of scan direction of Ti-6Al-4V build-up for figure 8.2.4
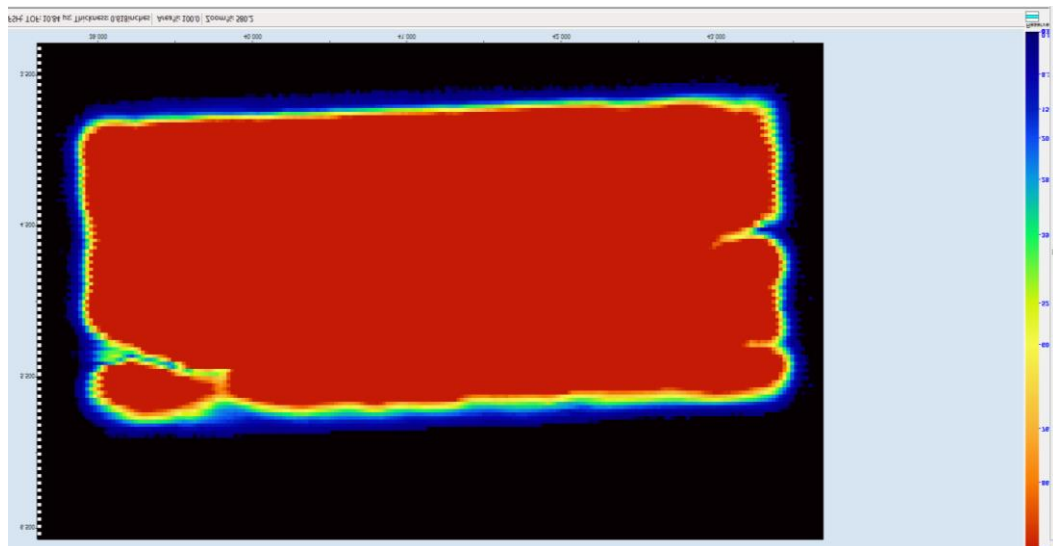
Figure 8.2.4: Screenshot of ultrasonic c-scan in amplitude mode showing obvious cracks on both sides which is related photo of the part in figure 8.2.2

In the figure 8.2.4, amplitude mode is firstly used. It is obvious to see that cracks occurred on both sides at different height and position. To make it easier, figure 8.2.2 and 8.2.4 can now be compared as figure 8.2.2 is a real photo of the build-up and figure 8.2.4 is the ultrasonic c-scan of the build-up. They both are in front view. Then, these cracks can be used as a control baseline to test what can be seen in top view below.

In addition to figure 8.2.4, this amplitude mode is used to see reflectivity of the whole part. Blue in the boundary is a leakage of the sound wave that is out of the boundary and it goes away in the water. Red color which is the most in figure 4 is the reflection from back wall (it goes to back wall and bounce back to the surface). This means the sound wave is able to go the set gate (back wall) and reflects back to indexing position at the surface.

Inspection direction

Ti-6Al-4V
build-up

Top of the wall
Bottom of the wall

Plate

Figure 8.2.6: Screenshot of ultrasonic c-scan in amplitude mode demonstrating high amplitude indications (red color) at various depths. All reflection in this case is in between front and back wall as shown in figure 8.2.5

After obtaining a scan from front view, figure 8.2.5 and 8.2.6 demonstrate top view of inspection direction of amplitude mode of the build-up. While figure 8.2.5 shows schematic of inspection direction, figure 8.2.6 illustrates reflectivity in amplitude mode of the Ti-6Al-4V build-up. As explained before, colors shown in this mode tell intensity of the reflectivity at various depths of the build-up. To explain colors shown in figure 8.2.6, blue is a leakage of the sound wave on the boundary. This is why it get the least reflectivity as indicated in blue. Yellow means something has been found inside the part that stays in about half way distance or in between front and black wall. This is probably because there is an imperfection between plate and the build-up. Red shows high amplitude reflectivity indications at various depth. With this information, it can be used to combine and understand the next figure (figure 8.2.7) which is the top view scan

in time of flight (TOF) mode.
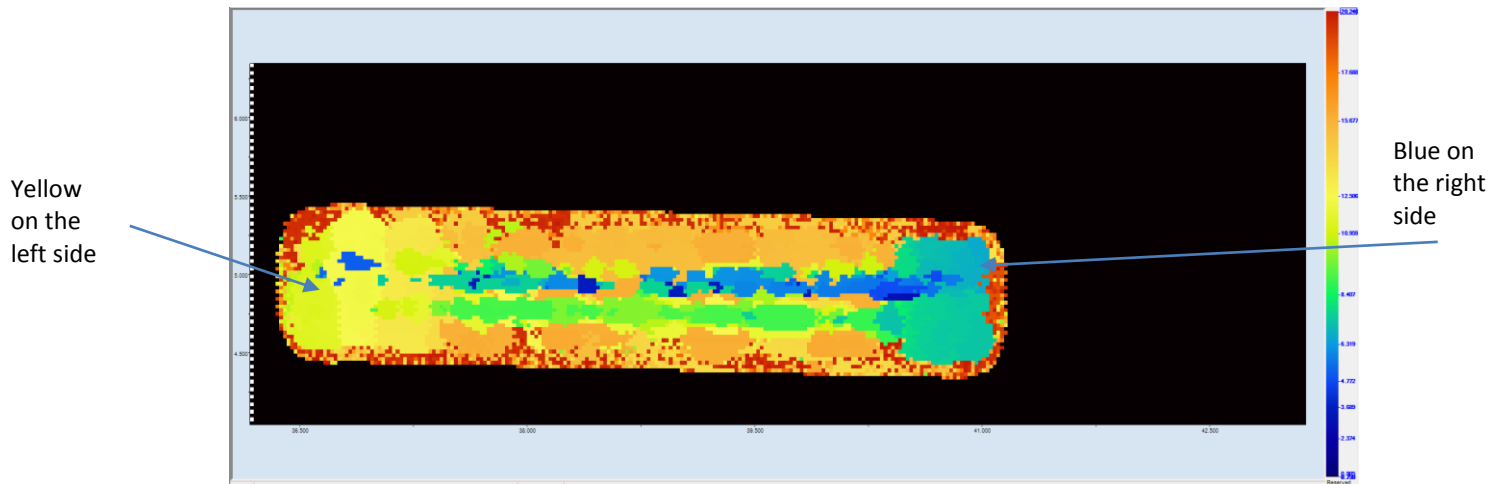
Figure 8.2.7: Screenshot of ultrasonic c-scan in time of flight (TOF) mode demonstrating top view similar to figure 6 and showing the depth of highest amplitude by different colors. On the left and right hand side, blue and yellow colors are used to indicate cracks respectively. This means that crack on the right side is closer to the indexing surface compared to the crack on left side.

For figure 8.2.7, the screenshot is shown in the top view of time of flight mode. This is the top view showing the highest amplitude from the amplitude mode in the figure 8.2.6. The depth of the largest reflection determines color. As can be seen, blue color on the right side represents the crack on right hand side which is relevant to figure 8.2.2 and 8.2.4. From blue color, one can conclude that the right crack is located around the middle area. For the left hand side, yellow color depicts the crack on the left. This means the left crack is further away from the indexing surface. This is very sensible as figure 8.2.7 can be compared to the figure 8.2.2 and 8.2.4 that distance from the top

(indexing surface) of the right crack is closer compared to the left crack.

Furthermore, in the middle of this figure, it is noticed that there is a blue and green color in the middle demonstrating that there is something reflecting the sound wave before reaching the back wall. In this case, it could be some defects, such as a lack of fusion occurred inside the part (not able to be seen by your eyes). Therefore, this inspection contributes value because it is able to find defects that is not able to be spotted by naked eyes. This is why it has been called "non-destructive evaluation" or NDE. Moreover, some of the orange and red areas are reflections from the back wall demonstrating that the emitted sound wave is able to get through internal structure to the back wall and reflects back to the surface without getting interfered.

9 References

1. What is Additive Manufacturing? Amazing. Retrieved from:

   http://additivemanufacturing.com/basics/

2. Additive Manufacturing definition. Royal Academy of Engineering. London.

   United Kingdom. Retrieved from:

   http://www.raeng.org.uk/publications/reports/additive-manufacturing

3. Katou, M., et al., *Freeform fabrication of titanium metal and intermetallic alloys by three-dimensional micro welding.* Materials & Design, 2007. **28**(7): p. 2093-2098.

4. Terakubo, M., et al., *Freeform fabrication of Ti-Ni and Ti-Fe intermetallic alloys by 3D Micro Welding.* Intermetallics, 2007. **15**(2): p. 133-138.

5. Mughal, M.P., et al., *Deformation modelling in layered manufacturing of metallic parts using gas metal arc welding: effect of process parameters.* Modelling and Simulation in Materials Science and Engineering, 2005. **13**(7): p. 1187-1204.

6. Song, Y.A., et al., *3D welding and milling: Part I - a direct approach for freeform fabrication of metallic prototypes.* International Journal of Machine Tools & Manufacture, 2005. **45**(9): p. 1057-1062.

7. Song, Y.A., S. Park, and S.W. Chae, *3D welding and milling: part II - optimization of the 3D welding process using an experimental design approach.* International Journal of Machine Tools & Manufacture, 2005. **45**(9): p. 1063-1069.

8. Taminger, K., *Electron Beam Freeform Fabrication.* Advanced Materials &

Processes, 2009. **167**(11-12): p. 45-45.

9. Wanjara, P., M. Brochu, and M. Jahazi, *Electron beam freeforming of stainless steel using solid wire feed.* Materials & Design, 2007. **28**(8): p. 2278-2286.

10. Zalameda, J.N., et al., *Thermal Imaging for Assessment of Electron-Beam Freeform Fabrication (EBF3) Additive Manufacturing Deposits.* Thermosense: Thermal Infrared Applications Xxxv, 2013. **8705**.

11. Domack, M.S., K.M.B. Taminger, and M. Begley, *Metallurgical mechanisms controlling mechanical properties of aluminum alloy 2219 produced by electron beam freeform fabrication.* Aluminium Alloys 2006, Pts 1 and 2, 2006. **519-521**: p. 1291-1296.

12. Murr, L.E., et al., *Metallographic Characterization of Additive-Layer Manufactured Products by Electron Beam Melting of Ti-6Al-4V Powder.* Praktische Metallographie-Practical Metallography, 2009. **46**(9): p. 442-453.

13. Brandl, E., C. Leyens, and F. Palm, *Mechanical properties of additive manufactured Ti-6Al-4V using wire and powder based processes.* Trends in Aerospace Manufacturing 2009 International Conference, 2011

14. Shea, William R., ed. (1983). Nature mathematized: historical and philosophical case studies in classical modern natural philosophy. Dordrecht: Reidel. P. 282. ISBN 9978-90-277-1402-2

15. Barbara K. Henon, PH.D., Arc Machines, Inc. and Michael D. Hayes, President, Acute Technological Services, Inc. Stainless Steel World, America 2002 Conference, Houston, Texas, February 2002

16. Welding Beads. Weldersuniverse. Retrieved from:

    http://www.weldersuniverse.com/welding_beads.html

17. Choosing a shielding gas for flux-cored welding. The Lincoln Electric Company.

    Retrieved from: http://www.lincolnelectric.com/en-us/support/process-and-

    theory/Pages/shielding-gas-for-flux-cored-welding.aspx

18. Saleh, B. E. A.; Teich, M. C. (1991). "Fundamentals of Photonics". New York: John

    Wiley & Sons: 521. ISBN 0471839655.

19. Fiber laser. Engineer review. Vol. 12 No.10. Feb 2013 Rs. 150. Retrieved from:

    http://content.yudu.com/Library/A23am4/EngineeringReviewFeb/resources/16

    4.htm

20. Duarte, F. J. (2003).*Tunable Laser Optics*. Elsevier Academic. ISBN 0-12-222696-8.

21. "Many lasers become one in Lockheed Martin's 30 kW fiber laser". Gizmag.com.

    Retrieved 2014-02-04.

22. H. Schultz. Electron beam welding. Abington Publishing (1993). Retrieved from:

    http://books.google.com/books?hl=en&lr=&id=AfaiAgAAQBAJ&oi=fnd&pg=PP1

    &dq=electron+beam+welding&ots=5OIhLhj0k7&sig=Ep5f6RP3EWi2zrflhq_rav52

    oSM#v=onepage&q=electron%20beam%20welding&f=false

23. Mikell P. Groover. Fundamentals of Modern Manufacturing: Materials,

    Processes, and Systems. 2009. Retrieved from:

    https://books.google.com/books?id=QU-

    Qvud3OvoC&pg=PA730&lpg=PA730&dq=electron+beam+welding+current+and+

    voltage+normal+use&source=bl&ots=yrOmO9TM0G&sig=95EVNMPpnAUzRpm1

JxM9ZluNPd0&hl=en&sa=X&ei=ex6JVIj-

HsWtyATe54H4Ag&ved=0CFEQ6AEwBg#v=onepage&q=electron%20beam%20w

elding%20current%20and%20voltage%20normal%20use&f=false

24. Dr. G. Schubert. Electron Beam Welding – Process, Applications and Equipment.

    Retrieved from: http://www.ptreb.com/Customer-

    Content/WWW/CMS/files/Electron_Beam_Welding_Process_Applications_and_

    Equipment2.pdf

25. Charlotte Weisman W. H. Kearns. Welding Handbook 7th version.1980

26. Liming, Liu, Wang Jifeng, and Song Gang. "Hybrid laser–TIG welding, laser beam

    welding and gas tungsten arc welding of AZ31B magnesium alloy."*Materials

    science and engineering: A* 381.1 (2004): 129-133.

27. Cui, H. 1991. Study of interaction between arc and focused laser beam and

    applicability of combined laser-arc technique. Thesis. Technical University

    Braunschweig.

28. Hybrid laser welding of pipes. Retrieved from:

    http://www.esab.com/global/en/education/Hybridlaser-welding-of-pipes.cfm

29. Zhou and H.L. Tsai. "Hybrid Laser-Arc Welding" Intech (2012): 1-32

30. French, I. E., & Bosworth, M. R. (1995). A comparison of pulsed and conventional

    welding with basic flux cored and metal cored welding wires.*Welding Journal-

    Including Welding Research Supplement*, *74*(6), 197-205.

31. Flux-cored welding. Retrieved from:

    http://www.weldersuniverse.com/advice.html

32. Horii, T., et al., *Development of freeform fabrication of metals by three dimensional micro-welding.* Designing of Interfacial Structures in Advanced Materials and their Joints, 2007. **127**: p. 189-194.

33. Flux-cored welding. Retrieved from: http://www.lincolnelectric.com/en-us/support/process-and-theory/Pages/flux-cored-overview-detail.aspx

34. Mukhopadhyay, S., & Pal, T. K. (2006). Effect of shielding gas mixture on gas metal arc welding of HSLA steel using solid and flux-cored wires. *The International Journal of Advanced Manufacturing Technology*, *29*(3-4), 262-268.

35. Liao, M. T., & Chen, W. J. (1999). A comparison of gas metal arc welding with flux-cored wires and solid wires using shielding gas. *The International Journal of Advanced Manufacturing Technology*, *15*(1), 49-53.

36. Atamert, S., and H. K. D. H. Bhadeshia. "Comparison of the microstructures and abrasive wear properties of stellite hardfacing alloys deposited by arc welding and laser cladding." *Metallurgical Transactions A* 20.6 (1989): 1037-1054.

37. A. Samant, E. Vogli, A. Sherman, and A. Ghidyal, "Corrosion resistant alloy cladding for the oil & gas industry using a high-density Infrared fusion cladding process" MesoCoat Inc., http://www.abakaninc.com/media/Cladding-Using-High-Density-Infrared-Fusion-Cladding-Process.pdf

38. Wanjara, P., M. Brochu, and M. Jahazi, *Electron beam freeform fabrication on stainless steel.* Thermec 2006, Pts 1-5, 2007. **539-543**: p. 4938-4943.

39. A survey of the U.S. commercial market, (June 2015). Retrieved from: Sciaky Inc. (Advantages of wire AM vs. Powder AM)

40. Sciaky Inc . Advantages of wire AM vs. powder AM. (2015)

41. Lincoln Electric Automation. Laser Hot Wire Cladding: How to know if it's right for your application. Retrieved from:

http://www.lincolnelectric.com/assets/US/EN/literature/mc13142.pdf

42. Choi, D. S., Lee, S. H., Shin, B. S., Whang, K. H., Song, Y. A., Park, S. H., & Jee, H. S. (2001). Development of a direct metal freeform fabrication technique using CO_2 laser welding and milling technology. *Journal of Materials Processing Technology*, *113*(1), 273-279.

43. Microstructural Evolution in Ti-6Al-4V Multi-Layer Builds Produced By Three Additive Manufacturing Processes; By S. Lathabai, M. Glenn, and D. R. Ritchie of CSIRO (June 17, 2014 AeroMat Conference presentation

44. Wire-feed additive manufacturing of metal components: technologies, developments and future interests; By D. Ding, Z. Pan, D. Cuiuri, and H. Li, 09 May 2015.

45. Dilution in arc welding. Retrieved from: http://www.helms-oiltools.com.cn/about-us

46. Lech Pawlowski,The science and Engineering of Thermal Spray Coatings, 2nd Edition, (2008): 1-656.

47. Kathuria, Y. P. "Some aspects of laser surface cladding in the turbine industry." *Surface and Coatings Technology* 132.2 (2000): 262-269.

48. Ghosh, P. K., P. C. Gupta, and V. K. Goyal. "Stainless steel cladding of structural steel plate using the pulsed current GMAW process." *Welding journal*77.7

(1998): 307s-314s.

49. Toyserkani, Ehsan; Stephen Corbin; Amir Khajepour (2004). *Laser Cladding*. Boca Raton, FL: CRC Press.

50. Kim, Jae-Do, and Yun Peng. "Plunging method for Nd: YAG laser cladding with wire feeding." *Optics and lasers in engineering* 33.4 (2000): 299-309.

51. Sexton, L., et al. "Laser cladding of aerospace materials." *Journal of Materials Processing Technology* 122.1 (2002): 63-68.

52. La Barbera, A., et al. "Electron beam cladding and alloying of AISI 316 on plain carbon steel: microstructure and electrochemical corrosion behaviour." *Surface and coatings technology* 46.3 (1991): 317-329.

53. Morimoto, Junji, et al. "Formation of a Cr 3 C 2/Ni–Cr alloy layer by an electron beam cladding method and evaluation of the layer properties." *Vacuum* 62.2 (2001): 203-210.

54. Abe, Nobuyuki, et al. "Formation of WC-Co layers by an electron beam cladding method and evaluation of the layer properties." *Vacuum* 59.1 (2000): 373-380.

55. Mathieu, Alexandre, et al. "Laser brazing of a steel/aluminium assembly with hot filler wire (88% Al, 12% Si)." *Materials Science and Engineering: A* 435 (2006): 19-28.

56. Kou, S., and Y. H. Wang. "Weld pool convection and its effect." *Weld. J* 65.3 (1986): 63s-70s.

57. Lv, S. X., et al. "Arc heating hot wire assisted arc welding technique for low resistance welding wire." *Science and Technology of Welding & Joining* 12.5

(2007): 431-435.

58. Possible causes of weld metal porosity. Retrieved from:

   http://www.thefabricator.com/article/arcwelding/22-possible-causes-of-weld-metal-porosity

59. K. Hori, H. Watanabe, T. Myoga, K. Kusano, Development of hot wire TIG welding methods using pulsed current to heat filler wire – research on pulse heated hot wire hot wire TIG welding processes, Welding International 2004 18 (6), pf. 456-468

60. TIG Hot Wire. Technical sheets. EWF. Retrieved from:

   http://www.ewf.be/media/documentosDocs/doc_85_tig_hot_wire.pdf

61. Barbara K. Henon, Avances in Automatic Hot-Wire GTAW (TIG) welding

62. Hori, K., et al. "Development of hot wire TIG welding methods using pulsed current to heat filler wire–research on pulse heated hot wire TIG welding processes." *Welding international* 18.6 (2004): 456-468.

63. Hybrid laser arc welding – Has its time finally arrived? Paul Denney. Lincoln Electric. Retrieved from:

   http://www.lincolnelectric.com/assets/US/EN/literature/mc1129.pdf

64. Liu, Wei, et al. "Real-time monitoring of the laser hot-wire welding process."*Optics & Laser Technology* 57 (2014): 66-76.

65. M. Kottman, S. Zhang, J. McGuffin-Cawley, P. Denney, & B. K. Narayanan, "Laser Hot Wire Process: A Novel Process for Near-Net Shape Fabrication for High-Throughput Applications," *JOM*, 67.3 (2015): 622-628.

66. Ruget G. "Manufacture of hollow cylindrical bodies ". US3789908A. Feb 5, 1974

    http://www.google.com/patents/US3789908

67. 108. Joshua E. Rabinovich "Rapid manufacturing system for metal, metal matrix

    composite materials and ceramics". US6144008A. Nov 7, 2000,

    http://www.google.com/patents/US3789908

68. The history of welding: From the middle ages to modern technology. Retrieved

    from: http://www.gowelding.org/articles/history-of-welding/

69. The history of welding – A brief overview of welding through the years – from

    the middle ages to today. Retrieved from:

    http://www.millerwelds.com/resources/articles/welding-history/

70. The harnessing of heat: A welding history. Retrieved from:

    http://www.weldguru.com/welding-history.html#timeline

71. Baker Raplh. "Method of making decorative articles." US1533300A, Apr 14, 1925

72. R. D. Simonson "History of Welding" Jefferson Pubns Inc, June 1969

73. Make metal parts faster & cheaper than ever with electron beam additive

    manufacturing (EBAM) system or services. Retrieved from:

    http://www.sciaky.com/additive-manufacturing/electron-beam-additive-

    manufacturing-technology

74. Prinz, Fritz, and Lee Weiss. "Method and support structures for creation of

    objects by layer deposition." U.S. Patent No. 5,286,573. 15 Feb. 1994.

75. Conley, J. G., and H. L. Marcus. "Rapid prototyping and solid free form

    fabrication." *Journal of Manufacturing Science and Engineering* 119.4B (1997):

811-816.

76. Song, Yong-Ak, and Sehyung Park. "Experimental investigations into rapid prototyping of composites by novel hybrid deposition process." *Journal of Materials Processing Technology* 171.1 (2006): 35-40.

77. Antonio Fernando Ribeiro and Prof. John Norrish, " Metal Based Rapid Prototyping for More Complex Shapes", 6th Biennial International Conference on "Computer Technology in Welding", TWI, Abington Publishing, 9-12 June 1996, Lanaken, Belgium

78. Antonio Fernando Ribeiro and Prof. John Norrish, " Rapid Prototyping Process Using Metal Directly", Proc. of the 7th Annual Solid Freeform Fabrication Symposium, Aug. 12-14, 1996, Austin, TX

79. Y. M. Zhang, P. Li, Y. Chen, and A. T. Male, "Automated system for welding-based rapid prototyping", Mechatronics, 12, 2002, pp.37-53.

80. Choi, D. S., Lee, S. H., Shin, B. S., Whang, K. H., Song, Y. A., Park, S. H., & Jee, H. S. (2001). Development of a direct metal freeform fabrication technique using CO 2 laser welding and milling technology. *Journal of Materials Processing Technology*, *113*(1), 273-279.

81. Cao, Y., Zhu, S., Liang, X., & Wang, W. (2011). Overlapping model of beads and curve fitting of bead section for rapid manufacturing by robotic MAG welding process. *Robotics and Computer-Integrated Manufacturing*, *27*(3), 641-645.

82. Song, Y. A., & Park, S. (2006). Experimental investigations into rapid prototyping of composites by novel hybrid deposition process. *Journal of Materials*

Processing Technology, *171*(1), 35-40.

83. Doumanidis, C., & Kwak, Y. M. (2002). Multivariable adaptive control of the bead profile geometry in gas metal arc welding with thermal scanning.*International Journal of Pressure Vessels and Piping*, *79*(4), 251-262.

84. Mutoh Industries unveils new metal arc welding 3D printer, the Value Arc MA5000-S1. Retrieved from: http://3dprint.com/84633/mutoh-industries-value-arc-3d/ end at old ref.110

85. Katou, M., et al., *Freeform fabrication of titanium metal and intermetallic alloys by three-dimensional micro welding.* Materials & Design, 2007. **28**(7): p. 2093-2098.

86. Terakubo, M., et al., *Freeform fabrication of titanium metal by 3D micro welding.* Materials Science and Engineering a-Structural Materials Properties Microstructure and Processing, 2005. **402**(1-2): p. 84-91.

87. Terakubo, M., et al., *Freeform fabrication of Ti-Ni and Ti-Fe intermetallic alloys by 3D Micro Welding.* Intermetallics, 2007. **15**(2): p. 133-138.

88. Horii, T., et al., *Development of freeform fabrication of metals by three dimensional micro-welding.* Designing of Interfacial Structures in Advanced Materials and their Joints, 2007. **127**: p. 189-194.

89. Horii, T., S. Kirihara, and Y. Miyamoto, *Freeform fabrication of Ti-Al alloys by 3D micro-welding.* Intermetallics, 2008. **16**(11-12): p. 1245-1249.

90. Horii, T., S. Kirihara, and Y. Miyamoto, *Freeform fabrication of superalloy objects by 3D micro welding.* Materials & Design, 2009. **30**(4): p. 1093-1097.

91. Jandric, Z., and R. Kovacevic. "Heat management in solid free-form fabrication based on deposition by welding." *Proceedings of the Institution of Mechanical Engineers, Part B: Journal of Engineering Manufacture* 218.11 (2004): 1525-1540.

92. Alec and Eddie Krassenstein. Mutoh industries unveils value arc MA5000-S1 metal arc welding 3D printer. 3D printer and 3D printing news. (2015). www.3Dprint.com

93. Haselhuhn, Amberlee S., et al. "In situ formation of substrate release mechanisms for gas metal arc weld metal 3-D printing." *Journal of Materials Processing Technology* 226 (2015): 50-59.

94. Drizo, Aleksandra, and Joseph Pegna. "Environmental impacts of rapid prototyping: an overview of research to date." *Rapid prototyping journal* 12.2 (2006): 64-71.

95. Taminger, Karen, and Robert A. Hafley. "Electron beam freeform fabrication: a rapid metal deposition process." (2003).

96. Karen M. B. Taminger and Robert A. Hafley. "Characterization of 2219 Aluminum produced by electron beam freeform fabrication." NASA Langley Research Center. Aug (2002)

97. Zalameda, J.N., et al., *Thermal Imaging for Assessment of Electron-Beam Freeform Fabrication (EBF3) Additive Manufacturing Deposits.* Thermosense: Thermal Infrared Applications Xxxv, 2013. **8705**.

98. Watt, F. (1999). Focused high energy proton beam micromachining: A perspective view. *Nuclear Instruments and Methods in Physics Research Section*

B: Beam Interactions with Materials and Atoms, *158*(1), 165-172.

99. Electron Beam Welding. Retrieved from:

http://www.weldingengineer.com/1%20Electron%20Beam.htm

100.   Laser Beam Vs. Electron Beam Welding Which process works best for

what?. May 2011. Retrieved from:

http://www.techbriefs.com/component/content/article/23-

ntb/features/feature-articles/9998

101.   Electron Beam vs. Laser Beam Welding. Feb 2014. Retrieved from.

http://www.accutektesting.com/about-us/blog/electron-beam-vs-laser-beam-

welding

102.   Heralić, Almir, Anna-Karin Christiansson, and Bengt Lennartson. "Height

control of laser metal-wire deposition based on iterative learning control and 3D

scanning." *Optics and lasers in engineering* 50.9 (2012): 1230-1241.

103.   W. Syed, A. Pinkerton, L. Li. A comparative study of wire feeding and

powder feeding in direct diode laser deposition for rapid prototyping**.** Appl Surf

Sci, 247 (2005), pp. 268–276

104.   J. Nurminen, Hot-wire laser cladding: process, materials and their

properties, PhD thesis, Tampere University of Technology, Publication 765, 2008.

105.   Song, Yong-Ak, et al. "3D welding and milling: Part I–a direct approach for

freeform fabrication of metallic prototypes." *International Journal of Machine

Tools and Manufacture* 45.9 (2005): 1057-1062.

106.   Choi, D.S., et al., *Development of a direct metal freeform fabrication*

technique using CO(2) laser welding and milling technology. Journal of Materials

Processing Technology, 2001. **113**(1-3): p. 273-279.

107.   Moures, F., Cicală, E., Sallamand, P., Grevey, D., Vannes, B., & Ignat, S.

(2005). Optimisation of refractory coatings realised with cored wire addition

using a high-power diode laser. *Surface and Coatings Technology*, *200*(7), 2283-

2292.

108.   156. Laser Beam vs. Electron Beam Welding: Which process works best

for what?. NASA. Tech Briefs. Engineering Solutions for design & manufacturing.

May (2011)

109.   Tolochko, N. K., Khlopkov, Y. V., Mozzharov, S. E., Ignatiev, M. B., Laoui,

T., & Titov, V. I. (2000). Absorptance of powder materials suitable for laser

sintering. *Rapid Prototyping Journal*, *6*(3), 155-161.

110.   I. Gibson, D.W. Rosen, B. Stucker, Additive Manufacturing Technologies:

Rapid Prototyping to Direct Digital Manufacturing. Springer New York. 2010

111.   Fischer, P., et al. "Sintering of commercially pure titanium powder with a

Nd: YAG laser source." *Acta Materialia* 51.6 (2003): 1651-1662.

112.   Mullen, Lewis, et al. "Selective Laser Melting: A regular unit cell approach

for the manufacture of porous, titanium, bone in-growth constructs, suitable for

orthopedic applications." *Journal of Biomedical Materials Research Part B:

Applied Biomaterials* 89.2 (2009): 325-334.

113.   Tolochko, Nikolay K., et al. "Absorptance of powder materials suitable for

laser sintering." *Rapid Prototyping Journal* 6.3 (2000): 155-161.

114.   Tolochko NK, Laoui T, Khlopkov YV, Mozzharov SE, Titov

115.   VI, Ignatiev MB. Absorptance of powder materials suitable

116.   for laser sintering. Rapid Prototyping J 2000;6:155–160

117.   Tolochko NK, Laoui T, Khlopkov YV, Mozzharov SE, Titov

118.   VI, Ignatiev MB. Absorptance of powder materials suitable

119.   for laser sintering. Rapid Prototyping J 2000;6:155–160

120.   Tolochko NK, Laoui T, Khlopkov YV, Mozzharov SE, Titov

121.   VI, Ignatiev MB. Absorptance of powder materials suitable

122.   for laser sintering. Rapid Prototyping J 2000;6:155–160

123.   olochko NK, Laoui T, Khlopkov YV, Mozzharov SE, Titov

124.   VI, Ignatiev MB. Absorptance of powder materials suitable

125.   for laser sintering. Rapid Prototyping J 2000;6:155–160Tolochko, Nikolay

K., et al. "Absorptance of powder materials suitable for laser sintering." *Rapid

Prototyping Journal* 6.3 (2000): 155-161.

126.   Khaing, M. W., J. Y. H. Fuh, and L. Lu. "Direct metal laser sintering for

rapid tooling: processing and characterisation of EOS parts." *Journal of Materials

Processing Technology* 113.1 (2001): 269-272.

127.   3ders.com; Wire-feed additive manufacturing might be the future of

metal-based 3D printing; By Simon http://www.3ders.org/articles/20150531-

wire-feed-additive-manufacturing-might-be-the-future-of-metal-based-3d-

printing.html

128.   Gibson, Ian, and Dongping Shi. "Material properties and fabrication

parameters in selective laser sintering process." *Rapid Prototyping Journal*3.4 (1997): 129-136.

129.   Osakada, Kozo, and Masanori Shiomi. "Flexible manufacturing of metallic products by selective laser melting of powder." *International Journal of Machine Tools and Manufacture* 46.11 (2006): 1188-1193.

130.   Frigola et al., "Fabricating Copper Components with Electron Beam Melting",http://www.asminternational.org/documents/10192/19735983/amp17 207p20.pdf/2a87d5ae-86ec-4f27-bdd1-f74af1a2f523

131.   Dinwiddie, R. B., Dehoff, R. R., Lloyd, P. D., Lowe, L. E., & Ulrich, J. B. (2013, May). Thermographic in-situ process monitoring of the electron-beam melting technology used in additive manufacturing. In *SPIE Defense, Security, and Sensing* (pp. 87050K-87050K). International Society for Optics and Photonics.

132.   Powder Bed Fusion. Additive Manufacturing Research Group. Loughborough University. (2015) Retrieved from: http://www.lboro.ac.uk/research/amrg/about/the7categoriesofadditivemanufac turing/powderbedfusion/

133.   Han C-M, Lee E-J, Kim H-E, Koh Y-H, Kim K N, Ha Y and Kuh S-U 2010 The electron beam deposition of titanium on polyetheretherketone (PEEK) and the resulting enhanced biological properties *Biomaterials* **31** 3465–70.

134.   Liu, W., & DuPont, J. N. (2003). Fabrication of functionally graded TiC/Ti composites by laser engineered net shaping. *Scripta Materialia*, *48*(9), 1337-1342.

135.   Liu, W., & DuPont, J. N. (2003). Fabrication of functionally graded TiC/Ti composites by laser engineered net shaping. *Scripta Materialia*, *48*(9), 1337-1342.

136.   Balla, V. K., DeVasConCellos, P. D., Xue, W., Bose, S., & Bandyopadhyay, A. (2009). Fabrication of compositionally and structurally graded Ti–TiO 2 structures using laser engineered net shaping (LENS). *Acta biomaterialia*, *5*(5), 1831-1837.

137.   España, F. A., Balla, V. K., Bose, S., & Bandyopadhyay, A. (2010). Design and fabrication of CoCrMo alloy based novel structures for load bearing implants using laser engineered net shaping. *Materials Science and Engineering: C*, *30*(1), 50-57.

138.   Terakubo, M., et al., *Freeform fabrication of titanium metal by 3D micro welding.* Materials Science and Engineering a-Structural Materials Properties Microstructure and Processing, 2005. **402**(1-2): p. 84-91.

139.   Total Materia. Corrosion of titanium and titanium alloys. (2001). Retrieved from: http://www.totalmateria.com/Article24.htm

140.   Optical Microscopy and Specimen Preparation. DoITPoMS. University of Cambridge. August 2009

141.   S. Thiru et al. Prediction and Measurement of weld dilution in robotic CO_2 Arc Welding. World Applied Sciences Journal 21 (Special Issue of Engineering and Technology) : 23-30, 2013

142.   Welding Cast Iron and Other Irons. Total Materia. 2006. Retrieved from: http://www.keytometals.com/page.aspx?ID=CheckArticle&site=kts&NM=185

143.   K.C. Mills (2002), "Recommended Values of Thermophysical Properties for Selected Commercial Alloys, ASM International, NPL, Woodhead Publishing, UK

144.   Xie & A. Kar. Laser Welding of Thin Sheet Steel with Surface Oxidation. Welding Research Supplement. Oct. 1999

145.   N. Ahmed, K.T. Voisey, and D.G. McCartney. Investigation into the effect of beam shape on melt pool characteristics using analytical modelling. Optics and Lasers in Engineering journal 48 (2010) 548-554

146.   R. I. L. Guthrie and T. Lida. Thermodynamic properties of liquid metals. Materials Science and Engineering A178 (1994) 35-41

147.   Ojo, O. A., & Chaturvedi, M. C. (2005). On the role of liquated γ' precipitates in weld heat affected zone microfissuring of a nickel-based superalloy. *Materials Science and Engineering: A*, *403*(1), 77-86.

148.   Arnold, J., and R. Volz. "Laser powder technology for cladding and welding."*Journal of thermal spray technology* 8.2 (1999): 243-248.

149.   Shea, William R., ed. (1983). Nature mathematized: historical and philosophical case studies in classical modern natural philosophy. Dordrecht: Reidel. P. 282. ISBN 9978-90-277-1402-2

150.   Antonysamy, A. A., J. Meyer, and P. B. Prangnell. "Effect of build geometry on the β-grain structure and texture in additive manufacture of Ti 6Al 4V by selective electron beam melting." *Materials Characterization* 84 (2013): 153-168.

151.	Lockheed Martin Aeronautics, Electron Beam, Direct Manufacturing of Large Scale Aerospace Components, Advanced Development Programs, Lockheed Martin, Aeromat 2014 Conference (2014)

152.	Antonysamy, A. A., J. Meyer, and P. B. Prangnell. "Effect of build geometry on the β-grain structure and texture in additive manufacture of Ti 6Al 4V by selective electron beam melting." Materials Characterization 84 (2013): 153-168.

153.	Lockheed Martin Aeronautics, Electron Beam, Direct Manufacturing of Large Scale Aerospace Components, Advanced Development Programs, Lockheed Martin, Aeromat 2014 Conference (2014)

154.	Zhou and H.L. Tsai. "Hybrid Laser-Arc Welding" Intech (2012): 1-32

155.	Iwasaki, K., Ohkawa, S., Uo, M., Akasaka, T., & Watari, F. (2004). Laser welding of titanium and dental precious alloys. *Materials Transactions*, *45*(4), 1140-1146.

156.	Barnes Jr, W. P. (1984). *U.S. Patent No. 4,424,435*. Washington, DC: U.S. Patent and Trademark Office.

157.	Baumers, M., Tuck, C., Wildman, R., Ashcroft, I., Rosamond, E., & Hague, R. (2012). Combined Build-Time, Energy Consumption and Cost Estimation for Direct Metal Laser Sintering. In *From Proceedings of Twenty Third Annual International Solid Freeform Fabrication Symposium—An Additive Manufacturing Conference* (Vol. 13).

158.	http://www.monarchserver.com/TableofEmissivity.pdf

159.   Mazumder, J., & Steen, W. M. (1980). Heat transfer model for CW laser material processing. *Journal of Applied Physics*, *51*(2), 941-947.

160.   Camci, C., & Herr, F. (2002). Forced convection heat transfer enhancement using a self-oscillating impinging planar jet. *Journal of heat transfer*, *124*(4), 770-782.

161.   Terakubo, M., et al., *Freeform fabrication of titanium metal by 3D micro welding.* Materials Science and Engineering a-Structural Materials Properties Microstructure and Processing, 2005. **402**(1-2): p. 84-91.

162.   Muthupandi, V., Srinivasan, P. B., Seshadri, S. K., & Sundaresan, S. (2003). Effect of weld metal chemistry and heat input on the structure and properties of duplex stainless steel welds. *Materials Science and Engineering: A*, *358*(1), 9-16.

163.   Yang, Z., Sista, S., Elmer, J. W., & DebRoy, T. (2000). Three dimensional Monte Carlo simulation of grain growth during GTA welding of titanium. *Acta Materialia*, *48*(20), 4813-4825.

164.   Mishra, S., & DebRoy, T. (2004). Measurements and Monte Carlo simulation of grain growth in the heat-affected zone of Ti–6Al–4V welds. *Acta Materialia*, *52*(5), 1183-1192.

165.   Lapostolle, F., Billard, A., & Von Stebut, J. (2000). Structure/mechanical properties relationship of titanium–oxygen coatings reactively sputter-deposited. *Surface and Coatings Technology*, *135*(1), 1-7.

166.   Finlay, W. L., & Snyder, J. A. (1950). Effects of three interstitial solutes (nitrogen, oxygen, and carbon) on the mechanical properties of high-purity, alpha

titanium. *J. Metals*, *188*.

167.   Liu, Z., & Welsch, G. (1988). Effects of oxygen and heat treatment on the
mechanical properties of alpha and beta titanium alloys. *Metallurgical
Transactions A*, *19*(3), 527-542.

168.   R. Jaffee: Presentation at TMS-AIME meeting, spring 1987, Denver, CO.

169.   G. Welsch, G. Liitjering, K. Gazioglu, and W. Bunk: Metall. Trans. A, 1977,
vol. 8A, pp. 169-77.

170.   R. Castro and L. Seraphin: Mem. Sci. Rev. Met., 1966, vol. 63, pp. 1025-58.

171.   R.E. Curtis and W. E Spurr: Trans. ASM, 1968, vol. 61, pp. 115-27.

172.   A. Lasalmonie and M. Loubradou: J. Mat. Sci., 1979, vol. 14, pp. 2589-95.

173.   Paul D. et al., Microstructure of titanium welds. Struers E-Journal of
Materialography (3/2004)

174.   Matthew J. Donachie. Titanium: A Technical Guide. 2nd Edition (2000)

175.   Cao, X., Jahazi, M., Immarigeon, J. P., & Wallace, W. (2006). A review of
laser welding techniques for magnesium alloys. *Journal of Materials Processing
Technology*, *171*(2), 188-204.

176.   Li, X., Xie, J., & Zhou, Y. (2005). Effects of oxygen contamination in the
argon shielding gas in laser welding of commercially pure titanium thin
sheet.*Journal of materials science*, *40*(13), 3437-3443.

177.   ROBERT P. MUDGE and NICHOLAS R. WALD. RPM & Associates, Inc.,
Welding Journal, Jan (2007). Retrieved
from:http://www.rpmandassociates.com/RPMILaserDepositionTechnologyAdva

ncesAdditiveManufacturingAndRepair.aspx

178.   Liu, W., & DuPont, J. N. (2003). Fabrication of functionally graded TiC/Ti

composites by laser engineered net shaping. *Scripta Materialia*, *48*(9), 1337-

1342.

179.   Nowotny, Steffen, et al. "Laser beam build-up welding: precision in

repair, surface cladding, and direct 3D metal deposition." *Journal of Thermal

Spray Technology* 16.3 (2007): 344-348.

180.   Yeo, Woon Seung, and Jonathan Berger. *Raster Scanning: A New

Approach to Image Sonification, Sound Visualization, Sound Analysis, and

Synthesis*. Diss. Department of Music, Stanford University, 2008.

181.   AWS A3.0:2001, Standard Welding Terms and Definitions Including Terms

for Adhesive Bonding, Brazing, Soldering, Thermal Cutting, and Thermal

Spraying, American Welding Society (2001), p. 117. ISBN 0-87171-624-0

182.   Duarte, F. J. (2003).*Tunable Laser Optics*. Elsevier Academic. ISBN 0-12-

222696-8.

183.   Zhenguo Nie. Experimental study and modeling of H13 steel deposition

using a laser hot-wire additive manufacturing (drafted paper). Tsinghua

University. Beijing. China. 2012

184.   M. Bourne. Radius of Curvature. Retrieved from:

http://www.intmath.com/applications-differentiation/8-radius-curvature.php